Lithium and boron in pyroclastic rocks from Bükkalja volcanic field

Mirt, Magdalena

Master's thesis / Diplomski rad

2024

Degree Grantor / Ustanova koja je dodijelila akademski / stručni stupanj: **University of Zagreb, Faculty of Mining, Geology and Petroleum Engineering / Sveučilište u Zagrebu, Rudarsko-geološko-naftni fakultet**

Permanent link / Trajna poveznica: https://urn.nsk.hr/urn:nbn:hr:169:129703

UNIVERSITY OF ZAGREB
FACULTY OF MINING, GEOLOGY AND PETROLEUM ENGINEERING
Graduate study of Geology

LITHIUM AND BORON IN PYROCLASTIC ROCKS FROM BÜKKALJA VOLCANIC FIELD

Master's Thesis

Magdalena Mirt
G485

Zagreb, 2024

KLASA: 602-01/24-01/13
URBROJ: 251-70-13-242
U Zagrebu, 13.02.2024.

Magdalena Mirt, studentica

RJEŠENJE O ODOBRENJU TEME

Na temelju vašeg zahtjeva primljenog pod KLASOM 602-01/24-01/13, URBROJ: 251-70-13-241 od 25.01.2024. priopćujemo vam temu diplomskog rada koja glasi:

LITHIUM AND BORON IN PYROCLASTIC ROCKS FROM BÜKKALJA VOLCANIC FIELD

Za mentoricu ovog diplomskog rada imenuje se u smislu Pravilnika o izradi i obrani diplomskog rada Prof.dr.sc. Sibila Borojević Šoštarić nastavnik Rudarsko-geološko-naftnog-fakulteta Sveučilišta u Zagrebu.

Mentorica:

(potpis)

Prof.dr.sc. Sibila Borojević Šoštarić
(titula, ime i prezime)

Predsjednica povjerenstva za završne i diplomske ispite:

(potpis)

Izv.prof.dr.sc. Ana Maričić
(titula, ime i prezime)

Prodekan za nastavu i studente:

(potpis)

Izv.prof.dr.sc. Borivoje Pašić
(titula, ime i prezime)

I would like to express my gratitude to…

..my mentor, professor Sibila Borojević Šoštarić, PhD, for her guidance, mentorship and support during my entire studies.

…Tomislav Brenko, PhD, for help with the XRD and XRF analyses and every useful advice in the past few years.

…my reviewers, Associate Professor Vesnica Garašić, PhD and Assistant Professor Duje Smirčić for every comment and advice that positively affected the quality of this paper.

…Michaela Hruškova Hasan, PhD, for help and cheerful company during laboratory work

…Vinko Baranašić, MS.c. and Branka Prša for help with the laboratory work and Mario Valent for the making of thin sections.

…my dearest colleague and best friend, Lucija Balaić, for being here every step of this journey.

….my friends and my family, especially my grandpa, for being my motivation when I needed it the most.

University of Zagreb Master's Thesis
Faculty of Mining, Geology and Petroleum Engineering

LITHIUM AND BORON IN PYROCLASTIC ROCKS FROM BÜKKALJA VOLCANIC FIELD

Magdalena Mirt

Thesis completed at: University of Zagreb
Faculty of Mining, Geology and Petroleum Engineering
Department of mineralogy, petrology and mineral resources
Pierottijeva 6, 10 000 Zagreb

Abstract

The aim of this Master's thesis is to analyse the mineralogical and chemical composition of pyroclastic rocks from the Bükkalja Volcanic Field and to determine which minerals host lithium and boron. A total of 12 samples were analysed from different Miocene pyroclastic units: Wind-Kalnik Unit, Eger Unit, Mango Unit, Demjén Unit, and Harsany Unit, with one sample from Kuchyna Tuff. Mineral composition was determined using polarisation microscopy and X-ray diffraction, chemical composition via X-ray fluorescence, lithium concentrations via atomic absorption spectrometry, and boron concentrations were determined using atomic emission spectrometry. Polarisation microscopy showed that samples consist of crystaloclasts, vitroclasts, and lithoclasts and mineralogical composition was further confirmed by the XRD analysis. Plagioclase, quartz, sanidine, biotite and hornblende are in the form of crystalloclasts. Lithoclasts are mostly andesitic to rhyolitic. Volcanic glass is abundant both as medium sieved glass shards and in the matrix as very fine to fine grained vitric particles. Clay minerals, mostly smectite, occur in the matrix. According to the XRF analysis, all of the analysed samples are rich in SiO_2 component with concentrations ranging from 61 to 73 wt%. Most of the samples fall under the High-K Calc-Alkaline magmatic series, according to the SiO_2/K_2O ratio. AAS and AES were performed separately for magnetic and non-magnetic fractions, where biotite separated into the magnetic fraction and other minerals in the non-magnetic fraction. In the non-magnetic fraction, the lithium concentrations obtained were mostly below the detection limit and could only be measured in 3 samples. In these samples, the lithium concentrations ranged from 4,2 to 21,7 mg/kg, whereas the lithium concentrations in the non-magnetic, <125 magnetic μm, fraction were below the detection limit in 5 analysed samples. In the remaining non-magnetic fraction, lithium concentrations range from 1,8 to 20,1 mg/kg. Lithium concentrations in magnetic fractions ranged from 15,2 to 41,2 mg/kg. The boron concentrations in the non-magnetic fraction range from 835 to 4505 mg/kg, while the boron concentrations in the magnetic fractions range from 3044 to 26204 mg/kg. Magnetic fractions of all samples show an enrichment of boron and lithium compared to the non-magnetic fractions. It follows that lithium and boron may be present in the crystal structure of biotite and its alterations, such as chlorite. Additionally, boron could be found adsorbed to the clay minerals.

Keywords: Bükkalja Volcanic Field, pyroclastic rocks, tuff, lithium, boron

Master's thesis includes: 92 pages, 10 tables, 31 figures, and 54 references.

Original in: English

Archived at: Library of the Faculty of Mining, Geology and Petroleum Engineering, Pierottijeva 6, Zagreb

Supervisors: Full Professor Sibila Borojević Šoštarić, PhD

Tech. assistance: Senior Assistant Tomislav Brenko, PhD

Reviewers: Full Professor Sibila Borojević Šoštarić, PhD
Associate Profesor Vesnica Garašić, PhD
Assistant Professor Duje Smirčić, PhD

Defense date: February 22nd 2024, Faculty of Mining, Geology and Petroleum Engineering, University of Zagreb

Sveučilište u Zagrebu
Rudarsko-geološko-naftni fakultet

Diplomski rad

LITIJ I BOR U PIROKLASTIČNIM STIJENAMA IZ VULKANSKOG POLJA BÜKKALJA

Magdalena Mirt

Rad izrađen: Sveučilište u Zagrebu
Rudarsko-geološko-naftni fakultet
Zavod za mineralogiju, petrologiju i mineralne sirovine
Pierottijeva 6, 10 000 Zagreb

Sažetak

Cilj ovog diplomskog rada je mineraloška i kemijska analiza piroklastičnih stijena s vulkanskog polja Bükkalja, u svrhu utvrđivanja minerala nosioca litija i bora. Analizirano je 12 uzoraka koji pripadaju različitim miocenskim piroklastičnim jedinicama: Wind-Kalnik, Eger, Mangó, Demjén i Harsany te jedan uzorak Kuchyna tufa. Mineralni sastav određen je metodama polarizacijske mikroskopije i rendgenske difracije na prahu (XRD), kemijski sastav određen je rendgenskom fluorescencijom (XRF), kocentracije litija određene su atomskom apsorpcijskom spektrometrijom (AAS) i koncentracije bora određen su atomskom emisijskom spektrometrijom (AES). Polarizacijskom mikroskopijom utvrđeno je da se uzorci sastoje od kristaloklasta, vitroklasta i litoklasta te je mineralni sastav potvrđen rendgenskom difrakcijom. Plagioklas, kvarc, sanidin, biotit i hornblenda pojavljuju se kao kristaloklasti. Litoklasti su andezitnog do riolitnog sastava. Vulkansko staklo pojavljuje se u velikim količinama, kao vitroklasti i u matriksu. Minerali glina, većinski određeni kao smektit, pojavljuju se u matriksu. Prema rezultatima rendgenske fluorescencije svi analizirani uzorci pokazuju visok sadržaj SiO_2 čije su koncentracije u rasponu od 61 do 73%. Prema omjeru SiO_2/K_2O većina uzoraka spada u visoko-kalijsku kalcijsko-alkalijsku magmatsku seriju. AAS i AES analize provedene su na uzorcima separiranima u magnetnu i nemagnetnu frakciju. Magnetna frakcija sastoji se većinski od biotita, a nemagnetna od ostalih prisutnih minerala. Koncentracije litija u nemagnetnoj frakciji su ispod granice detekcije u većini uzorka, dok se 3 uzorka u kojima su mjerljive kreću od 4,2 do 21,7 mg/kg. U nemagnetnoj, <125 μm frakciji koncentracija litija je u 5 uzoraka bila ispod granice detekcije, dok se koncentracije u uzorcima u kojima su mjerljive su u rasponu od 1,8 do 20,1 mg/kg. Koncentracije litija u magnetnoj frakciji su u rasponu od 15,2 do 41,2 mg/kg. Koncentracije bora u nemagnetnoj frakciji su u rasponu od 835 do 4505 mg/kg, a u magnetnoj od 3044 do 26240 mg/kg. Magnetne frakcije ovih uzoraka pokazuju obogaćenje litijem i borom u usporedbi s nemagnetnim frakcijama, iz čega slijedi da oba elements mogu biti prisutni u strukturi biotita i njegovim alteracijama, poput klorita, dok se bor još može pojaviti adsorbiran na minerale glina.

Ključne riječi: Vulkansko polje Bükkalka, piroklastične stijeme, tuf, litij, bor

Završni rad sadrži: 92 stranice, 10 tablica, 31 sliku i 53 reference.

Jezik izvornika Engleski

Pohrana rada: Knjižnica Rudarsko-geološko-naftnog fakulteta, Pierottijeva 6, Zagreb

Mentori: Dr. sc. Sibila Borojević Šoštarić, redovita profesorica RGNF

Pomagao pri izradi: Dr. sc. Tomislav Brenko

Ocjenjivači: Dr.sc. Sibila Borojević Šoštarić, redovita profesorica RGNF
Dr.sc. Vesnica Garašić, izvanredna profesorica RGNF
Dr.sc. Duje Smirčić, docent RGNF

Datum obrane: 22.02.2024., Rudarsko-geološko-naftni fakultet Sveučilišta u Zagrebu

TABLE OF CONTENTS

LIST OF FIGURES

LIST OF TABLES

LIST OF USED SYMBOLS AND UNITS

Symbol		Description
AAS	–	atomic absorption spectrometry
AES	–	atomic emission spectrometry
A	-	ampere
Å	-	ågström
Apt	–	apatite
Bt	-	biotite
BVF	–	Bükkalja Volcanic Field
Cal	–	calcite
Hbl	-	hornblende
km^2	–	squared kilometre
LC	–	lithoclast
Ma	–	million years
m	–	meter
mm	–	millimeter
mg/kg	–	milligram per kilogram
Ms	-	muscovite
µm	–	micrometer
n	–	refraction index
N	–	parallel polars
N+	-	crossed polars
Pl	-	plagioclase
ppm	–	parts per million
PUM	–	pumice
R	-	radius
Qtz	–	quartz
VG	–	volcanic glass
XRD	–	X-ray diffraction
XRF	–	x-ray fluorescence

1. INTRODUCTION

Effusive magmatic rocks are formed on the Earth's surface as a result of crystallization processes caused by the rapid cooling of erupted lava.

Pyroclastic rocks, such as pyroclastic breccia or tuff, are directly related to explosive eruptions of viscous, volatile rich magmas. Pyroclastic material can be both lithified and non-lithified, which is called tephra, and can be further classified according to the grain or clast size. Pyroclastic rocks with grains/clasts larger than 64 mm are defined as pyroclastic breccias, those with grain/clast size between 2-64 mm are defined as lapillistone, and those with grain/clast size smaller than 2 mm are defined as tuff (Fisher, 1966). Tuffs can be further subdivided according to the main component of the rock as vitroclastic, crystaloclastic, or lithoclastic tuff (Pettijhon, 1975) (Figure 1-1).

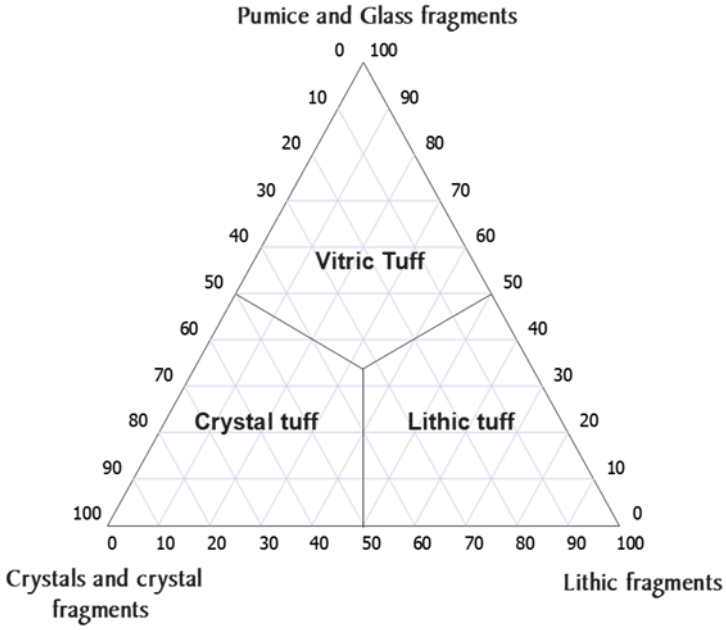

Figure 1-1. Tuff classification diagram (Pettijhon, 1975).

The term ignimbrite refers to all pyroclastic flow deposits, welded or not. Their groundmass is usually devitrified and non-devitrified volcanic glass, but they can contain crystal and lithic fragments (Fisher, 1966).

Pumice is a volcanic rock which is created during a violent ejection of super-heated, highly pressurised rock from a volcano. Predominantly, it is porous and very light volcanic

rock having vesicular texture and consists of volcanic glass which can include crystals (Cox et al., 1979).

According to Biró et al., (2020) and references therein, the Miocene silicic volcanism in the Bükkalja Volcanic Field is characterized by phreatomagmatic, explicitly, phreatoplinian eruptions. Phreatomagmatic eruptions imply explosive reactions of magma and water, whereas Plinian eruptions are characterized by forming extremely high ash columns. Plinian eruptions are usually caused by gas boiling in gas-rich magmas during their ascend to the surface. The expression phreatoplinian is applied to silicic eruptions which result in pyroclastic deposition of a larger extent than Plinian eruptions (>500km^2) along with a high degree of fragmentation.

The purpose of this master thesis is to define the mineralogical and geochemical composition of the Miocene volcaniclastic rocks from the Bükkalja Volcanic Field, along with determining the contents and sources of lithium and boron. In addition, the obtained results will be compared with Western Balkan Li-B zone and Miocene tuffs from Dinarides. For that matter, 11 samples of volcanoclastic pyroclastic rocks from differenc volcanoclastic units from Bükkalja Volcanic Field along with 1 sample of Kuchyna tuff, were analysed.

Mineral composition was determined using the methods of polarisation microscopy and x-ray diffraction (XRF), geochemical composition was determined using x-ray fluorescence (XRF) and targeted lithium and boron contents were obtained using the atomic absorption spectrometry (AAS), and atomic emission spectrometry (AES).

Lithium is a silvery-white, extremely soft, reactive, and flammable alkali metal with the atomic radius of 1,82 Å. The main sources of lithium are brines, where it occurs as lithium carbonate, and silicate/borosilicate minerals such as spodumene ($LiAlSi_2O_6$) or jadarite ($LiNaSiB_3O_7(OH)$). Recently, clay minerals are being researched as another potential source of lithium (Royal Society of Chemistry, 2024a).

Boron is a metalloid with an atomic radius of 1,92 Å. In its elementary state, it occurs as an amorphous brown powder or crystalline solid, but it is usually found in borate minerals such as borax ($Na_2(B_4O_5)(OH)_4 \cdot 8H_2O$), ulexite ($NaCa[B_5O_6(OH)_6] \cdot 5H_2O$), and colemanite ($Ca[B_3O_4(OH)_3] \cdot H_2O$) (Royal Society of Chemistry, 2024b).

Due to its various industrial implications, both boron and lithium are categorized as critical and strategic raw materials in the recent European critical raw materials act (European Commission, 2023).

The samples examined in this research were conceded by the kindness of Réka Haranginé Lukács, Ph.D., from Eötvös Loránd University. This work is a part of the follow-up activities proceeding the EIT RawMaterials project 18036 iTARG3T Innovative targeting & processing of W-Sn-Ta-Li ores: towards EU's self-supply.

2. GEOGRAPHICAL SETTING

The Bükkalja Volcanic Field is located in Northern Hungary, eastern-central Europe (Figure 2-1a). Regionally, it is a part of the Inner Western Carpathians. Bükkalja Volcanic Field is located in the southern part of the Bükk mountain range. It is known for the volcanic tuffs, lava flows, and post-volcanic hot springs. Bükk mountains (Figure 2-1.b) are a part of North Hungarian mountains and they cover an area of about 1 500 km^2. It has 20 peaks reaching a height of over 900 m, with the highest one called Istállós-kő, reaching a height of 961 m. The area is known for its diverse wildlife and over a thousand documented caves which are of great biological and geological interest.

The climate in this area is continental and it is one of the most rugged places in Hungary with trees covering most of the area. The nearest big city is Miskolc, which administratively belongs to the Borsod-Abaúj-Zemplén county.

Historically, this area is known for the neolithic Bükk pottery culture.

Kuchyna tuff sample analysed in this Masters thesis was collected in Kisbeszterce, a small village in the Northern Baranya county in the south of Hungary, close to Pécs (Figure 2-1.b).

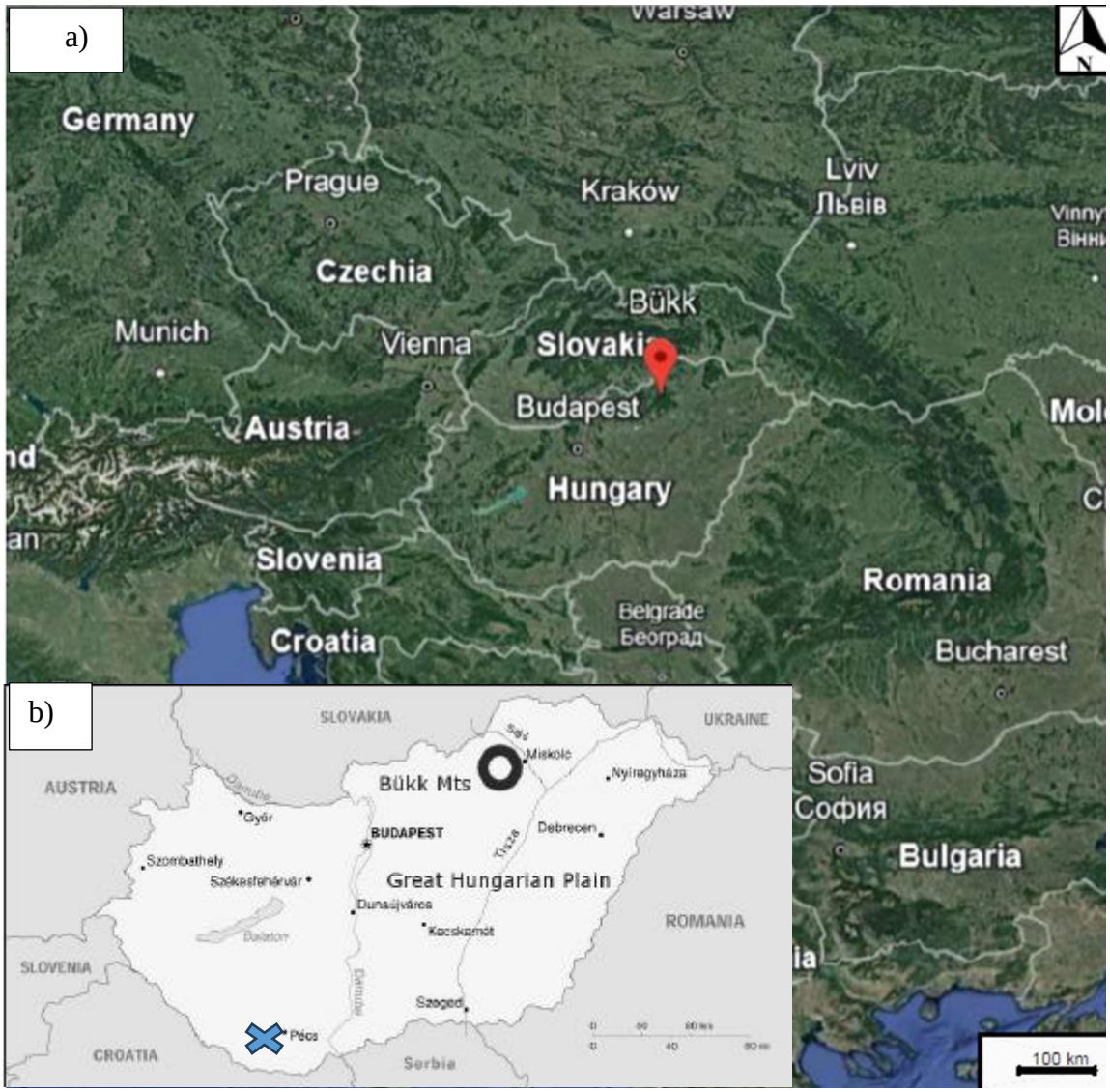

Figure 2-1. Geographic setting of Bukk Mts. a) in Central-Eastern Europe (https://earth.google.com/web/) b) in Hungary; X-Kisbeszterce (Németh & Petho (2009))

3. GEOLOGICAL SETTING

3.1. Regional geological setting

The Carpathian-Pannonian Region consists of an arcuate orogenic belt (the Carpathians) and the back-arc basin, which would be the Pannonian basin, formed as a part of the Alpine-Mediterranean orogenic region (Harangi et al., 2005 and references therein).

Pannoniann basin was formed during the Early to Middle Miocene due to the combined effect of the collapse of overthickened crust and slab pull in the retreating subduction zone beneath the Outer Carpathians which was accompanied by widespread volcanic activity (Harangi et al., 2005 and references therein).

Konečny (1995) suggests a close temporal and spatial relationship between silicic magmatism and back-arc extension of the Pannonian Basin.

Most of the volcanic rocks are situated along the Mid-Hungarian Tectonic zone which separates Alpine-Carpathian-Pannonian (ALCAPA) and Tisza-Dacia microplates. Harangi (2001 and references therein) suggested that Early Miocene silicic volcanism could have been the result of strike-slip movements along the southern margin of the ALCAPA and the northern margin of the Tisza-Dacia microplates (Figure 3-1).

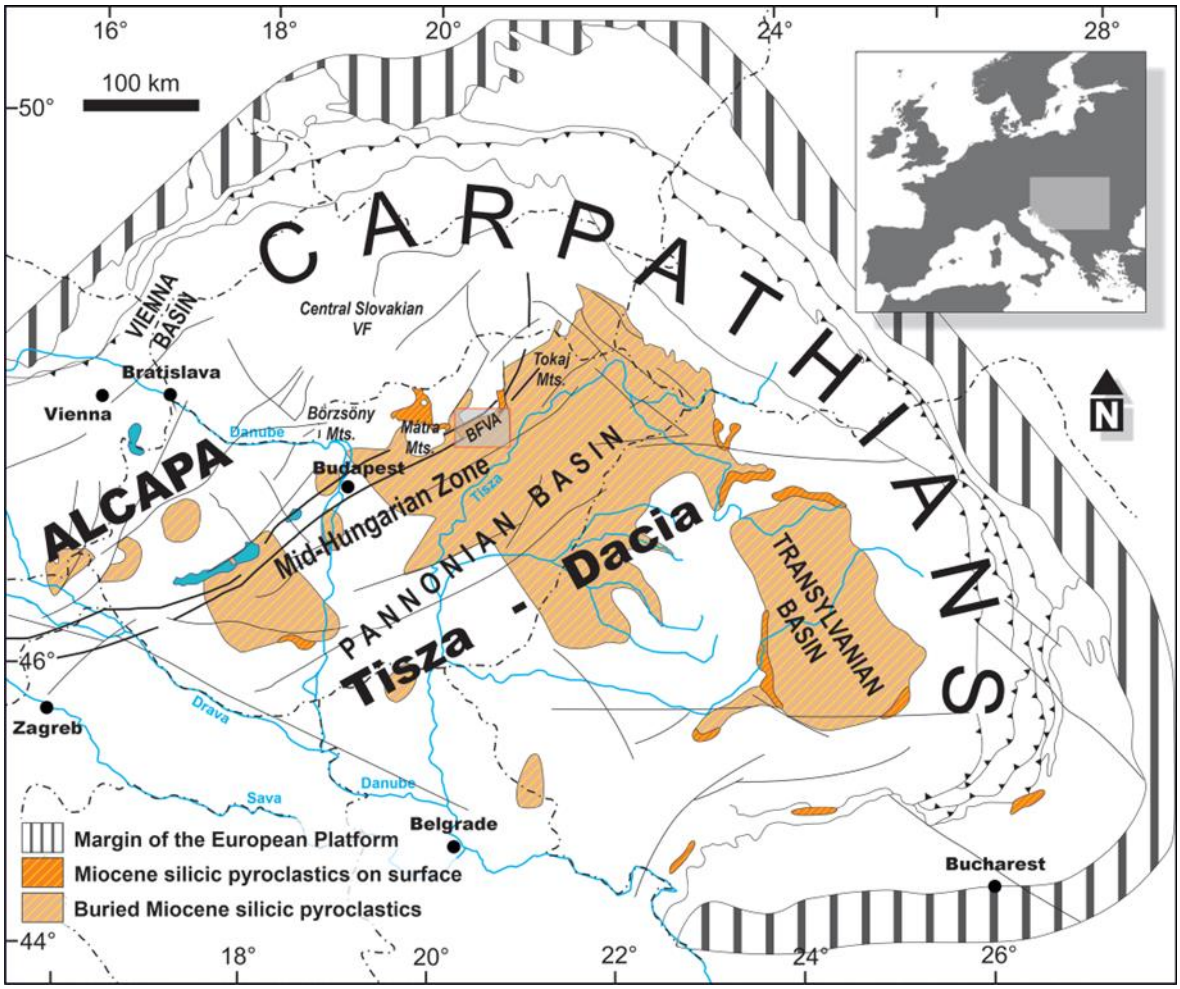

Figure 3-1. Regional geological setting of Bükkalja Volcanic Field (BVFA) and silicic pyroclastic rocks (Hencz et al, 2021).

3.2. Neogene to Quaternary volcanism

The Carpathian-Pannonian region is characterized by various volcanic products which range from strongly undersaturated nephelines through ultrapotassic rocks to high-silica rhyolites (Harangi, 2001).

According to Harangi (2001) above mentioned volcanic rocks can be classified into four groups based on their composition and age:

1). Miocene silicic volcanism

2.) Miocene to Pliocene potassic and ultrapotassic volcanism

3.) Miocene to Quaternary calc-alkaline volcanism

4.) Late Miocene to Quaternary alkaline volcanism

All of the above-mentioned volcanic rocks are abundant all over the Carpathian-Pannonian Region and they can be found in various volcanic fields, e.g. Styrian Basin Volcanic Field, Little Hungarian Plain Volcanic Field, Bakony-Balaton Volcanic Field, Štiavnica-Nógrád-Gömör Volcanic Field, Kecel Volcanic Field, Banat Volcanic Field, and Bükkalja Volcanic Field (Figure 3-2), but they are mostly covered by younger sedimentary formations (Harangi, 2001).

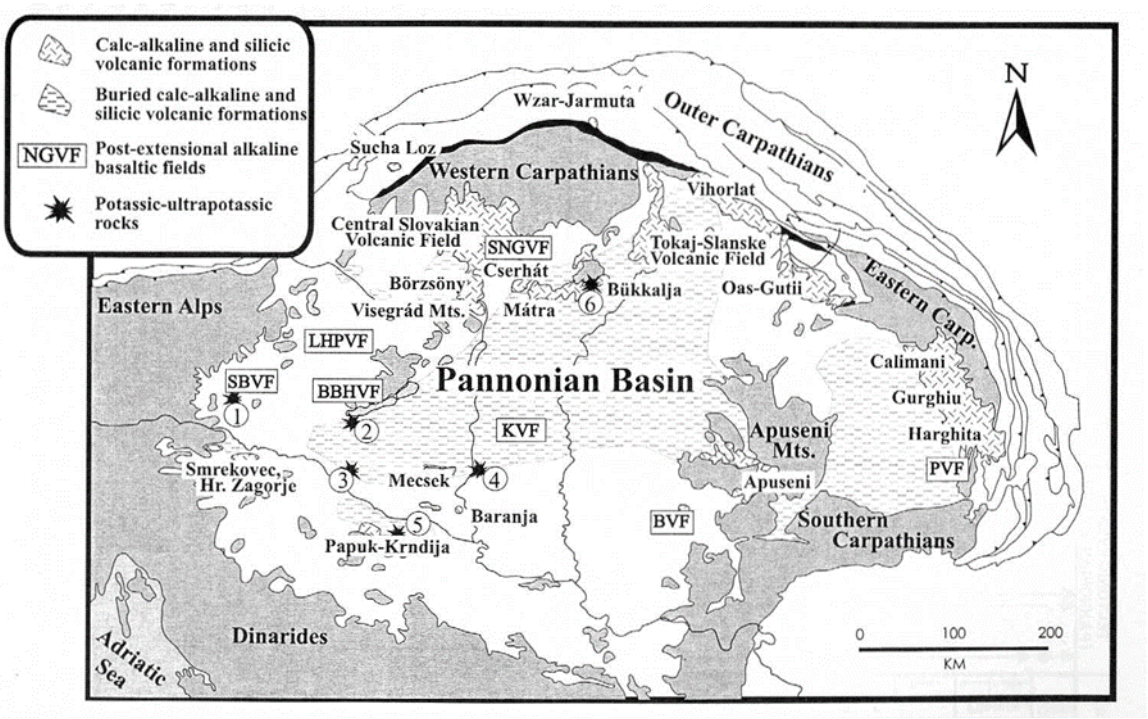

Figure 3-2. Distribution of the Neogene to Quaternary volcanic field in the Carpatian-Pannonian region. SBVF – Styrian Basin Volcanic Field; LHPVF- Little Hungarian Plain Volcanic Field; BBHVF – Bakony-Balaton Highland Volcanic Field; SNGVF - Štiavnica-Nógrád-Gömör Volcanic Field; KVF – Kecel Volcanic Field; BVF – Banat Volcanic Field; PVF – Persany Volcanic Field; 1 – Styrian Basin; 2 – Balatonmária; 3 – Szenta; 4 – Bár; 5 – Krndija Mt; 6 – Bükkalja (Harangi, 2001)

Bükkalja Volcanic Field belong to the Miocene silicic volcanism which is almost exclusively represented by volcaniclastic rocks mostly characterised as block-bearing lapilli tuffs suggesting proximal pyroclastic facies. They often contain less than 10% lithic clasts classified as basaltic andesite and andesite and are both sodic and potassic. Rhyodacite to rhyolitic pumices, rich in potassium, are also common. The strong potassium enrichment indicates a magma mixing process which is a characteristic for the Miocene silicic volcanism (Harangi, 2001 and references therein).

According to Czuppon (2001), the intrusion of andesitic magma into the shallow crustal rhyolitic magma chamber during the Middle Miocene triggered the explosive eruption of the silicic magma from the upper part of the chamber. The explosive eruption was then followed by a dacite-rhyodacite effusive eruption and resulted in the occurrence of rhyolitic pumices and dacitic scoriae in the same pyroclastic deposit.

3.3. Local geological setting and volcanoclastic units of the Bükkalja Volcanic Field

The Bükkalja Volcanic Field (BVF) is located in the Carpathian-Pannonian basin and it belongs to the Neogene volcanic fields of the Pannonian basin (Figure 3-3) (Harangi, 2001; Harangi et al., 2005).

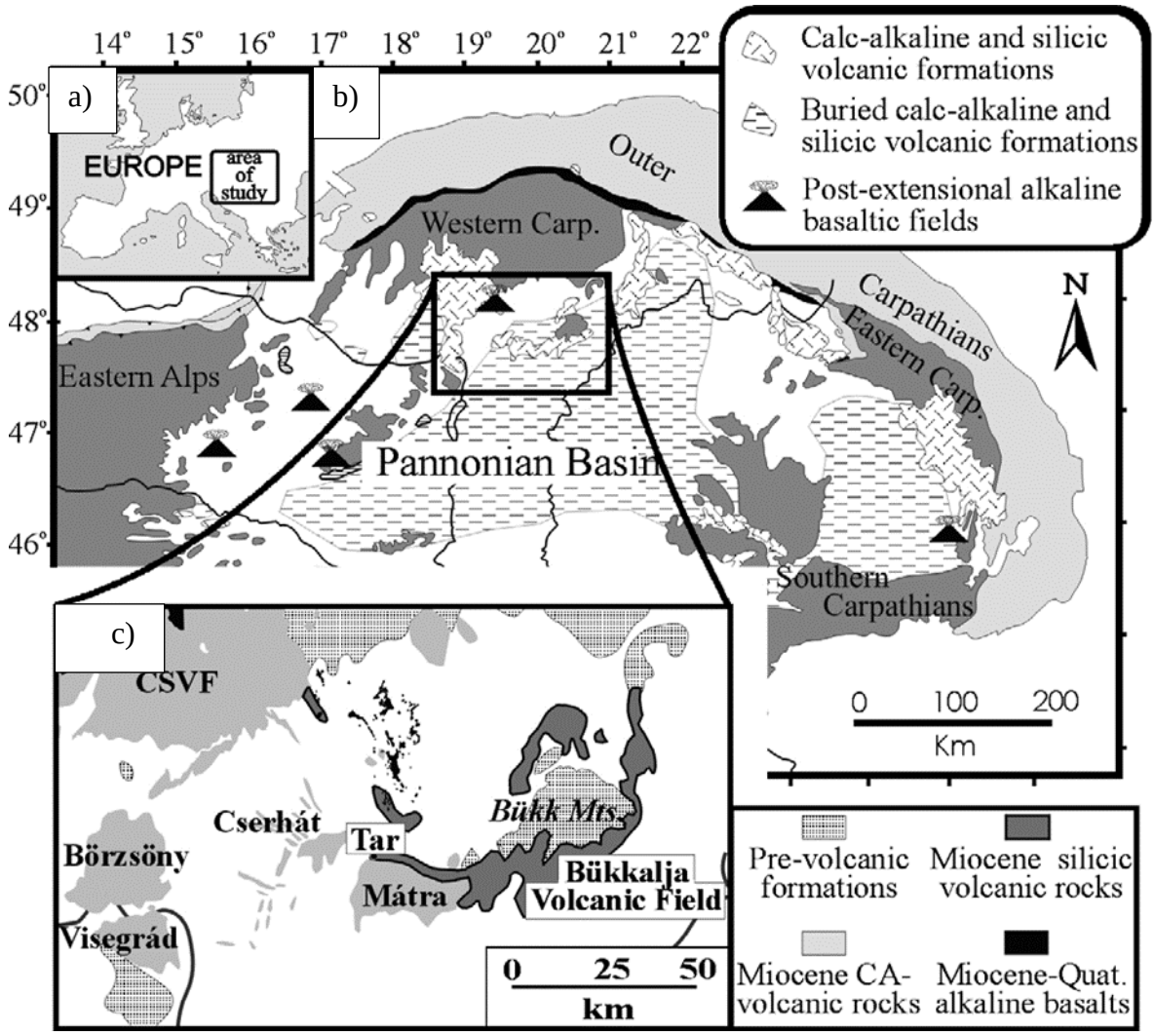

Figure 3-3. 3. Location of the BFV a) in Europe; b) in the Carpathian-Pannonian region; c) in the Northern Hungary ;Carp—Carpathians,CSVF—Central Slovakia. (Harangi et al, 2005).

Locally, according to Hencz et al. (2021), BVF in its current position is located in an inflexion zone between the upward-moving Bükk Mountains and the subsiding Great Hungarian Plain, whereas the Bükk Mountains are mostly consisted of Mesozoic Bükkfennsíki Limestone Formation.

Bükkalja Volcanic Field represents the volcanic products of the Middle Miocene silicic ignimbrite flare-up episode and is cropping out in the largest area. The outcropping rocks are presented by the fresh silicic pyroclastic rocks which show very similar macroscopic features, making them difficult to differentiate on the field (Harangi et al., 2005; Lukács et al., 2005; Harangi and Lenkey, 2007). Extensive silicic volcanic activity was present in the area of BVF from 21 to 13 Ma in 4 separate phases (Lukács et al, 2018). Harangi et al. (2005) state that the Early Miocene volcanic activity, older than 18 Ma is coeval with the formation of the back-arc basin area by lithospheric extension and can therefore be considered as pre-extensional, while younger volcanic activity can be considered syn-extensional. The thickness of Miocene volcanic sequence reaches up to 750m (Szakacs et al., 1998; Harangi et al, 2005), and cover approximately 300 km^2. They are determined as ignimbrite-type pyroclastic flow deposits, locally intercalated with accretionary lapilli-bearing tuffs as the products of phreatomagmatic eruptions. The ignimbrites of the BVF range from un-welded to welded and somewhere are capped with thin pyroclastic fall deposits with locally occurring reworked tephras between major ignimbrite units (Biró et al, 2020 and references therein). According to Lukács et al. (2005) and references therein BVF ignimbrites contain rhyolitic and dacitic pumice and scoria clasts and basaltic andesitic to andesitic lithic clasts. According to Biró (2020) and references therein, quartz, sanidine, plagioclase, biotite, amphibole, and orthopyroxene occur as phenocrystals in most of the described volcanoclastics from Bükkalja Volcanic Field.

Firstly, according to Noszky (1931) and Schréter (1939), BVF was divided into three tuff horizons. Later, pyroclastic complexes were further divided and characterized according to the results of the K/Ar and the paleomagnetic data on which basis three main eruption periods in the BFV can be distinguished; 21.0–18.5, 17.5–16.0 and 14.5–13.5 Ma (Lukacs et al., 2015; Márton and Pécskay, 1998). Considering the paleomagnetic data three main pyroclastic units were distinguished (Figure 3-4): Lower, Middle, and Upper Ignimbrite Units (Harangi, 2005; Martón and Fodor, 1995; Martón and Pecskay, 1998).

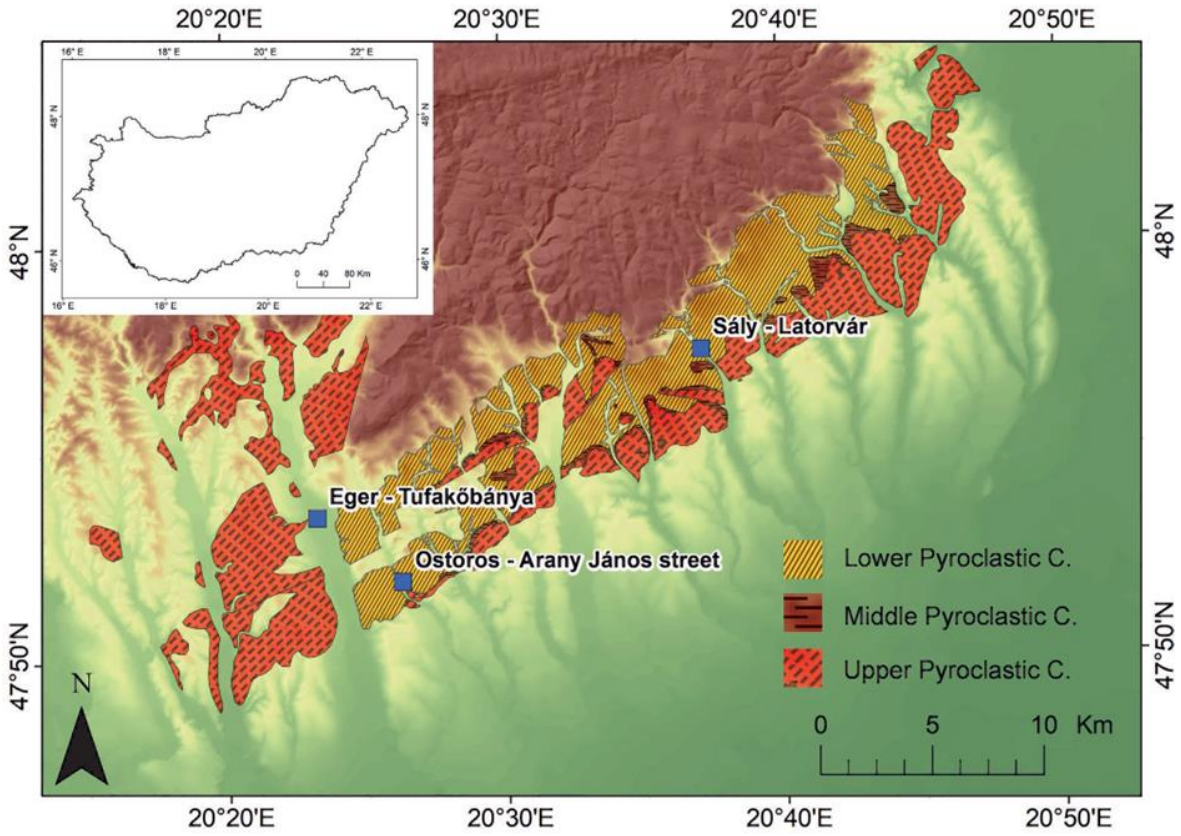

Figure 3-4. Volcanological map of the Bükk Foreland Volcanic Area showing the three main pyroclastic complexes where the Lower unit was dated at 21,0–18.5 Ma, Middle unit at 17.5–16.0 Ma, and Upper unit at 14.5–13.5 Ma (Hencz et al. (2021), based on Szakács et al. (1998))

Non-welded pumiceous pyroclastic flow deposit is the most common facies both in the Lower and Upper Ignimbrite Unit (Harangi et al., 2005). They are defined as poorly sorted block-bearing lapilli tuffs. Pumices contain less than 5% phenocrystals. Quartz, plagioclase, and biotite occur as main phenocrystals in the mentioned pyroclastic flow deposits whereas hornblende and sanidine occur sporadically. Zircon, allanite, and ilmenite are present as accessory minerals. The mentioned pumiceous pyroclastic flow deposits contain around 5-10% lithoclasts which are mostly of igneous origin (basaltic andesite, andesite, and rhyolite). Lithoclasts are composed of plagioclase and orthopyroxene phenocrystals which occur as main minerals, whereas biotite, quartz, hornblende, and clinopyroxene also occur as phenocrystals, but in much smaller amounts. The matrix is mostly composed of glass shards and loose crystals. Welded pyroclastic flow deposits occur both in the Lower and Middle Ignimbrite Unit and are characterized as *fiamme*-bearing lapilli tuffs which occur in various colours such as grey, white, and red. The *fiamme* consists of fresh volcanic glass with

structural remnants of pumice clasts and glass shards. Quartz, plagioclase, and biotite occur as phenocrystals in the Lowe and Middle Ignimbrite Unit, whereas orthopyroxene occurs as phenocrystals only in the Middle Ignimbrite Unit. Allanite and ilmenite occur as accessory minerals in both the Lower and Middle Ignimbrite Unit, whereas zircon is characteristic only for the Lower Ignimbrite Unit. The matrix consist of similar mineral phases as the coarser part of the rock and can occupy up to 50% of the rock. Czuppon et al. (2001) and Harangi et al (2002.) additionally mention the scoria-flow deposits in the Middle Ignimbrite Unit overlying the *fiamme*-bearing pyroclastics. It contains mixed juvenile clasts, dark scoria fragments, and composite clasts. Accretionary lapilli-bearing tuffs can also occasionally be found in the BVF (Harangi et al., 2005). They are described as crystal-poor vitric tuffs containing cuspate and rare loose quartz, plagioclase, biotite, and, rarely, hornblende phenocrystals.

The volcanic activity was dated using the U-Pb method as 18-14 Ma (Lukacs et al., 2015; 2018; Harangi and Lukacs, 2019). Based on the U-Pb data and zircon trace elements composition Lukacs et al (2018) further divided the volcanism into 8 eruption phases as follows: Csv-2 eruption phase (from a borehole) (18.2 ± 0.3 Ma); Eger ignimbrite unit (17.5 ± 0.3 Ma); Mangó ignimbrite unit (17.055 ± 0.024 Ma); Bogács unit (16.816 ± 0.059 Ma); Td-J eruption (16.2 ± 0.3 Ma); Demjén ignimbrite unit (14.880 ± 0.014 Ma); Tibolddaróc unit (14.7 ± 0.2 Ma); and Harsány ignimbrite unit (14.358 ± 0.015 Ma).

In the Figure 3-5. the comparison between the above-mentioned classifications is given.

Márton & Pécskay 1998 (paleomagnetic rotations, K–Ar age)	**Szakács et al. 1998** (field observations and main lithological properties)	**Lukács et al. 2018** (zircon U–Pb age)
Upper Pyroclastic Complex (0°; 13.5–14.5 Ma)	*Upper Tuff Complex* (*UTC*; reworked tephra, phreatomagmatic deposits, non-welded ignimbrites)	*Harsány ignimbrite unit* (14.358±0.015 Ma) *Tibolddaróc unit* (14.7±0.2 Ma) *Demjén ignimbrite unit* (14.880±0.014 Ma)
Middle Pyroclastic Complex (30°; 16–17.5 Ma)	*Upper Middle Tuff Complex* (*UMTC*; obsidian fiamme-rich welded ignimbrites, reddish-dark grey non-welded mixed pumice-scoria ignimbrites, accretionary lapilli-bearing phreatomagmatic deposits) *Lower Middle Tuff Complex* (*LMTC*; welded red ignimbrites, phreatomagmatic deposits)	*Td-J unit* (16.2±0.3 Ma) *Bogács unit* (16.816±0.059 Ma)
Lower Pyroclastic Complex **(80–90°; 18.5–21 Ma)**	***Upper Lower Tuff Complex* (*ULTC*; reworked tuffs, pumice fall deposits, phreatomagmatic fall deposits, non-welded ignimbrites, welded ignimbrites)** *Lower Lower Tuff Complex* (*LLTC*; non-welded ignimbrites, interbedded in red conglomerates)	***Mangó ignimbrite unit* (17.055±0.024 Ma)** *Eger ignimbrite unit* (17.5±0.3 Ma) *Csv-2 unit* (18.2±0.3 Ma)

Figure 3-5. Stratigraphic subdivision of the BFV succession in former studies; units mentioned in this Master thesis are underlined in yellow (from Hencz et al., 2021)

According to Brlek et al. (2023) and Lukács (personal communication, 19th October 2022) Csv-2 Unit is coeval with the Mts. Kalnik and Požeška gora volcanoclastites, therefore the name Wind-Kalnik Unit can be used.

3.4. Kuchyna Tuff

According to Rybar et al. (2019), Kuchyna tuff is a product of felsic volcanism found on the Eastern margin of the Vianna Basin (Western Carpathian Mountain Range), as shown in Figure 3-6.. It is dated at 15 Ma using the $^{40}Ar/^{39}Ar$ method on sanidine together with the paleobotanic data due to the fact that Kuchyna tuff contains fossil leaf prints (Fordinal et al, 2010).

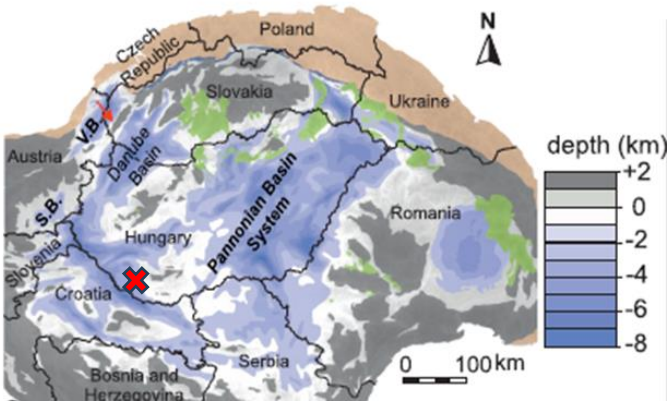

Figure 3-6. Location of the Vienna Basin within the Pannonian Basin; Kiszbeszterce (marked with X) – Kuchyna tuff locality in Hungary (Rybar et al., 2019).

The total thickness of the Kuchyan tuff layer is estimated at 30 cm (Fordinal et al., 2010). It is determined as fine-grain tuff with vitroclasts and phenocrystals of quartz, plagioclase, biotite, and orthopyroxene as main minerals, while apatite, ilmenite, and titanomagnetite are found as accessory minerals in clay matrix (Šimon et al., 2009).

According to the U-Pb data deposition of the Kuchyna tuff is coeval with the Demjén Ignimbrite Unit from the Bükkalja Volcanic Field and they show similar mineralogical composition. The difference is that Kuchyna tuff shows an Eu anomaly of 0.59 whereas tuffs from Demjén Ignimbrite Unit has no pronounced Eu anomaly which makes this correlation questionable (Lukács et al., 2018; Rybar et al., 2019).

4. MATERIALS AND METHODS

For the purpose of this study, 11 samples from different Miocene Ignimbrite Units from the Bükkalja Volcanic Field were analysed, alongside one Kuchyna tuff sample from Kiszbezterce.The list of analysed samples with their classification and associated pyroclastic units is given in Table 1, according to Lukács (personal communication, 19th October 2022). Macroscopically, all of the samples look similar. They are white and powdery, almost without any visible minerals except an occasional black biotite which can range in size up to a maximum of 2 milimetres.

Table 4-1. List of analysed samples (Lukács, personal communication, 19th October 2022)

Sample	macroscopic identification	unit
EG-HOM-1	lapilli tuff	Wind-Kalnik unit
EG-HOM-1	lapilli tuff	
EG-1	lapilli tuff	Eger unit
Cskly-1f	accretionary lapilli bearing tuff	Mangó unit
EG-2	lapilli tuff	
Dem-9_E/6	lapilli tuff	Demjén unit
Dem-30	lapilli tuff	
KMJ-01	fine tuff	
KMJ-02	medium tuff	
Hh-01	fine tuff	
Td-A	pumice clasts	Harsány unit
KISBESZ	tuff with plant prints	Kuchyna tuff sample

All 12 samples were analysed using polarisation microscopy, x-ray fluorescence, x-ray diffraction, atomic absorption spectrometry, and atomic emission spectrometry (Fig. 4-1). Polarised light microscopy and X-ray diffraction were used to determine the mineral composition of the samples, while X-ray fluorescence was used to determine the bulk chemical composition. As shown in figure 5-1. one-quarter of the samples were milled to the size of fine powder and used for XRF and XRD analyses, while three-quarters of the crushed samples were then sieved through 2 mm, 1mm, 500 μm, 250 μm, and 125 μm sized sieves and separated to extract biotite for further analysis. The separation was done using the magnetic separation for fractions smaller than 125 μm, between 125-250 μm, and 250-500

μm. The hand selection method was used for fractions between 500 μm-1mm, 1-2 mm, and coarser than 2 mm. For each sample, magnetic and non-magnetic fractions were obtained, with the magnetic fraction consisting mainly of biotite and sporadically, hornblende. Atomic absorption spectrometry was used for the determination of lithium concentration in individual fractions, while atomic emission spectrometry was used for the determination of boron concentration in individual fractions.

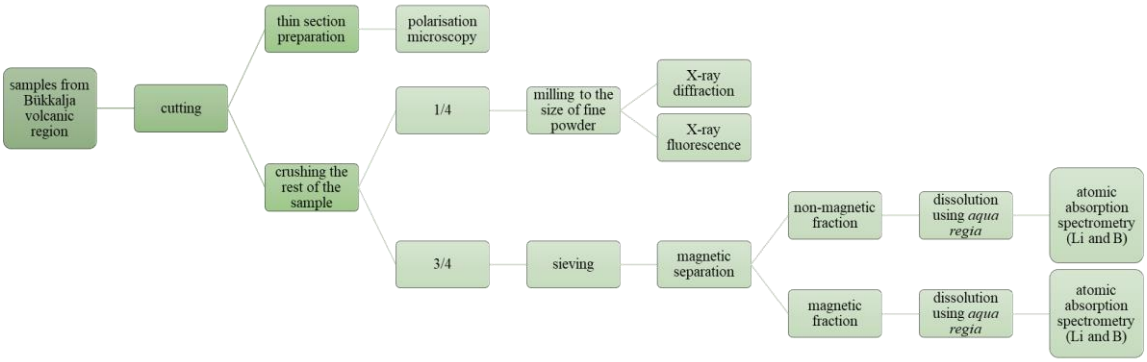

Figure 4-1. Sample handling scheme

Polarisation microscopy, XRF, XRD, magnetic separation, AAS, and AES analyses were conducted in the Department of Mineralogy, Petrology and Mineral Resources at the Faculty of Mining, Geology and Petroleum Engineering, University of Zagreb.

4.1. Polarisation microscopy

Polarized light microscopy is a fundamental method for determining the mineral composition, paragenesis, grain size, and classification of certain rocks. It is based on the fact that each mineral has unique optical properties that can be used for its determination.

To prepare thin sections, first the rocks are cut with a diamond saw and then their dimensions are adjusted to fit on the covering glass. After the desired thickness of 30 μm is achieved, the thin section is bonded with Canadian balsam (refractive index n=1,537).

Microphotographs were taken using an OPTIKA B-1000 microscope with 5x, 10x, and 20x magnification, OPTIKA C-P6 FL camera, and OPTIKA ProView software.

4.2. X-ray fluorescence

X-ray fluorescence (XRF) is a non-destructive analytical method used for determining the elemental composition of materials. It is based on the detection of secondary X-rays emitted by the analysed sample when excited by an external primary X-ray source.

For the purpose of this research, the Hitachi X-MET8000 Expert Geo portable XRF was used. Each measurement lasted 40 seconds and was repeated 5 times for each sample. The results are reported in ppm.

4.3. X-ray diffraction

X-ray diffraction (XRD) is a fast and non-destructive analytical method for determination the mineral composition of rocks. X-rays are electromagnetic waves with a wavelength of 10^{-10} m which equals 1Å. When an X-ray beam hits the sample it is diffracted and by applying Bragg's law the distances between the planes of the atoms in the crystal can be calculated:

$$n\lambda = 2d\sin\theta \qquad (4\text{-}1)$$

where n is the order of the diffracted beam, λ is the wavelength of the incident X-ray beam, d is the distance between adjacent atoms and θ is the angle of incidence of the X-ray beam.

Spacings generated in the XRD scan are characteristic of each mineral and are therefore used to determine the mineralogical composition of the analysed samples.

A Malvern PanAnalytical vertical X–ray goniometer (type X'Pert MPD) equipped with a Cu tube and a graphite crystal monochromator was used. Porfex software was applied for crystalline phase quantification. The calculation algorithm first reads the structural information of all the present mineral phases and calculates their peak position from the cell parameters and space group, which is followed by the calculations of structure factors from atomic sites and converting them into intensities. Then obtained peaks are fitted to the observed peaks. The relative weight fraction of certain crystalline phases is then calculated using the formula:

$$W_a = \frac{S_a x (ZxMxV)_a}{\sum S_i x (ZxMxV)_i} \quad (4\text{-}2)$$

Where *W* is the relative weight fraction; *S* is the Rietveld scale factor*; Z* is the number of formula units per unit cell; *M* is the mass of the formula unit; *V* is the volume of the unit cell; *a* is the crystalline phase which weight fraction is being calculated and *i* is the sample (Döbelin, 2020).

4.4. Magnetic separation

Magnetic separation is based on the way the force of the magnetic field acts on mineral particles that have different magnetic susceptibility. The used Frantz isodynamic magnetic separator consists of two electromagnets with two specially designed different magnetic fields. Between them is a gap in which a vibrating groove is inserted. Both the groove and the electromagnets can be inclined. Mineral particles are poured through a funnel and are then impacted by both the magnetic force and gravity causing them to separate based on their magnetic properties. The standard conditions for magnetic separation are shown in Figure 5-2.

For the purpose of this paper, it was necessary to extract biotite, therefore magnetic separation was performed using current of 0,8 A and 20° incline. Fractions <125, from 125 to 250, and from 250 to 500 µm were separated, whereas biotite grains were handpicked from the larger fractions.

Sample KMJ-01 wasn't separated because polarisation microscopy didn't reveal any ferromagnesium minerals.

4.5. Atomic absorption spectrometry and atomic emission spectrometry

Atomic absorption spectrometry is based on the absorption of visible or ultraviolet light with wavelengths from 190 to 680. The source of eradiation is usually a hollow cathode lamp. The anode of the lamp is made out of tungsten and the cathode is made out of the element that needs to be detected, in this case lithium. For the boron measurement, the emission method was used, so the lamp was not needed.

The sample solution prepared in the laboratory enters the instrument through a thin tube and turns into an aerosol, which then mixes with acetylene gas and ignites. This allows the electromagnetic rays to pass through the sample in the flame where absorption occurs.

Atomic emission spectrometry is based on the emission of outer electrons into higher energy levels. Those emitted electrons emit radiation whose wavelengths are characteristic of each element.

The magnetic and non-magnetic fractions of all samples except KMJ-01, which was analysed in bulk, were analysed for lithium and boron, where AAS was used for lithium and AES for the determination of boron concentrations.

Measurements were performed using the Perkin Elmer Analyst 700.

4.5.1. Sample preparation

First, the samples had to be dissolved using *aqua reggia* which is a 1:3 solution of HCl and HNO_3. On average 0,5 grams of samples were dissolved in 10 ml of *aqua reggia*, then, a solution of 1% HNO_3 was added to the 20 ml mark. For the non-magnetic fractions, the 125-250 µm fractions were used. Biotite from all size fractions was used for measurements of the magnetic fractions.

For sample KMJ-01 both the 125-250 and 250-500 µm fractions were used.

Furthermore, lithium contents of non-magnetic <125 µm fractions were analysed from all samples; along with the <125 µm fraction of the KMJ-01 sample. For this purpose, 1 g of every sample was dissolved, and samples were prepared as previously described.

Calibration solutions were prepared prior to the measurement procedure. Lithium standard solutions were prepared at concentrations of 0,1, 0,25, 0,50, 0,75, 1, 1,5 and 2 ppm with the addition of caesium chloride as an ionisation buffer. Boron standard solutions were prepared at concentrations of 50, 100, 150, 200, 250 and 400 ppm.

Alongside samples and standards, 6 BLANK solutions of *aqua reggia* were also prepared.

For the boron measurements of the samples from non-magnetic fractions and sample KMJ-01, the standard addition method was used. Also, the magnetic fraction of the sample EG-2 and KMJ-02 were diluted because the first results were above the calibration limit where 2 ml of sample was diluted with 2 ml of 1% HNO_3.

5. RESULTS

5.1. Polarisation microscopy

Mineral compositions acquired by the method of polarisation microscopy of all samples are given in Table 5-1. Samples are further categorized according to the percentages of crystalloclasts, vitroclasts, and lithoclasts.

Table 5-1. Mineral composition according to the results of polarisation microscopy.

sample	EG-HOM-1	EG-HOM-2	EG-1	Cskly-1f	EG-2	Dem-9_E/6	Dem-30	KMJ-01	KMJ-02	Hh-01	Td-A	KISBESZ
unit	Wind-Kalnik unit		Eger unit	Mangó unit		Demjén unit					Harsány unit	Kuchyna tuff sample
Quartz	+	+	+	+	+	+	+	+	+	+	+	+
Plagioclase	+	+	+	+	+	+	+	+	+	+	+	+
Sanidine	+	+			+	+	+		+			+
Biotite	+	+	+	+	+	+	+	+	+	+	+	+
Hornblende	+				+	+	+				+	+
white mica (Ms)	+	+				+	+	+	+			+
Apatite			+		+	+			+			
Zircon					+							
opaque mineral	+			+	+	+	+		+	+		+
Calcite									+			
Chlorite		+	+	+	+	+	+					+
Hematite						+	+		+			
Limonite												
Sericite											+	
Clay minerals	+	+	+	+	+	+	+	+	+	+	+	+
Volcanic Glass	+	+	+	+	+	+	+		+	+	+	+
Lithoclasts	+	+	+	+	+	+		+	+	+		+

5.1.1. Wind-Kalnik unit

Samples EG-HOM-1 and EG-HOM-2 belong to the Wind-Kalnik unit. Quartz, plagioclase, sanidine, biotite and hornblende (sample EG-HOM-1) appear as crystalloclasts, whereas opaque minerals (sample EG-HOM-1), chlorite (sample EG-HOM-2) and clay minerals appear as their alteration products. White mica appears as accessory mineral phase occupying less than 1% of the samples.

Quartz appears in both samples as colourless, anhedral mineral grains. Its dimensions vary from 0,55×0,35 mm to 0,04×0,02 mm. It's characterised by undulose extinction and grey interference colour of 1st order. Some of the grains in sample EG-HOM-1 show jigsaw-fit texture and rounded habit, often with oval cavities characteristic of pyroclastic quartz. It occupies around 10% of each sample.

Plagioclase appears in both samples as colourless, subhedral 4-sided mineral grains. Its dimensions vary from 0,85×0,75 mm to 0,15×0,1 mm. It is characterised by the grey interference colour of 1st order and polysynthetic twinning lamellae as well as zoning. Some of the grains are cracked and moderately to heavily altered into clay minerals. Few grains in the sample EG-HOM-2 show jigsaw-fit texture (Figure 5-1. a; b). It occupies around 10% of each sample.

Sanidine appears in both samples as colourless, subhedral to anhedral mineral grains. Its dimensions vary from 0,7×0,45 mm to 0,1×0,1 mm. It is characterised by grey interference colour of 1st order. Most of the grains are moderately cracked and show moderate alteration into clay minerals. It occupies less than 5% of each sample.

Biotite appears in both samples as subhedral, elongated 4-sided grains which show pleochroism in the shades of brown colour. Its dimensions vary from 1,2×0,15 mm to 0,4×0,02 mm. Mineral grains are mostly fresh, in the sample EG-HOM-1 some show very light opacitization, whereas, in the sample EG-HOM-2, some show light to moderate chloritization with some biotite grains being completely green. It occupies 10-15% of each sample.

Hornblende appears in the sample EG-HOM-1 as subhedral to euhedral grains with an average size of 0,2×0,15 mm. It shows pleochroism in the shades of brown and green to greenish-yellow interference colours of 2nd order. Most of the grains are heavily cracked and disintegrated. It occupies less than 1% of the sample.

White mica appears in both samples as colourless, subhedral, 4-sided grains that show pseudoabsorption. Its dimensions vary from 0,12×0,06 mm to 0,08×0,02 mm. It shows various interference colours of 2nd order. It occupies less than 1% of each sample.

Opaque minerals appear in the sample EG-HOM-1 as a product of biotite alteration. It occupies less than 1% of the sample.

Chlorite appears in the sample EG-HOM-2 as a product of biotite alteration. It is green in colour. It occupies around 2% of the sample.

Clay minerals appear in both samples, both as the product of feldspar alteration and in the matrix. They occupy around 10% of the sample.

Lithoclasts appear in both samples. They vary in size from 1,9×1,25 mm to 0,9×0,6 mm. Some of them are heavily altered into sericite and clay minerals and they can be possibly determined as rhyolite (Figure 5-1. c;d). Lithoclasts occupy around 10% of each sample.

Volcanic glass appears in the matrix and as vitroclastic components, which are pumice fragments and glass shards. Pumice fragments consist mostly of non-devitrified volcanic glass and are exhibit holohyaline texture. Additionally, bubble-wall shards, as a pumice fragments, are present in both samples. Volcanic glass is present as devitrified and non-devitrified volcanic glass, where devitrified volcanic glass shows its characteristic Y to irregular shape (Fig 5-1. c). In the sample EG-HOM-1 dark, flattened, glassy clasts which can be categorized as *fiamme* appear. Volcanic glass altogether occupies around 40% of the sample.

Matrix is composed mostly of fine ash particles altered into clay minerals. Among the fine ash, both devitrified and non-devitrified shards can be seen. It occupies around 10% of the samples.

Fluid inclusions are present in quartz and feldspars in both samples.

Samples from the Wind-Kalnik Unit are determined as **ignimbrite deposits dominated by vitroclastic and crystalloclastic particles**.

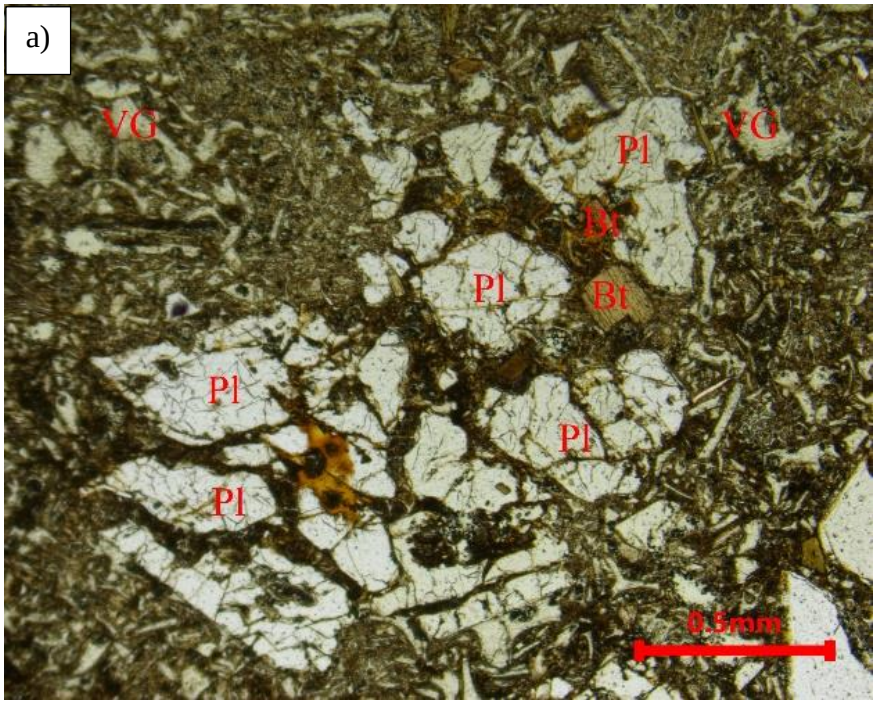

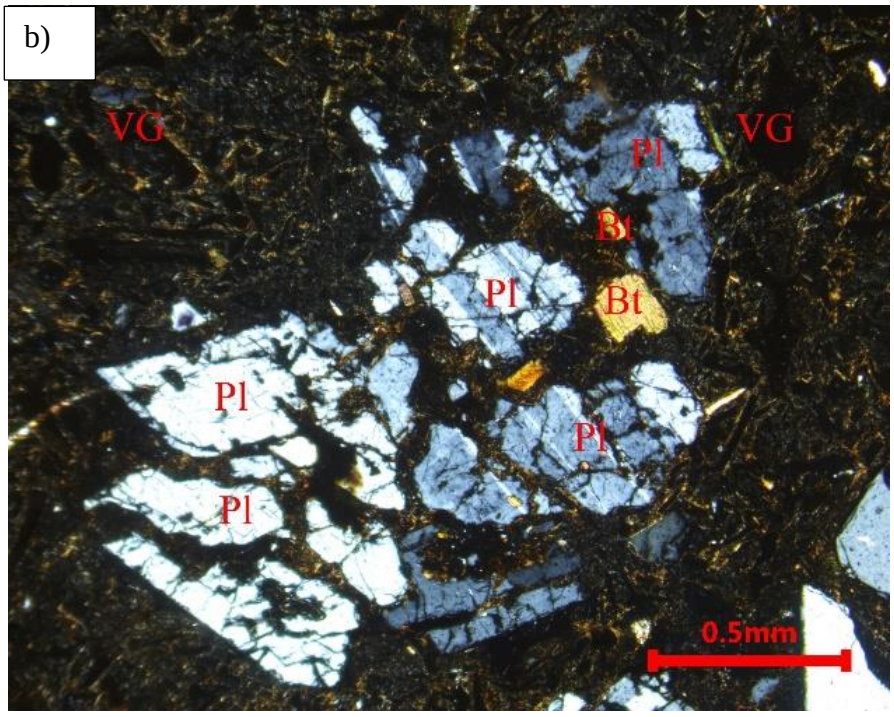

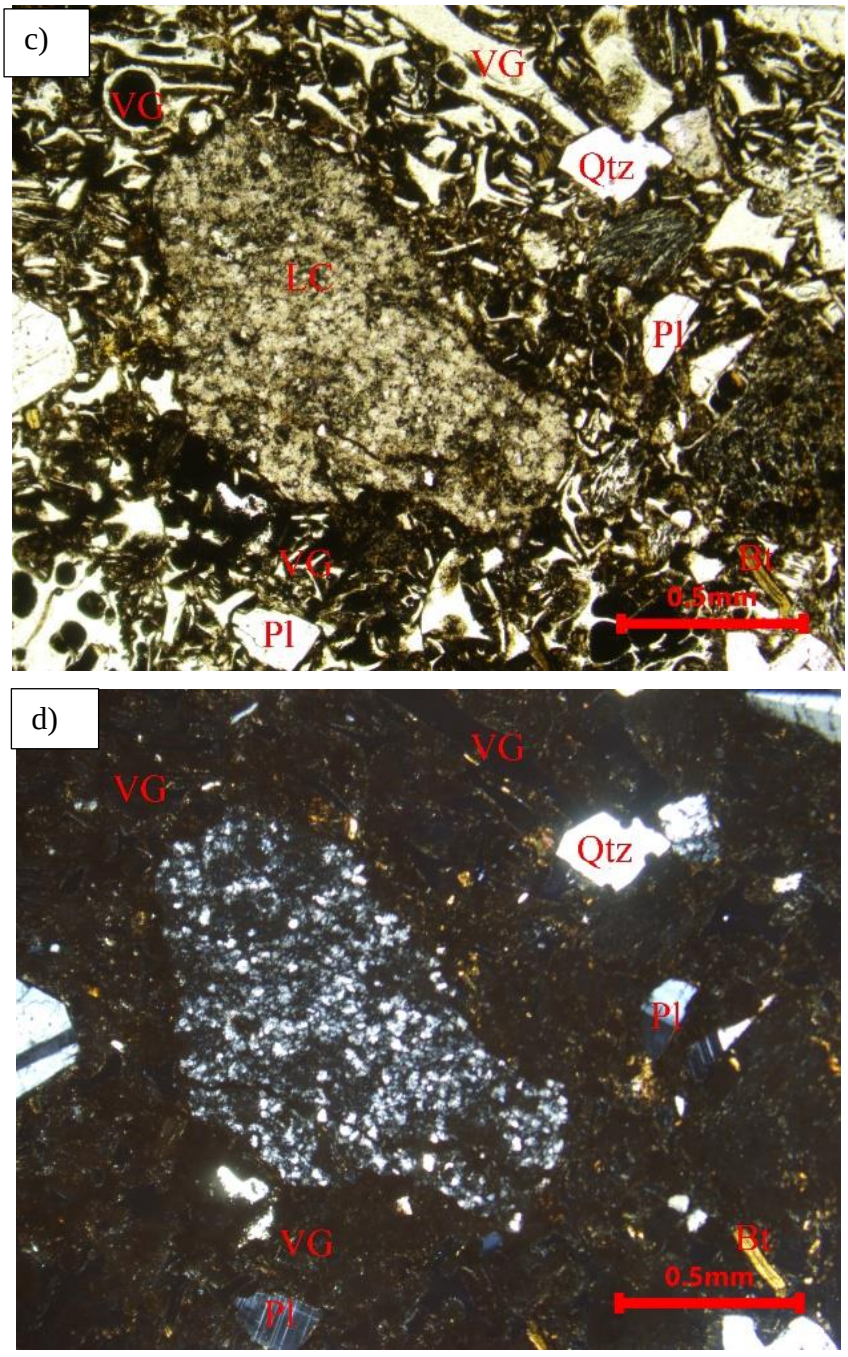

Figure 5-1. a) Jigsaw-fit texture in Plagioclase in sample thhe EG-HOM-2; b) Jigsaw-fit texture in plagioclase in the sample EG-HOM-2, N+; c) Volcanic glass and lithoclast in the sample EG-HOM-1; d) Volcanic glass and lithoclast in sample the EG-HOM-1, N+

The average mineral composition alongside volcanic glass and lithoclast distribution of samples from the Wind-Kalnik unit is presented in Figure 5-2.

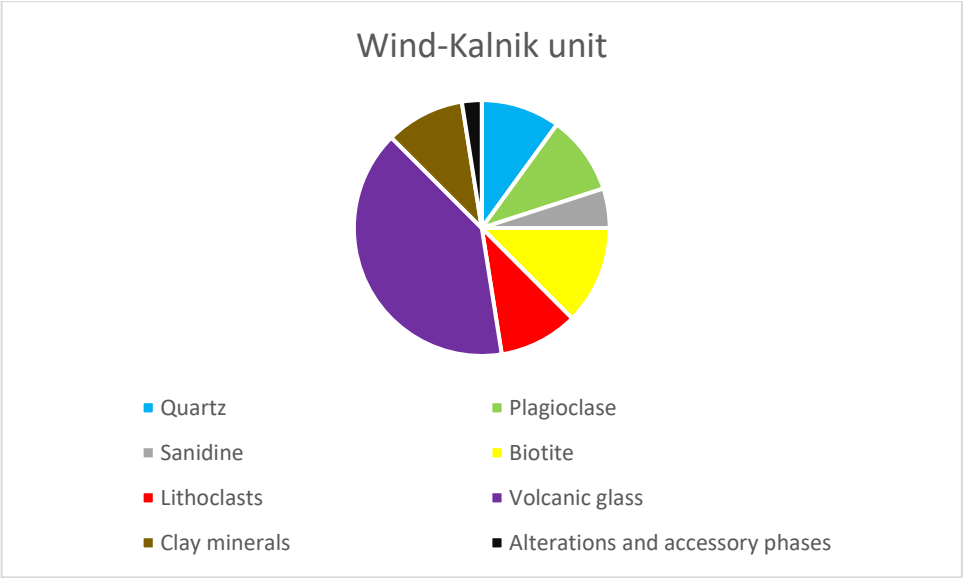

Figure 5-2. Average mineral, lithoclast, and volcanic glass distribution in samples from the Wind-Kalnik unit.

5.1.2. Eger unit

Sample EG-1 belongs to the Eger unit. In this sample, quartz, plagioclase and biotite and appear as crystalloclasts, whereas chlorite and clay minerals appear as their alterations. Apatite appears as an accessory mineral phase occupying less than 1% of the sample.

Quartz appears as colourless, anhedral mineral grains. Its dimensions vary from 1,34×0,45 mm to 0,1×0,06 mm. It's characterised by undulose extinction and grey interference colour of 1st order. Some of the grains exhibit round habit characteristic for pyroclastic quartz. It occupies around 10% of the sample.

Plagioclase appears as colourless, subhedral 4-sided mineral grains. Its dimensions vary from 0,75×0,45 mm to 0,1×0,04 mm. It is characterised by grey interference colour of 1st order and polysynthetic twinning lamellae as well as zoning. Some of the grains are cracked, disintegrated and moderately to heavily altered into clay minerals. Few grains show jigsaw-fit texture. It occupies around 15% of the sample.

Biotite appears as subhedral, elongated 4-sided grains which show pleochroism either in the shades of brown or yellow to yellowish-brow. Its dimensions vary from 1,35×0,7 mm to 0,15×0,15 mm. Grains show moderate chloritization, exhibiting green colour. It occupies less than 10% of the sample.

Apatite appears as subhedral, elongated, and slightly rounded, colourless mineral grains with high relief. The average size of mineral grains is 0,14×0,1 mm and sometimes it can be found as an inclusion in biotite (Figure 5-3 a, b). It occupies less than 1% of the sample.

Chlorite appears as a product of biotite alteration. It is green in colour. It occupies around 5% of the sample.

Clay minerals appear both as the product of plagioclase alteration and in the matrix. They occupy around 10% of the sample.

Lithoclasts vary in size from 2,1×0,65 mm to 0,65×0,45 mm. One type of lithoclast consists of mostly alkali feldspars and quartz, although most of them are heavily altered into clay minerals and sericite. According to the mineral composition of the fresh lithoclasts, they can possibly be defined as rhyolite. Lithoclasts altogether occupy around 30% of the sample.

Volcanic glass appears in the matrix and as vitroclastic components, which are pumice fragments and glass shards. Pumice fragments consist mostly of non-devitrified volcanic glass and are exhibit holohyaline texture. Additionally, bubble-wall shards (Figure 5-3.c), as a pumice fragments, are present in the sample from this unit. Volcanic glass is present as devitrified and non-devitrified volcanic glass, where devitrified volcanic glass shows its characteristic Y to irregular shape. Additionally, dark, flattened clasts which can be categorized as *fiamme* appear. Volcanic glass altogether occupies 40% of the sample.

Matrix is composed mostly of altered fine sized ash clasts. These clasts are altered to clay minerals, Among the altered particles tiny particles of both devitrified and non-devitrified volcanic glass are observed. Matrix occupies approximately 15% of the whole sample.

According to the ratios of crystalloclasts, vitroclasts, and lithoclasts this sample can be determined as **crystalo- to lithoclastic tuff**.

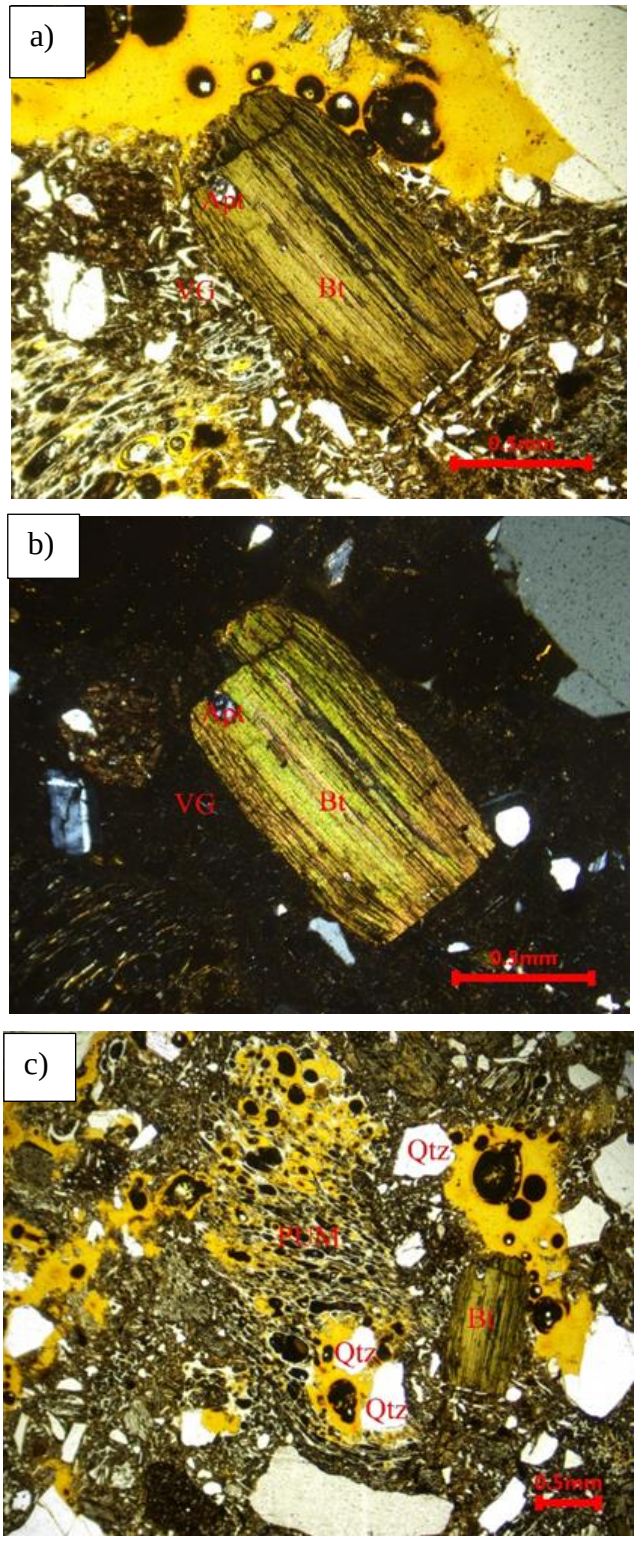

Figure 5-3. a) Apatite as an inclusion in biotite in the sample EG-1, N; b) Apatite as an inclusion in biotite in the sample EG-1, N+; c) Pumice lithoclast in the sample EG-1, N.

Mineral, lithoclastic, and volcanic glass distribution of the Eger unit based on the sample EG-1 is given in Figure 5-4.

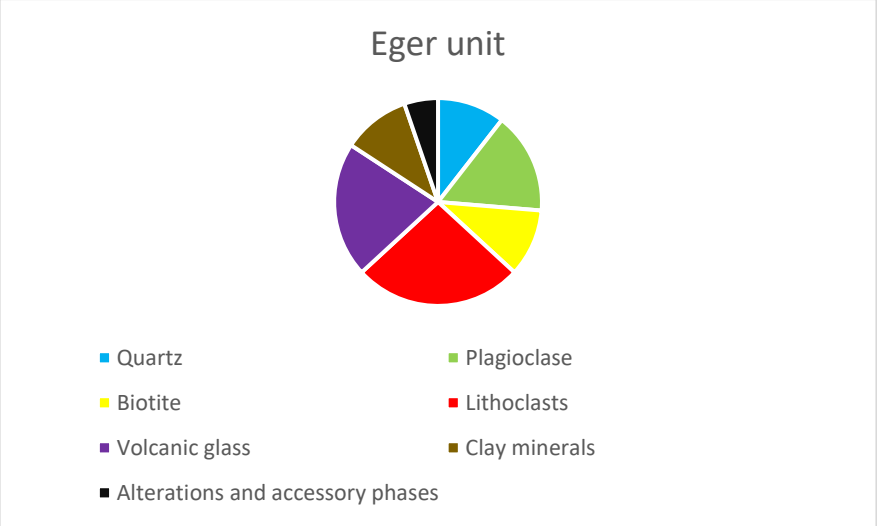

Figure 5-4. . Minerals, lithoclasts, and volcanic glass distribution in the sample from the Eger unit.

5.1.3. Mangó unit

Sample Cskly-1f and EG-2 belong to the Mangó unit. Quartz, plagioclase, sanidine (sample EG-2), biotite and hornblende (sample EG-2) appear as crystalloclasts whereas chlorite, opaque minerals, limonite, and clay minerals appear as their alterations. Apatite (sample EG-2) and zircon (EG-2) appear as accessory mineral phases occupying less than 1% of the sample EG-2.

Quartz appears in both samples as colourless, anhedral mineral grains. Its dimensions vary from 0.7x0.4 mm to 0.08x0.06 mm. It's characterised by undulose extinction and grey interference colour of 1st order. Some of the grains in the sample EG-2 show jigsaw-fit texture and rounded habit characteristic for pyroclastic quartz. It occupies less than 10% of samples.

Plagioclase appears in both samples as colourless, subhedral 4-sided mineral grains. Its dimensions vary from 2,4x2,25 mm to 0,6x0,14 mm. It is characterised by the grey interference colour of 1st order and polysynthetic twinning lamellae as well as zoning. Some of the grains are cracked and lightly to moderately altered into clay minerals. Few grains in the sample Cskly-1f show jigsaw-fit texture. It occupies around 10-15% of samples.

Sanidine appears in the sample EG-2 as colourless, subhedral mineral grains. Its dimensions vary from 0,9x0,5 mm to 0,04x0,02 mm. It is characterised by the grey

interference colour of 1st order. Most of the grains are moderately cracked and show moderate to heavy alteration into clay minerals. It occupies less than 5% of the sample.

Biotite appears in both samples as subhedral, elongated 4-sided grains. Its dimensions vary from 1,8x0,4 mm to 0,6x0,15 mm (Figure 5-5 c; d). Due to heavy chloritizations, most grains show pleochroism in shades of green. Biotite in both samples also shows moderate opacitization, where opaque minerals are formed around the edges and along the cleavage planes. It occupies around 5% of each sample.

Hornblende appears in the sample EG-2 as 6-sided, euhedral grains which exhibit pleochroism in the shades of brown. Its dimensions vary in size from 0,6x0,45 mm to 0,3x0,06 mm in size. It is moderately to heavily chloritized and disintegrated. It occupies less than 5% of the sample.

Apatite appears in the sample EG-2 as a subhedral, elongated colourless grain with high relief. Its dimensions vary from 0,1x0,06 mm to 0,03x0,01 mm. Sometimes it occurs as an inclusion in biotite. It occupies less than 1% of the sample.

Zircon appears in the sample EG-2 as a subhedral, elongated colourless grain with high relief. The average size of mineral grains is 0,06x0,04 mm. It exhibits various interference colours of 3rd order. It occupies less than 1% of the sample.

Chlorite appears as a product of biotite and hornblende alteration (sample EG-2). It is green in colour. It occupies around 5% of the sample.

Opaque minerals appear in both samples as a product of biotite alteration. Some parts of opaque minerals show limonitization. They occupy less than 1% of the sample.

Limonite appears in both samples as a light brown to orange amorphous mass around opaque minerals as a product of their alteration. It occupies less than 1% of the sample.

Clay minerals appear in both samples, both as the alteration of feldspars and in the matrix. They occupy around 15% of the sample.

Lithoclasts appear in both samples. They vary in size from 10x4 mm to 0,45x0,2 mm and mostly correspond to andesite. They occupy 20-30% of the samples.

Volcanic glass appears in the matrix and as vitroclastic components, which are pumice fragments and glass shards. Pumice fragments consist mostly of non-devitrified volcanic glass and are exhibit holohyaline texture. Additionally, bubble-wall shards occur in the sample EG-2, as a pumice fragments, are present in the sample from this unit. Volcanic glass is present as devitrified and non-devitrified volcanic glass, where devitrified volcanic glass shows its characteristic Y to irregular shape (Figure 5-5. a). Additionally, dark, flattened clasts which can be categorized as *fiamme* appear in both samples. Volcanic glass altogether occupies 20% of the samples.

Matrix is composed mostly of fine ash altered to clay minerals and tiny particles of both devitrified and non-devitrified volcanic glass. The matrix is light brown. It occupies approximately 15% of the samples.

Accretionary lapilli seen in the sample Cskly-1f are spherical in shape and occupy less than 5% of the sample. They are composed of fine ash sized shards altered to clay minerals and fine ash fragments of devitrified volcanic glass.(Fig 5-5. b).

According to the partially welded structure, the aforementioned samples can be determined as **ignimbrite deposits dominated by lithoclsastic and crystalloclastic particles**.

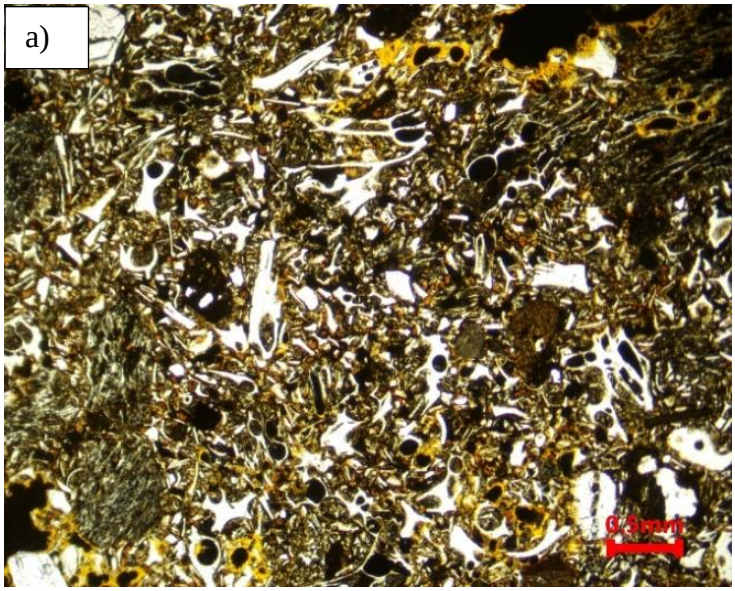

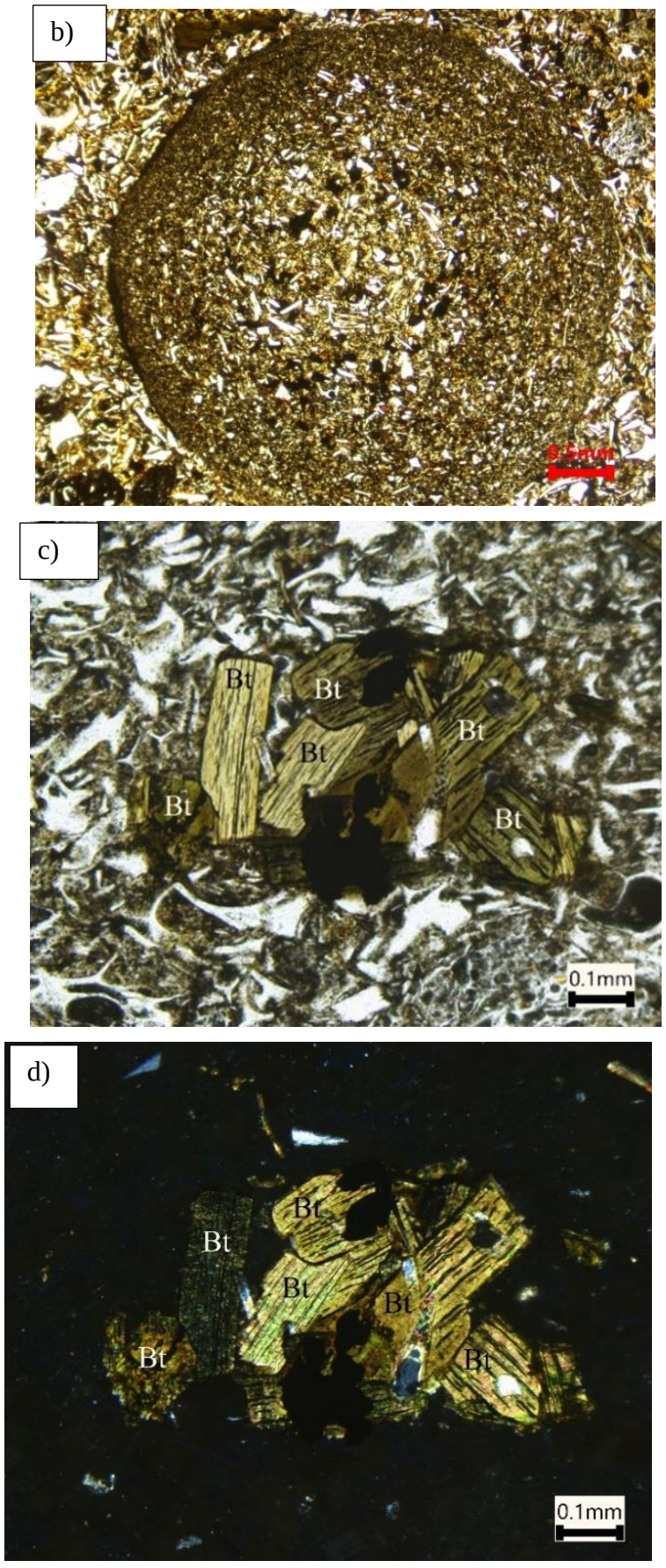

Figure 5-5. a) Volcanic glass shards in the sample Cskly-1f, N; b) Lapili in the sample Cskly-1f, N; c) Biotite in the sample EG-2, N; d) Biotite in the sample EG-2, N+.

The average mineral composition alongside volcanic glass and lithoclast distribution of samples from the Mangó unit is presented in Figure 5-6.

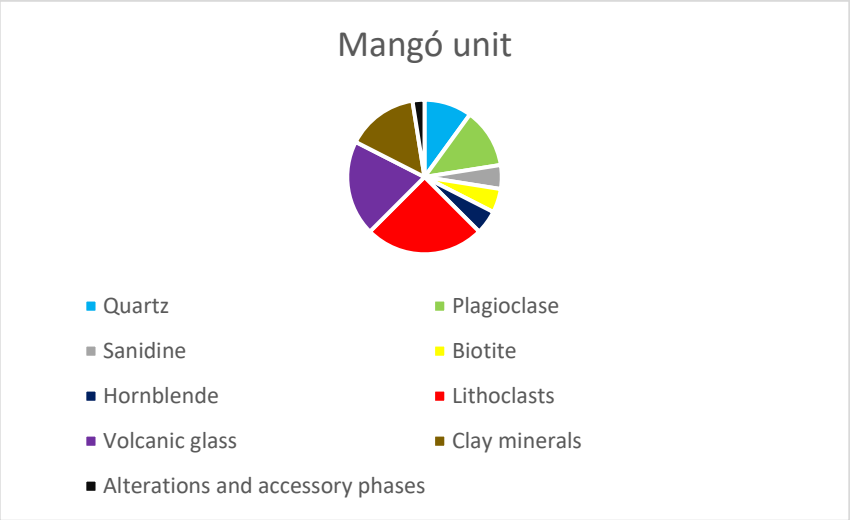

Figure 5-6. Mineral composition, volcanic glass, and lithoclasts distribution in the samples from Mangó unit

5.1.4. Demjén unit

Samples Dem-9_E/6, Dem-30, KMAJ-01, KMJ-02, and Hh-01 belong to the Demjén unit. Quartz, plagioclase, sanidine (samples Dem-9_E/6; Dem-30; KMJ-02), biotite and hornblende (samples Dem-9_E/6; Dem-30) appear as crystalloclasts, whereas chlorite (samples Dem-9_E/6; Dem-30; Hh-01), opaque minerals, hematite (samples Dem-30), limonite (samples Dem-30; KMJ-01) and clay minerals appear as their alterations and calcite as pseudomorphosis (sample KMJ-02). White mica (samples Dem-9_E/6; Dem-30; KMJ-01; KMJ-02), apatite (samples Dem-9_E/6; KMJ-02) and opaque minerals (samples Dem-30; KMJ-01) appear as accessory mineral phases occupying less than 1% of the samples.

Quartz appears as colourless, anhedral mineral grains. Its dimensions vary from 0,44×0,32 mm to 0,06×0,02 mm. It's characterised by undulose extinction and grey interference colour of 1st order. It occupies 5% of the sample.

Plagioclase appears in all samples as colourless, subhedral 4-sided mineral grains. (Figure 5-7 a, b) Its dimensions vary from 2,9×1 mm to 0,1×0,05 mm. It is characterised by the grey interference colour of 1st order and polysynthetic twinning lamellae as well as zoning (Figure

5-7 b). Some of the grains are slightly cracked and lightly altered into clay minerals. Few grains in the sample Dem-30 show jigsaw-fit texture and in the sample KMJ-02 some grains show colloidal texture. It occupies around 10-30% of samples.

Sanidine appears in the samples Dem-9_E/6, Dem-30, and KMJ-02 as colourless, subhedral to anhedral mineral grains. Its dimensions vary from 1,1×0,4 mm to 0,1×0,05mm. It is characterised by grey interference colour of 1st order. Most of the grains are moderately cracked and disintegrated. It occupies around 5% of the aforementioned samples.

Biotite appears in all samples as subhedral, 4-sided, elongated grains. Its dimensions vary in size from 0,78×0,16 mm to 0,02×0,01 mm. It shows pleochroism in the shades of brown, or due to chloritization, shades of green whereas some of the grains show gradation to red colour. Biotite is fresh in the sample KMJ-01, but it is lightly chloritized and moderately opacitized in all other samples. Opacitization usually occurs around the edges of the grains and alongside the cleavage planes. It occupies less than 1% of the sample KMJ-01 and around 5-15% of the rest of the samples.

Hornblende appears in samples Dem-9_E/6 and Dem-30 as 4- and 6-sided, subhedral to euhedral mineral grains, whereas its presence in the sample KMJ-01 can't be determined with certainty. Its dimensions vary in size from 1,25×0,4 mm to 0,3×0,25 mm. It shows pleochroism in shades of brown or, rarely, green due to chloritization. Some grains in the sample Dem-9_E/6 are disintegrated. It occupies around 2% of the sample Dem-30 and less than 1% of the sample Dem-9_E/6.

White mica appears in samples Dem-9_E/6, Dem-30, KMJ-01, and KMJ-02 as colourless, subhedral, 4-sided grains that show pseudoapsorption. Its dimensions vary from 02×0,06 mm to 0,03×0,005 mm. It shows various interference colours of 2nd order. It occupies less than 1% of samples.

Apatite appears in samples Dem-9_E/6 and KMJ-02 as subhedral, elongated, and slightly rounded, colourless mineral grains with high relief. The average size of mineral grains is 0,08x0,02 mm. It occupies less than 1% of samples.

Calcite appears in the sample KMJ-02 as pseudomorphosis over subhedral, 4-sided minerals (Figure 5-7 e, f) which are, according to their habit, probably feldspars. It is characterised by pseudoapsorption and white interference colours of higher order. It occupies less than 1% of the sample.

Chlorite appears in samples Dem-9_E/6, Dem-30, and Hh-01 as a product of biotite and hornblende alteration. It's green in colour and it occupies less than 5% of each of the aforementioned samples.

Opaque minerals appear in all of the aforementioned samples both as individual, euhedral 4-sided mineral grains (possibly pyrite) and as a product of biotite alteration. In the sample Dem-30 they show alteration to hematite and limonite, whereas in sample KMJ-01 they show light limonitization. They occupy less than 1% of each sample.

Hematite appears in the sample Dem-30 as an amorphous mass around opaque minerals, as a product of their alteration. It is red and it occupies less than 1% of the sample.

Limonite appears in samples Dem-30 and KMJ-01 as a light brown to orange amorphous mass around opaque minerals as a product of their alteration. It occupies less than 1% of the samples.

Clay minerals appear in all of the aforementioned samples as the product of feldspar and volcanic ash alteration. They occupy 5-15% of the samples.

Lithoclasts appear in the samples Dem-9_E/6, KMJ-02, and Hh-01. In the sample Dem-9_E/6, their dimensions vary from 6,15×3,7 mm to 1,45×0,8 mm. They are heavily altered into sericite and clay minerals but are possibly rhyolithic to andesitic (Figure 5-7 d). Some lithoclasts show slight fluidal structure. Biotite occurs in some of the lithoclasts in this sample and is slightly strained due to the ductile deformations. In the sample, Dem-30 lithoclasts vary in dimensions from 0,45×0,3 mm to 0,15×0,1 mm. They are moderately to heavily altered into clay minerals and are possibly from rhyolitic to andesitic in composition. In the sample, Hh-01 lithoclasts vary in size from 0,44×0,38 mm to 0,1×0,1 mm. They are moderately altered into clay minerals and possibly rhyolithic in composition. Lithoclasts altogether occupy 10-40% of the samples.

Volcanic glass appears in the matrix and as vitroclastic components, which are pumice fragments and glass shards. Pumice fragments are present in the sample Dem-9_E/6 and they consist mostly of non-devitrified volcanic glass and are exhibit holohyaline texture. Volcanic glass is present as devitrified and non-devitrified volcanic glass, where devitrified volcanic glass shows its characteristic Y to irregular shape, although in the sample KMJ-01 non-devitrified volcanic glass is predominant (Figure 5-7. c). Additionally, dark, flattened clasts which can be categorized as *fiamme* appear in samples KMJ-02 and Hh-01. Volcanic glass altogether occupies around 15-55% of the samples.

Matrix is composed mostly of fine ash sized particles altered into clay minerals, and tiny particles of both devitrified and non-devitrified volcanic glass. The matrix varies in colour from greyish light brown to dark brown, depending on the sample. It occupies 5-25% of the samples.

Fluid inclusions are present in both feldspars and quartz in the samples fom this unit, some of which are two-phased, consisting of fluid and vapour.

According to the ratios of crystaloclasts, vitroclasts, and lithoclasts samples KMJ-01, KMJ-02, and Hh-01 can be determined as **vitroclastic tuff**, sample Dem-30 can be determined as **crystalo- to vitroclastic tuff** and sample Dem-9_E/6 can be determined as partially welded **ignimbrite deposit dominated by crystalloclastic and lithoclastic particles.**

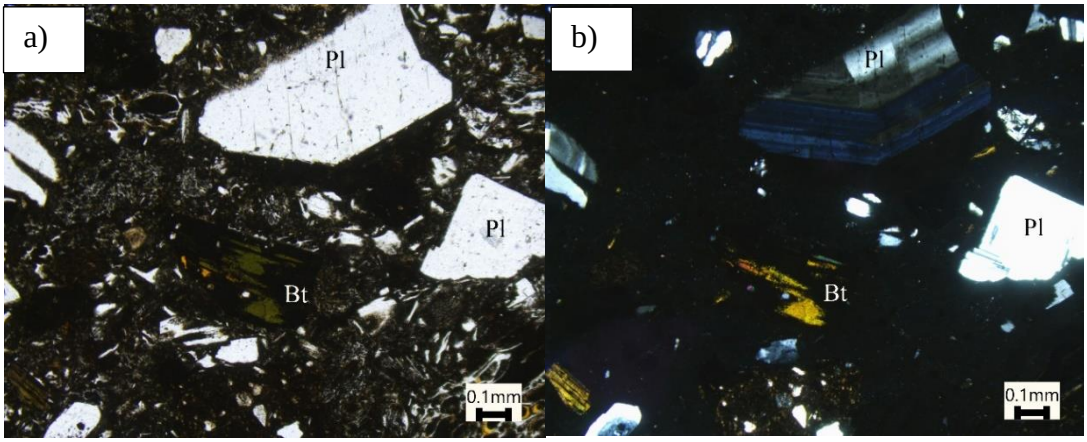

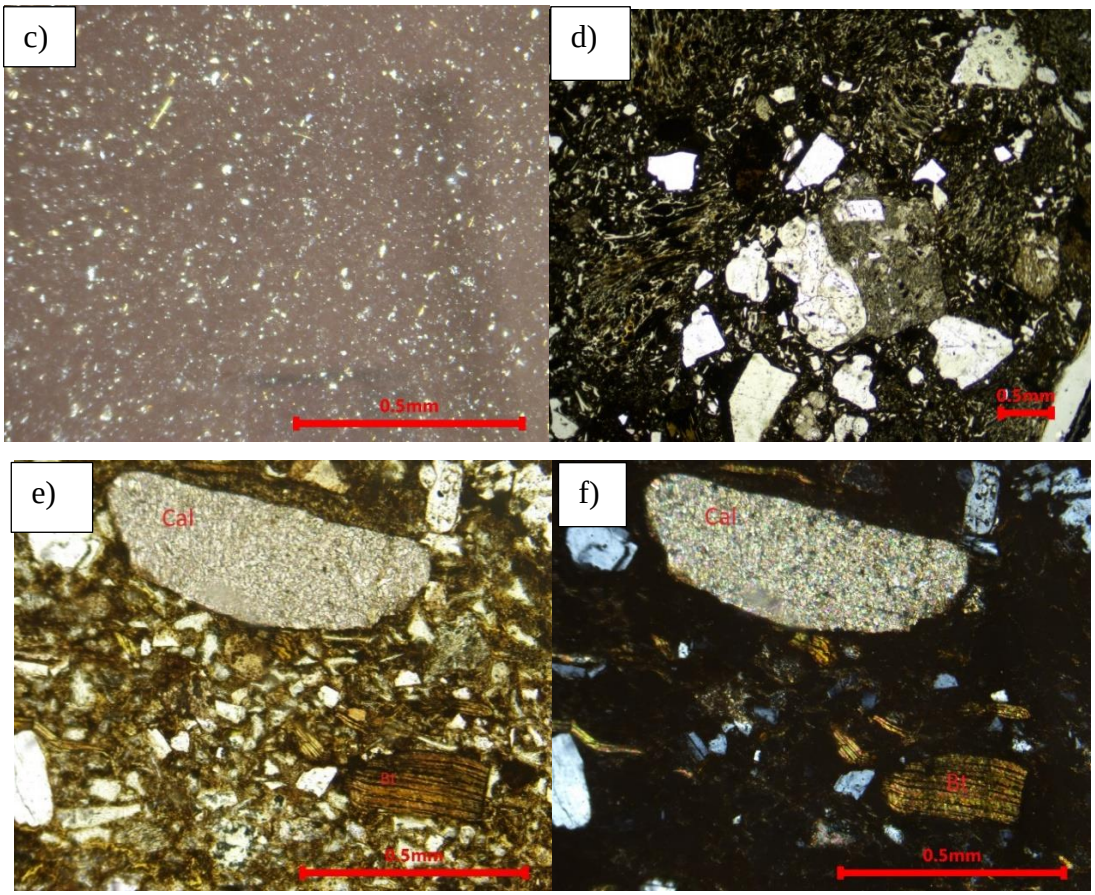

Figure 5-7. a) Plagioclase and biotite in sample Dem-30, N; b) Zoned plagioclase and biotite in sample Dem-30, N+, c) Dark volcanic glass particles in sample KMJ-01, N+; d) Litchoclast in sample Dem-9_E/6, N; e) Calcite pseudomorphosis after feldspar in sample KMJ-02, N; f) Calcite pseudomorphosis after feldspar in sample KMJ-02, N+

The average mineral composition alongside volcanic glass and lithoclast distribution of samples from the Demjén unit is presented in Figure 5-8.

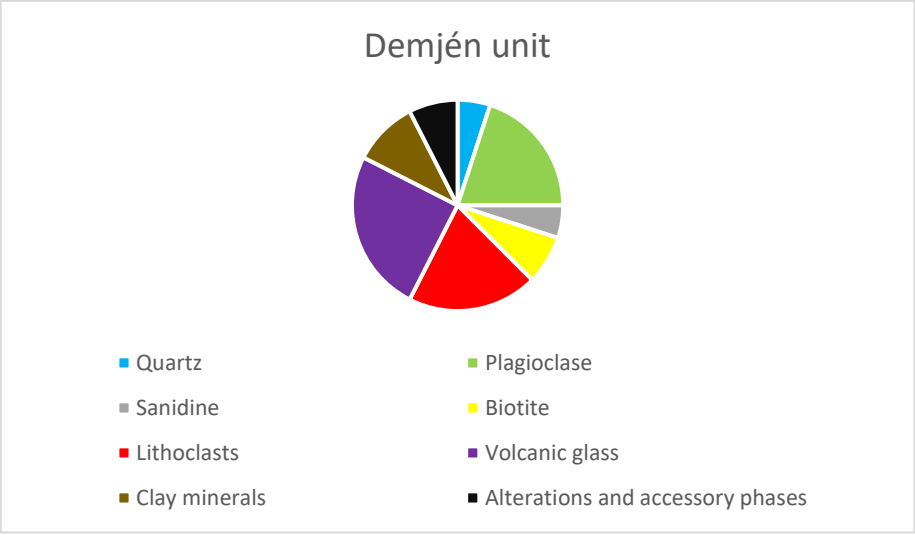

Figure 5-8. Mineral, lithoclast, and volcanic glass distribution in samples from the Demjén unit

5.1.5. Harsány unit

Sample Td-A belongs to the Harsány unit. Quartz, plagioclase, and biotite occur as phenocrystals, opaque minerals appear both as phenocrystals and as a product of alteration, whereas hematite, sericite, and clay minerals appear only as the product of alteration.

Quartz appears as colourless, anhedral mineral grains. Its dimensions vary from 0,75×0,4 mm to 0,2×0,2 mm. It's characterised by undulose extinction and grey interference colour of 1st order. Some of the grains exhibit jigsaw-fit texture. It occupies less than 5% of the sample.

Plagioclase appears as colourless, subhedral, 4-sided mineral grains. Its dimensions vary from 2,45×0,85 mm to 0,18×0,02 mm. It is characterised by grey interference colour of 1st order and polysynthetic twinning lamellae as well as zoning. Some of the grains are cracked, disintegrated and moderately altered to clay minerals. It occupies around 10% of the sample.

Sanidine appears in both samples as colourless, subhedral to mostly anhedral mineral grains. Its dimensions vary from 0,95×0,4 mm to 0,25×0,1 mm. It is characterised by grey interference colour of 1st order. Most of the grains are moderately cracked and show moderate alteration into clay minerals as well as light sericitization. It occupies less than 2% of each sample.

Biotite appears as subhedral, elongated 4-sided grains (Figure 5-9. a) which show pleochroism in the shades of brown. Its dimensions vary from 0,5×0,16 to 0,15×0,1 mm. Grains show moderate to heavy opacitization around the edges and along the cleavage planes. It occupies approximately 3% of the sample.

Opaque minerals appear as individual, 4- and 6- 6-sided euhedral grains (possibly pyrite and/or magnetite) as well as the product of biotite alteration. They show alteration to hematite. They occupy less than 1% of the sample.

Hematite appears as an amorphous, red mass around opaque minerals as the product of their alteration. It occupies less than 1% of the sample.

Sericite appears as a product of feldspar alteration. It appears as tiny, colourless grains which exhibit vivid interference colours. It occupies less than 1% of the sample.

Clay minerals appear as the product of alteration of feldspars and fine volcanic ash in the matrix. They occupy around 10% of the sample.

Volcanic glass, both devitrified and non-devitrified, occupies around 65% of the sample. According to that, the texture of this sample is hypohyaline (Figure 5-9, b).The structure is homogenous and the samples id categorized as pumice.

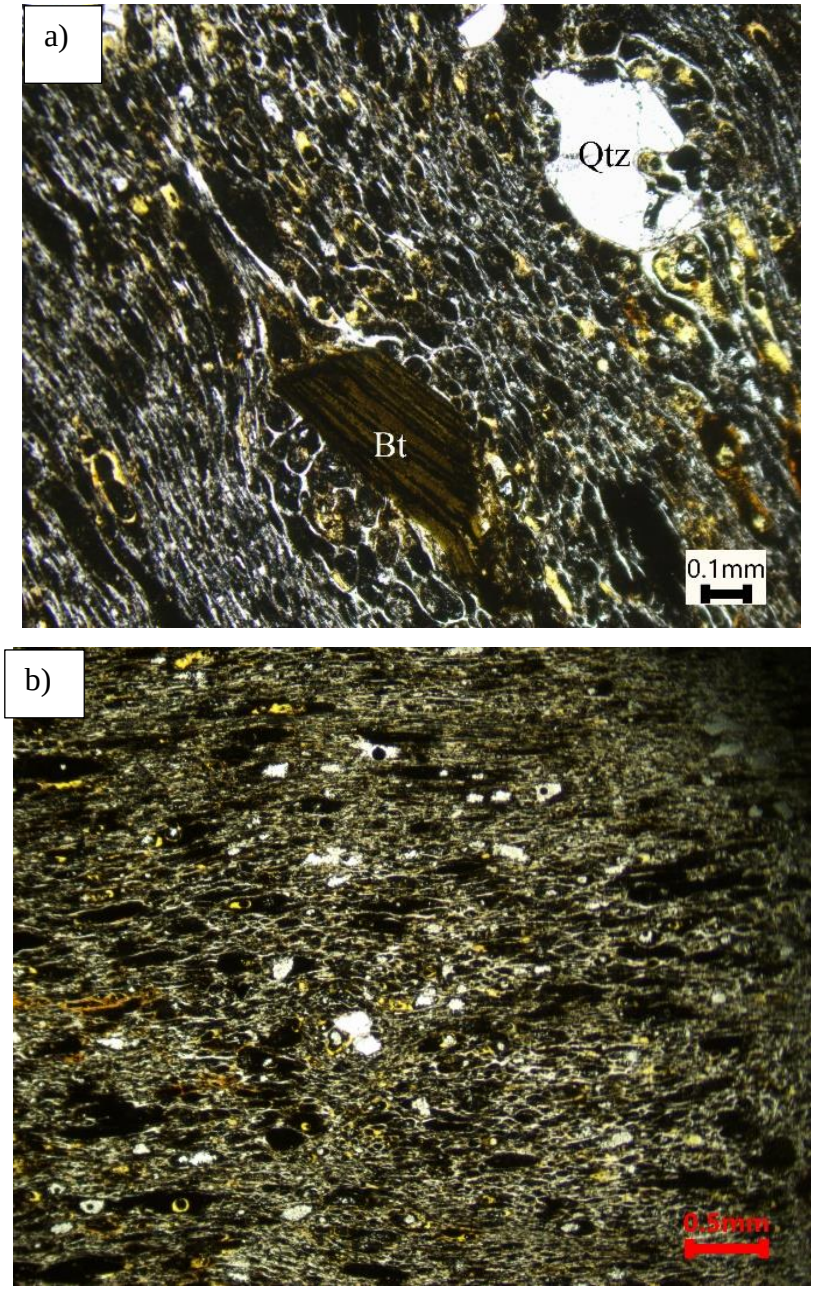

Figure 5-9 a) Biotite in the sample Td-A, N; b) Texture of the sample described as holohyaline in the sample Td-A, N

The mineral composition of the sample Td-A from the Harsány unit is shown in Figure 5-10.

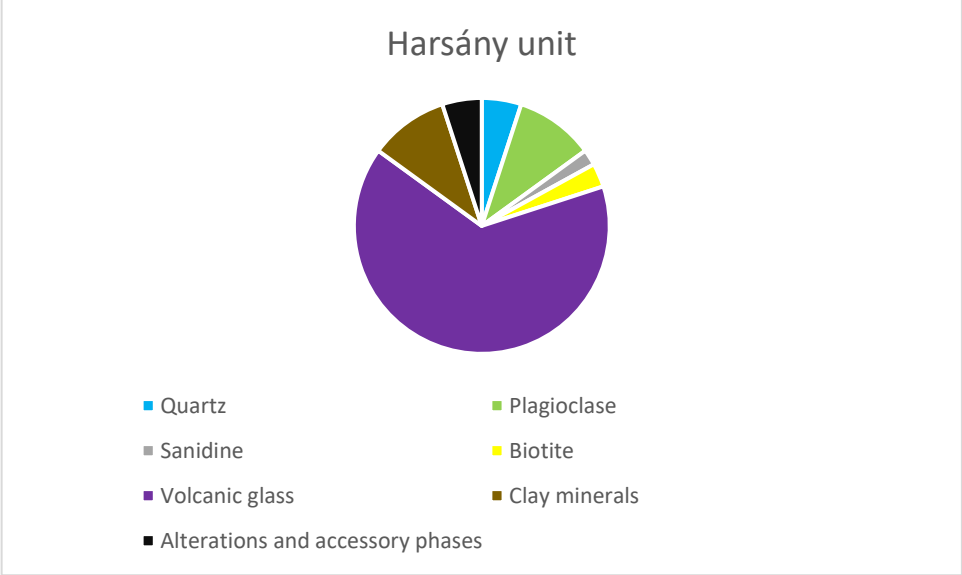

Figure 5-10. Mineral composition of the sample from the Harsány unit

5.1.6. Kuchyna tuff

Sample KISBESZ is the sample of Kuchyna tuff. In this sample, quartz, plagioclase, sanidine, biotite and hornblende appear as crystalloclasts (Figure 5-11, a; b), whereas opaque minerals, chlorite, and clay minerals appear as their alterations. Opaque minerals additionally occur as accessory mineral phase occupying less than 1% of the sample.

Quartz appears as colourless, anhedral mineral grains. Its dimensions vary from 1,34×0,45 mm to 0,1×0,06 mm. It's characterised by undulose extinction and grey interference colour of 1st order. It occupies around 5% of the sample.

Plagioclase appears as colourless, subhedral 4-sided mineral grains. Its dimensions vary from 0,42×0,28 mm to 0,08×0,04 mm. It is characterised by grey interference colour of 1st order and polysynthetic twinning lamellae as well as zoning. It occupies around 10% of the sample.

Sanidine appears as colourless, subhedral to anhedral mineral grains. Its dimensions vary from 0,6×0,4 mm to 0,26×0,16 mm. It is characterised by grey interference colour of 1st order and it's lightly altered into clay minerals. It occupies less than 5% of each sample.

Biotite appears as subhedral, elongated 4-sided grains which show pleochroism the shades of brown. Its dimensions vary from 0,7×0,16 mm to 0,18×0,04 mm. Grains are moderately chloritized and opacitizied and resorbed. It occupies around 3% of the sample.

Hornblende appears as brown pleochroic, 4-sided subhedral to euhedral grains. Its dimensions vary in size from 0,56×0,16 mm to 0,4×0,1 mm in size. It is moderately chloritized. It occupies less than 1% of the sample.

Opaque minerals appear both as individual, 4-sided euhedral mineral grains (possibly pyrite) and as a product of alteration of biotite. It is lightly altered into hematite, and it occupies less than 1% of the sample.

Chlorite appears as a product of biotite and hornblende alteration. It is green in colour and it occupies around 2% of the sample.

Clay minerals appear both as the product of alterations of sanidine and in the matrix. They occupy around 25% of the sample.

Lithoclasts vary in size from 0,56×0,32 mm to 0,1×0,1 mm. According to their mineral composition of quartz, plagioclase, and alkali feldspars, they can be determined as rhyolites to andesites. Lithoclasts occupy around 5% of the sample.

Also, lenses of dark, glassy material identified as *fiamme* occur in this sample.

The volcanic glass appears both in the matrix and as vitroclasts with sizes similar to the crystalloclasts. Shards exhibit their characteristic Y shape. It occurs mostly as devitrified volcanic glass. Also, lenses of dark, glassy material identified as *fiamme* occur in this sample. Volcanic glass altogether occupies around 45% of the sample.

Matrix is composed mostly of altered volcanic ash into clay minerals and tiny particles of both devitrified and non-devitrified volcanic glass and is brown. It occupies 10% of the sample.

Fluid inclusions are present in the sample from this unit.

According to the ratios of crystalloclasts, vitroclasts and lithoclasts, this sample can be categorized as **vitroclastic tuff.**

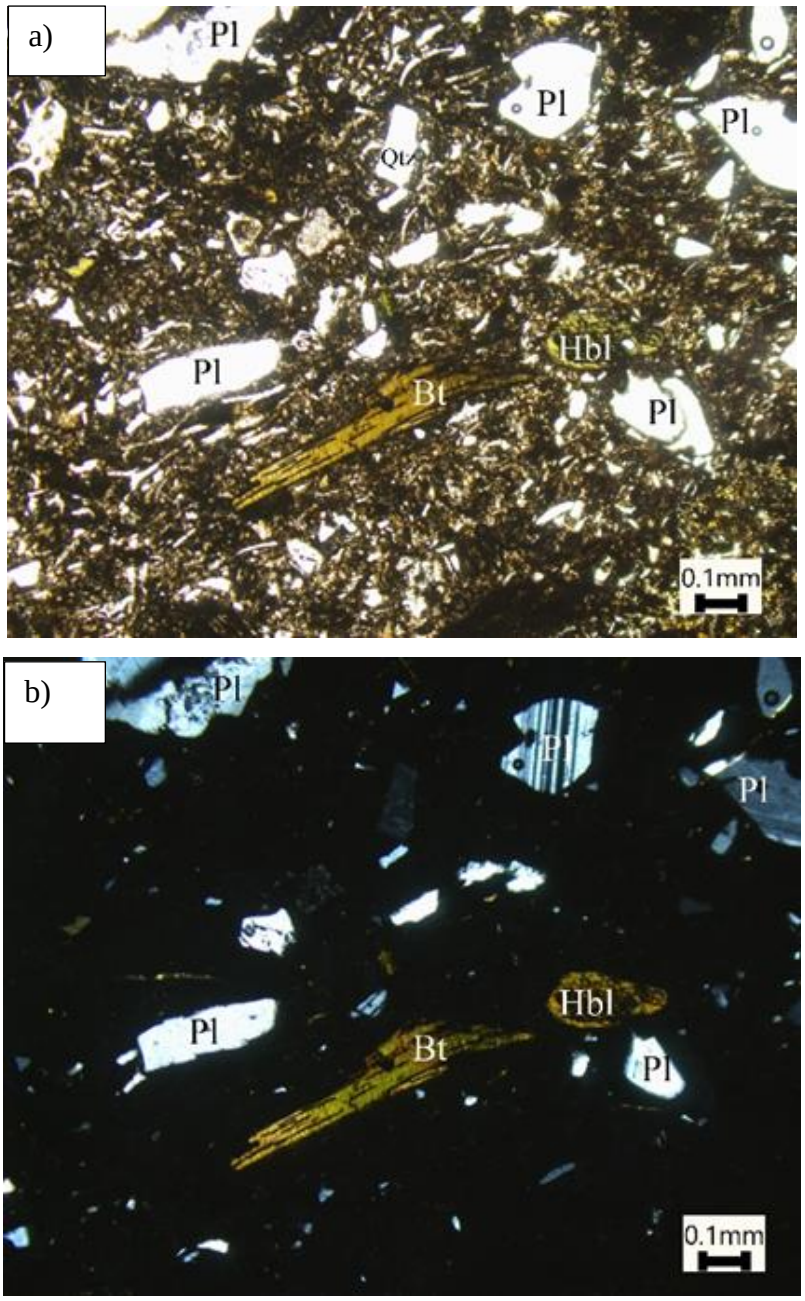

Figure 5-11. a) Mineral composition of the sample KISBESZ, N; b) Mineral composition of the sample KISBESZ, N+.

Mineral, lithoclastic, and volcanic glass distribution of Kuchyna uff based on the sample KISBESZ is given in Figure 5-12.

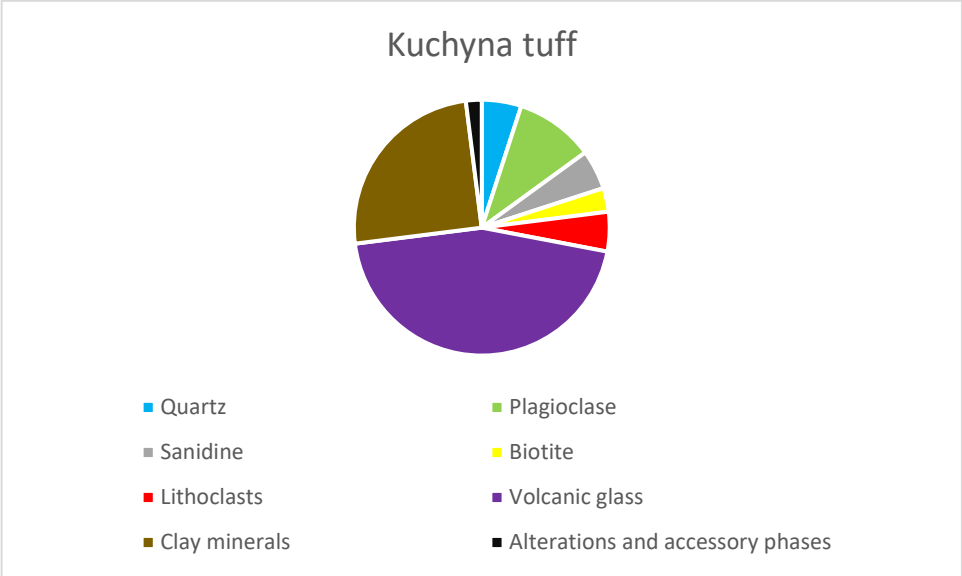

Figure 5-12. Mineral phases, lithoclast, and volcanic glass distribution in Kuchyna tuff sample

5.2. X-ray fluorescence

X-ray fluorescence shows the contents of all elements heavier than sodium. Alongside sodium, loss of ignition can't be determined by this method, hence it isn't presented in the following results. The results for the main elements are given as the weight percentage of their oxides, as shown in Table 5-2.

The microelement contents (Table 5-3) are given in ppm. The elements not shown here, which are heavier than sodium, have contents below the detection limit.

Table 5-2. Major oxides in analysed samples

Name	unit	SiO_2 [wt.%]	TiO_2 [wt. %]	Al_2O_3 [wt. %]	FeO [wt. %]	MnO [wt. %]	MgO [wt. %]	CaO [wt.%]	K_2O [wt. %]	P_2O_5 [wt. %]	Total [wt%]
EG-HOM-1	Wind-Kalnik	72,97	0,09	12,36	1,87	0,05	0,62	1,7	4,23	0,05	93,94
EG-HOM-2		70,95	0,13	13,68	2,79	0,04	1,18	1,78	3,41	0,04	94
EG-1	Eger	71,62	0,15	12,95	2,82	0,04	1,07	2,34	3,21	0,09	94,29
Cskly-1f	Mangó	71,63	0,15	14,3	2,17	0,05	0,24	1,54	4,08	0,06	94,22
EG-2		72,98	0,09	12,24	2,05	0,04	0,38	2,19	4,25	0,09	94,31
Dem-9_E/6	Demjén	61,28	0,33	12,73	3,04	0,07	0,8	8,19	3,58	3,78	93,8
Dem-30		70,75	0,2	12,88	2,62	0,06	0,77	2,72	4,26	0,1	94,36
KMJ-01		73,18	0,06	12,7	1,99	0,06	0,62	1,97	3,57	0,14	94,29
KMJ-02		65,91	0,45	15,73	4,05	0,09	2,15	3,36	2,38	0,13	94,25
Hh-01		70,8	0,16	13,57	2,44	0,05	1,18	2,06	4,02	0,09	94,37
Td-A	Harsány	73,36	0	10,75	1,48	0,06	0,42	1,69	6,14	0,07	93,97
KISBESZ	Kuchyna tuff	66,24	0,17	16,18	4,53	0,04	2,59	2,68	1,73	0,09	94,25

Table 5-3. Microelements in analysed samples

Name	EG-HOM-1	EG-HOM-2	EG-1	Cskly-1f	EG-2	Dem-9_E/6	Dem-30	KMJ-01	KMJ-02	Hh-01	Td-A	KISBESZ	Bulk continental crust according to Rudnick & Gao (2003)
Unit	Wind-Kalnik		Eger	Mangó		Demjén					Harsány	Kuchyna tuff	
Cr [ppm]	124	0	0	0	257	63	0	0	0	0	62	0	135
Co [ppm]	15	9	20	0	13	13	15	0	27	13	15	6	26,6
Zn [ppm]	43	42	44	44	38	52	45	45	67	52	42	55	72
As [ppm]	10	9	1	7	6	4	14	13	10	14	4	3	2,5
Se [ppm]	0	0	0	0	0	0	0	0	1	0	0	1	0,13
Rb [ppm]	164	160	140	188	183	164	183	170	174	215	168	91	49
Sr [ppm]	128	110	172	150	147	238	181	94	198	100	72	141	320
Zr [ppm]	102	103	107	153	81	115	112	82	157	89	75	145	132
Nb [ppm]	4	8	0	13	0	0	0	0	4	0	0	22	8
Mo [ppm]	7	3	3	0	7	0	0	0	0	2	7	0	0,8
Sb [ppm]	0	17	18	9	0	0	0	0	0	0	0	0	0,2
Ba [ppm]	308	198	284	397	88	243	219	86	177	87	227	49	456

Ta [ppm]	28	27	16	23	9	17	11	16	29	23	33	27	0,1
W [ppm]	0	0	2	0	4	0	0	3	3	2	0	0	1
Hg [ppm]	5	8	1	9	0	3	3	4	2	4	11	1	0,03
Tl [ppm]	1	1	1	3	4	2	1	0	2	2	1	5	0,5
Pb [ppm]	34	36	23	26	27	42	34	37	36	29	23	27	11
Bi [ppm]	0	1	0	0	0	1	0	0	0	0	0	0	0,18
Th [ppm]	21	24	21	26	19	19	21	26	26	23	15	21	5,6
U [ppm]	0	0	0	0	0	7	0	2	0	0	2	2	1,3

5.2.1. Wind-Kalnik unit

The most abundant oxide is SiO_2, with contents ranging from 70,95 to 72,97 %. Al_2O_3 is the second most abundant oxide, with contents ranging from 12,35 to 13,68 %. K_2O content ranges from 3,41 to 4,23 %, FeO content ranges from 1,87 to 2,79 %, CaO content ranges from 1,7 to 2,78 %, and MgO content ranges from 0,62 to 1,18 %. The contents of MnO, TiO_2 and P_2O_5 are less than 1 %.

The microelements present in both samples from this unit are Co, Zn, As, Rb, Sr, Zr, Nb, Mo, Ba, Ta, Hg, Tl, Pb and Th, while Cr is present only in the sample EG-HOM-1 and Sb and Bi are present in the sample EG-HOM-2.

In comparison with the composition of the bulk continental crust according to Rudnick and Gao (2003) As, Rb, Mo, Sb Ta, Hg, Pb and Th have larger contents while Zn, Sr and Ba have lower contents and Cr, Co, Zr, Nb, Tl and Bi are present in similar amounts.

5.2.2. Eger unit

The most abundant oxide is SiO_2, with contents of 71,62%. Al_2O_3 is the second most abundant oxide, with contents of 12,95%. K_2O content is 3,20%, FeO content is 2,82%, CaO content is 2,34%, and MgO content is 1,07%. The contents of MnO, TiO_2 and P_2O_5 are less than 1 %.

The microelements present in the sample from this unit are Co, Zn, As, Rb, Sr, Zr, Mo, Sb, Ba, Ta, W, Hg, Tl, Pb and Th.

In comparison with the composition of the bulk continental crust according to Rudnick and Gao (2003) Rb, Mo, Sb, Ta, Hg, and Th have larger contents while Zn and Sr have lower contents, and Co, As, Zr, W, Tl and Pb are present in similar amounts.

5.2.3. Mangó unit

The most abundant oxide is SiO_2, with contents ranging from 71,63 to 72,98 %. Al_2O_3 is the second most abundant oxide with contents ranging from 12,24 to 14,30 %. K_2O content ranges from 4,08 to 4,25 %, FeO content ranges from 2,05 to 2,17 % and CaO content ranges from 1,54 to 2,19 %. The contents of MgO, MnO, TiO_2 and P_2O_5 are less than 1 %.

The microelements present in both samples from this unit are Zn, As, Rb, Sr, Zr, Ba, Ta, Tl, Pb and Th, while Nb, Sb and Hg are present only in the sample Cskly-1f and Cr, Co, Mo and W are present only in the sample EG-2.

In comparison with the composition of the bulk continental crust according to Rudnick and Gao (2003) Cr, Rb, Nb, Mo, Ta, Hg and Th have larger contents, while Zn, Sr and Ba have lower contents, and Co, As, Zr, Sb, Mo, W and Tl are present in similar amounts.

5.2.4. Demjén unit

The most abundant oxide is SiO_2, with contents ranging from 61,27 to 73,18 %. Al_2O_3 is the second most abundant oxide with contents ranging from 12,70 to 15,73 %. CaO content ranges from 1,97 to 8,19%, K_2O content ranges from 2,38 to 4,26 %, FeO content ranges from 1,99 to 4,05 % and MgO content ranges from 0,62 to 2,15%. The contents of, MnO and TiO_2 are less than 1% in all samples from this unit, and P_2O_5 contents are below 1% in every sample except from Dem-9_E/6 where it is 3,76%.

The microelements present in all samples from this unit are Zn, As, Rb, Sr, Zr, Ba, Ta, Hg, Ta, Pb and Th. In addition to above-mentioned microelements present in every sample from this unit Cr, Co, Tl, Bi, and U are present in sample Dem-9_E/6; Co and Tl are present in sample Dem-30; W and U are present in sample KMJ-01; Co, Se, Nb, W, and Tl are present in sample KMJ-02; and Co, Mo, W, and Tl are present in sample Hh-01.

In comparison with the composition of the continental crust according to Rudnick and Gao (2003), As, Rb, Ta, Hg, Pb, and Th have larger contents, while Cr, Sr, Na, and Ba have lower contents, and Co, Zn, Se, Mo, W, Tl, Bi and U are present in similar amounts.

5.2.5. Harsány unit

The most abundant oxide is SiO_2, with a content of 73,96 %. Al_2O_3 is the second most abundant oxide, with contents of 10,73%. K_2O content is 6,14%, CaO content is 1,69% and FeO content is 1,48% The contents of MgO, MnO, TiO_2 and P_2O_5 are less than 1 %.

The microelements present in the sample from this unit are Cr, Co, Zn, As, Rb, Sr, Zr, Mo, Ba, Ta, Hg, Tl, Pb, Th and U.

In comparison with the composition of the bulk continental crust according to Rudnick and Gao (2003) Rb, Mo, Ta, Hg, Tl, Pb and Th show have larger contents while Cr, Sr and Ba have lower contents, and Co, Zn, As, Zr and U are present in similar amounts.

5.2.6. Kuchyna tuff

The most abundant oxide is SiO_2, with a content of 66,24%. Al_2O_3 is the second most abundant oxide, with contents of 16,18%. FeO content is 4,53%, CaO content is 2,68%, MgO content is 2,59% and K_2O content is 1,72% The contents of MnO, TiO_2 and P_2O_5 are less than 1%.

The microelements present in the sample from this unit are Co, Zn, As, Se, Rb, Sr, Zr, Nb, Ba, Ta, Hg, Tl, Pb, Th and U.

In comparison with the composition of the bulk continental crust according to Rudnick and Gao (2003) Rb, Ta, Hg, Pb and Th have larger contents while Co and Sr have lower contents, and Zn, As, Se, Zr, Nb, Tl and U are present in similar amounts.

5.3. X-ray diffraction

The mineral composition of the analysed samples acquired by x-ray diffraction is given in Table 5-4. and the estimated proportions are given in Table 5-5.

Table 5-4. Mineral composition of analysed samples according to XRD. ++++ predominant phase; +++ dominant phase, ++- moderately represented phase, +-poorly represented phase,?- phase can't be determined with certainty

sample	unit	Gypsum	Biotite	Hornblende	Hydroxylapatite	Sanidine/K-feldspar	Plagioclase	Quartz	Smectite	Illite-smectite
EG-HOM-1	Wind-Kalnik		+	+	?	++	+++	++	+++	
EG-HOM-2		?	+	+	?	+	++	++	++++	+
EG-1	Eger		+	?	?	+	+++	++	+++	++
Cskly-1f	Mangó		+	+	?	+	+++	+	++++	+
EG-2			+	+	?	+	++++	++	++	
Dem-9_E/6	Demjén		+	+	++	+	++++	+	+++	+
Dem-30			+	+	?	++	++++	+	+++	+
KMJ-01			+	+	?	+	++	+	++++	+
KMJ-02			+	?		+	+++	+	++++	+
Hh-01			+	+	?	+	++	+	++++	+
Td-A	Harsány		+		+	+++	+++	++		++
KISBESZ	Kuchyna tuff		+	?	?	+	++	+	++++	

Table 5-5. Estimated proportions (%) of mineral phases. Orange - value probably too high; blue – unrealistic values due to the preferred orientation of certain mineral phases.

sample	unit	Gypsum	Biotite	Hornblende	Hydroxylapatite	Sanidine/K-feldspar	Plagioclase	Quartz	Smectite	Illite-smectite
EG-HOM-1	Wind-Kalnik		3	3	1	11	31	17	34	
EG-HOM-2		2	6	2	1	5	16	12	52	6
EG-1	Eger		6	1	0.5?	2	37	13	26	15
Cskly-1f	Mangó		8	3	2	9	27	4	44	3
EG-2			5	2	2	8	45	15	23	
Dem-9_E/6	Demjén		4	2	15	5	41	5	24	4
Dem-30			4	2	1	12	43	4	29	5
KMJ-01			4	2	2	3	12	6	68	3
KMJ-02			4	1		2	31	4	52	6
Hh-01			6	2	1	7	21	3	57	3
Td-A	Harsány		5		4	24	38	15		14
KISBESZ	Kuchyna tuff		5	1	1	5	23	3	62	

5.3.1. Wind-Kalnik unit

Smectite is a predominant phase in the sample EG-HOM-2 and a dominant phase in the sample EG-HOM-1. Plagioclase is the dominant phase in the sample EG-HOM-1 and is moderately represented in the sample EG-HOM-2. Quartz is moderately represented in both samples. K-feldspar (sanidine) is moderately represented in the sample EG-HOM-1 and poorly represented in the sample EG-HOM-2. Biotite and hornblende are poorly presented in both of the samples and mixed-layer illite-smectite is poorly presented in the sample EG-HOM-1. Hydroxyapatite can't be determined with certainty in both of the samples as well as gypsum in the sample EG-HOM-2.

5.3.2. Eger unit

Plagioclase and smectite are dominant minerals in the sample EG-2. Quartz and mixed-layer illite-smectite are moderately represented. K-feldspar (sanidine) and biotite are poorly presented and hornblende and hydroxyapatite can't be determined with certainty.

5.3.3. Mangó unit

Smectite is the predominant mineral phase in the sample Cskly-1 and dominant in the sample EG-2. Plagioclase is the predominant mineral phase in the sample EG-2 and dominant in the sample Cskly-1f. Quartz is moderately represented in the sample EG-2 and poorly represented in the sample Cskly-1f. K-feldspar (sanidine) is poorly represented in both of the samples as well as biotite and hornblende, whereas mixed-layer illite-smectite is poorly represented in the sample Cskly-1f. Hydroxyapatite can't be determined with certainty in both of the samples.

5.3.4. Demjén unit

Smectite is the predominant phase in the samples KMJ-01, KMJ-02, and Hh-01 and the dominant phase in the samples Dem-9_E/6 and Dem-30. Plagioclase is the predominant phase in the samples Dem-9_E/6 and Dem-30, dominant in the sample KMJ-02 and moderately represented in the samples KMJ-01 and Hh-01. K-feldspar is moderately

represented in the sample Dem-30 whereas it is poorly represented in other samples from this unit. Quartz, biotite, and mixed-layer illite-smectite are poorly represented in all of the aforementioned samples, whereas hornblende is poorly represented in all of the aforementioned samples except KMJ-02 where it can't be determined with certainty. Hydroxyapatite is moderately represented in the sample Dem-9_E/6 and it is possibly present in the samples Dem-30, KMJ-01, and Hh-01 but its occurrence can't be determined with certainty.

5.3.5. Harsáany unit

Plagioclase and K-feldspar are dominant mineral phases in the sample Td-A. Quartz and mixed-layer illite-smectite are moderately represented, whereas biotite and hydroxyapatite are poorly represented in the sample.

5.3.6. Kuchyna tuff

Smectite is the predominant mineral phase in the sample KISBESZ. Plagioclase is the dominant mineral phase whereas quartz, K-feldspar, and biotite are poorly represented in the aforementioned sample. The occurrence of hornblende and hydroxyapatite can't be determined with certainty.

5.4. Atomic absorption spectrometry

From all samples except for EG-1 one solution from both magnetic and non-magnetic fractions was prepared, whereas both non-magnetic and magnetic fractions from sample EG-1 were analysed in three parallels, alongside non-magnetic, <125 μm fractions of all the samples except KMJ-01 which was analysed in bulk.

5.4.1. Lithium in >125 μm fractions

The results of atomic absorption spectrometry measurements for lithium in >125 μm fractions are given in Table 5-6.

Table 5-6. Lithium concentrations in >125 µm non-magnetic (NM) and magnetic (M) fractions of the analysed samples; BDL – below detection limit

sample name	unit	M/NM	m (sample) [g]	V (solution) [mL]	measured c (Li) [ppm]	Li [mg/kg]	standard deviation	confidence interval	Li [mg/kg]
EG-HOM-1	Wind-Kalnik	NM	0,5033	20	0,034	BDL	-	-	BDL
		M	0,3439	20	0,262	15,24	-	-	15,2
EG-HOM-2		NM	0,5028	20	0,043	BDL	-	-	BDL
		M	0,3734	20	0,345	18,48	-	-	18,5
EG-1	Eger	NM	0,5006	20	0,055	BDL	BDL	BDL	BDL
		NM	0,5031	20	0,059				
		NM	0,5002	20	0,061				
		M	0,5012	20	0,975	38,91	0,5539928	0,9339558	38,9
		M	0,5011	20	0,995	39,71			
		M	0,5004	20	1	39,97			
Cskly-1f	Mangó	NM	0,5028	20	0,075	BDL	-	-	BDL
		M	0,3547	20	0,313	17,65	-	-	17,6
EG-2		NM	0,5037	20	0,051	BDL	-	-	BDL
		M	0,5029	20	0,483	19,21	-	-	19,2
Dem-9_E/6	Demjén	NM	0,5023	20	0,119	4,74	-	-	4,7
		M	0,5003	20	0,598	23,91	-	-	23,9
Dem-30		NM	0,5027	20	0,084	BDL	-	-	BDL
KMJ-01		/	0,5038	20	0,08	BDL	-	-	BDL
KMJ-02		NM	0,5016	20	0,093	BDL	-	-	BDL
		M	0,5016	20	0,423	16,87	-	-	16,9
Hh-01		NM	0,5014	20	0,106	4,23	-	-	4,2
		M	0,1314	20	0,271	41,25	-	-	41,2
Td-A	Harsány	NM	0,5008	20	0,067	BDL	-	-	BDL
		M	0,4704	20	0,811	34,48	-	-	34,5
KISBESZ	Kuchyna tuff	NM	0,5004	20	0,543	21,70	-	-	21,7
		M	0,5001	20	0,494	19,76	-	-	19,8
Bulk contitnental crusto composition according to Rudnick & Gao (2003)									16

5.4.1.1. *Wind-Kalnik unit*

In the non-magnetic fractions of the samples from the Wind-Kalnik unit, the lithium content is below the detection limit, while the lithium content in magnetic fractions of the samples is between 15,24 and 18,48 mg/kg.

5.4.1.2. *Eger unit*

In the non-magnetic fraction of the sample from the Eger unit, the lithium content is below the detection limit, whereas the lithium content in the magnetic fraction of the samples is 39,53 mg/kg.

5.4.1.3. *Mangó unit*

In the non-magnetic fractions from the sample from Mangó unit the lithium content is below the detection limit, while the lithium content in magnetic fractions from the samples is between 17,65 and 19,21 mg/kg.

5.4.1.4. *Demjén unit*

In the sample KMJ-01 and non-magnetic fractions of samples Dem-30 and KMJ-02, from the Demjén unit, the lithium content is below the detection limit, while in the non-magnetic fractions of the samples, Dem-9_E/6 lithium contents are between 4,32 and 4,74 mg/kg. Lithium is present in magnetic fractions from all the samples from this unit with contents between 16,87 and 41,25 mg/kg.

5.4.1.5. *Harsány unit*

In the non-magnetic fraction of the sample from the Harsány unit, the lithium content is below the detection limit, while the lithium content in the magnetic fraction from the sample is 34,48 mg/kg.

5.4.1.6. *Kuchyna tuff*

In the non-magnetic fraction of the sample from the Kuchyna tuff unit, the lithium content is 21,7 mg/kg, while the lithium content in the magnetic fraction from the samples is 19,76 mg/kg.

In comparison with the composition of the bulk continental crust according to Rudnick and Gao (2003) lithium contents in non-magnetic fractions in all of the samples analysed in this master's thesis are lower while lithium contents from magnetic fractions are either similar or slightly higher.

5.4.2. Lithium in <125 μm fractions

The results of atomic absorption spectrometry measurements for lithium in >125 μm fractions are given in Table 5-7.

Table 5-7. Lithium concentrations in <125 μm, non-magnetic (NM) fractions of analysed samples; BDL - below detection limit

sample name	unit	NM/M	m (sample) [g]	V (solution) [mL]	measured c (Li) [ppm]	Li [mg/kg]	stan. dev.	conf. interval	Li [mg/kg]
EG-HOM-1	Wind-Kalnik	NM	1,0006	20	BDL	BDL			BDL
EG-HOM-2		NM	1,0025	20	BDL	BDL			BDL
EG-1	Eger	NM	1,0013	20	0,086	1,72	0,2022697	0,34099896	1,80
		NM	1,0013	20	0,103	2,06			
		NM	1,0017	20	0,085	1,70			
Cskly-1f	Mangó	NM	1,0006	20	0,353	7,06	-	-	7,10
EG-2		NM	1,0002	20	BDL	BDL	-	-	BDL
Dem-9_E/6	Demjén	NM	1,0023	20	0,236	4,71	-	-	4,70
Dem-30		NM	1,0004	20	0,115	2,30	-	-	2,30
KMJ-01		/	1,0006	20	BDL	BDL	-	-	BDL
KMJ-02		NM	1,0011	20	0,099	1,98	-	-	2,00
Hh-01		NM	1,001	20	0,103	2,06	-	-	2,10
Td-A	Harsány	NM	1,0007	20	BDL	BDL	-	-	BDL
KISBESZ	Kuchyna tuff	NM	1,001	20	1,003	20,04	-	-	20,00
Bulk contitnental crusto composition according to Rudnick & Gao (2003)									**16**

5.4.2.1. *Wind-Kalnik unit*

In non-magnetic fractions from analysed samples lithium contents are below the detection limit.

5.4.2.2. *Eger unit*

In the non-magnetic fraction of the sample from the Eger unit, the lithium content is 1,8 mg/kg.

5.4.2.3. *Mangó unit*

In the non-magnetic fractions from the sample from Mangó unit the lithium content is below the detection limit in the sample EG-2 and 7,1 mg/kg in the sample Cskly-1f.

5.4.2.4. *Demjén unit*

In the sample KMJ-01 lithium content is below the detection limit, whereas in the rest of the non-magnetic fraction of the analysed samples from this unit, it ranges from 2 to 4,7 mg/kg.

5.4.2.5. *Harsány unit*

In the non-magnetic fraction of the sample from the Harsány unit, the lithium content is below the detection limit.

5.4.2.6. *Kuchyna tuff*

In the non-magnetic fraction of samples from the Kuchyna tuff unit, the lithium content is 20 mg/kg.

In comparison with the composition of the bulk continental crust according to Rudnick and Gao (2003) lithium contents in non-magnetic fractions in all of the samples, except the Kuchyna tuff sample, analysed in this master's thesis are lower.

5.5. Atomic emission spectrometry

The results from atomic absorption spectrometry measurements for boron in fractions >125 μm are given in Table 5-8.

Table 5-8. Boron concentrations in non-magnetic (NM) and magnetic (M) fractions of the analysed samples. Method of standard addition was used for NM fractions.

sample name	unit	M/NM	m (sample) [g]	V (original solution) [mL]	c (B) measured [ppm]	c (B) in original solution [ppm]	B [mg/kg]	stan. dev.	conf. Interval	B [mg/kg]
EG-HOM-1	Wind-Kalnik	NM	0,5033	20	17,56 56,85 112,1	21,01	835,05	-	-	835,00
		M	0,3439	20	365,8	365,80	21273,63	-	-	21273,60
EG-HOM-2		NM	0,5028	20	26,93 72,79 118,2	39,45	1569,24	-	-	1569,20
		M	0,3734	20	367,8	367,80	19700,05	-	-	19700,10
EG-1	Eger	NM	0,5006	20	31,23 80,68 121,3	48,41	1934,07	113,34	191,08	1881,50
		NM	0,5031	20	30,5 75,6 122,1	44,06	1751,41			
		NM	0,5002	20	33,15 82,8 126,2	48,99	1958,99			
		M	0,5012	20	371,3	371,30	14816,44	937,87	1581,11	15897,10
			0,5011	20	410,3	410,30	16375,97			
			0,5004	20	412,8	412,80	16498,80			
Cskly-1f	Mangó	NM	0,5028	20	20,23 59,74 120	22,41	891,58	-	-	891,60
		M	0,3547	20	250,3	250,30	14113,34	-	-	14113,30
EG-2		NM	0,5037	20	17,5	26,90	1068,17	-	-	1068,20

					67,13					
					109,9					
		M	0,5029	20	300,1	600,20	23869,56	-	-	23869,60
Dem-9_E/6	Demjén	NM	0,5023	20	71,04	89,28	3554,90	-	-	3554,90
					122,5					
					176,5					
		M	0,5003	20	272,9	272,90	10909,45	-	-	10909,50
Dem-30		NM	0,5027	20	32,43	43,14	1716,16	-	-	1716,20
					82,15					
					132,4					
		M	0,504	20	313,7	313,70	12448,41	-	-	12448,40
KMJ-01		/	0,5038	20	46,51	60,46	2400,13	-	-	2400,10
					104,9					
					152,9					
KMJ-02		NM	0,5016	20	53,8	70,62	2815,74	-	-	2815,70
					101,5					
					153,9					
		M	0,5016	20	328,6	657,20	26204,15	-	-	26204,10
Hh-01		NM	0,5014	20	51,03	67,55	2694,53	-	-	2694,50
					102,7					
					152,4					
		M	0,1314	20	148,5	20,00	3044,14	-	-	3044,10
Td-A	Harsány	NM	0,5008	20	15,13	21,02	839,50	-	-	839,50
					52,9					
					100,6					
		M	0,4704	20	417,3	417,30	17742,35	-	-	17742,30
KISBESZ	Kuchyna tuff	NM	0,5004	20	89,1	112,73	4505,41	-	-	4505,40
					139,4					
					193,7					
		M	0,5001	20	343	343,00	13717,26	-	-	13717,30
Bulk contitnental crusto composition according to Rudnick & Gao (2003)										11

5.5.1.1. *Wind-Kalnik unit*

In the non-magnetic fractions of samples from the Wind-Kalnik unit, the boron content is between 835 and 1569,2 mg/kg, whereas the boron content in magnetic fractions from the samples is between 19 700 and 21 273,6 mg/kg.

5.5.1.2. *Eger unit*

In the non-magnetic fraction of the sample from the Eger unit, the boron content is 1881,45+/- 191 mg/kg, while in the magnetic fractions of the sample, the boron content is 15 897 +/- 937,9 mg/kg.

5.5.1.3. *Mangó unit*

In the non-magnetic fractions of samples from the Mangó unit the boron content is between 891,6 and 1068,2 mg/kg, while in the magnetic fractions of the samples, the boron content is between 14 113,3 and 23 869,6 mg/kg.

5.5.1.4. *Demjén unit*

In the non-magnetic fractions from samples from the Demjén unit, the boron content is between 1716,2 and 3554,9 mg/kg, while in the magnetic fractions of the samples, the boron content is between 3044,1 and 26 204,2 mg/kg. The boron content in the sample KMJ-01 is 2400,1 mg/kg.

5.5.1.5. *Harsány unit*

In the non-magnetic fraction of the sample from the Harsány unit the boron content is 839,5 mg/kg, while in the magnetic fraction of the sample, the boron content is 17 742,4 mg/kg.

5.5.1.6. *Kuchyna tuff*

In the non-magnetic fraction of the sample from the Kuchyna tuff unit, the boron content is 4505,4 mg/kg, while in the magnetic fraction of the sample, the boron content is 13 717,3 mg/kg. is highly increased, although the ones from magnetic fraction are larger than the ones from non-magnetic fractions.

In comparison with the composition of the bulk continental crust according to Rudnick and Gao (2003) boron contents from both magnetic and non-magnetic fractions from all samples are highly increased, although the ones from magnetic fractions are larger than the ones from non-magnetic fractions.

6. DISCUSSION

6.1. Mineral composition

The mineral composition of all the analysed samples was determined using the methods of polarisation microscopy and x-ray diffraction. Some differences can be noticed while comparing the results of those methods considering that polarisation microscopy observes only a small part of the analysed rock, while XRD was used on the powdered, bulk sample. Due to the fact that the bulk sample was analysed without any additional treatments, XRD results couldn't show the specific type of clay minerals present. Also, some percentages of certain mineral phases obtained by XRD are higher than percentages obtained by polarisation microscopy, which could be the result of the occurrence of certain mineral phases as fine grains in the matrix or the lithoclasts and not considering amorphous matter during XRD analysis.

Samples were categorized as litho-, vitro-, or crystaloclastic tuff based on the results of the polarisation microscopy.

6.1.1. Wind-Kalnik unit

Tuffs from the Wind-Kalnik unit consist of crystalloclasts (quartz, plagioclase, sanidine, biotite, and hornblende), vitroclasts, and lithoclasts. Crystalloclasts occupy approximately 30-50% of the samples from which 10% quartz, 10-30% plagioclase, 5-10% sanidine, and 5% biotite, whereas 1-3% hornblende occurs in the one sample from this unit. Plagioclase grains exhibit jigsaw-fit texture and zoning. Biotite is opacitizied in one and chloritized in second of two analysed samples from this unit. Opaque minerals occupy approximately 1% and chlorite approximately 2% of the sample. In both samples, XRD analysis show the possible occurrence of hydroxylapatite and additionally gypsum in one of the analysed samples. Clay minerals occupy approximately 10-30% of the samples. XRD identifies them as mostly smectite. Vitroclasts are predominantly devitrified volcanic glass shards and occupy approximately 40% of the samples according to polarisation microscopy. Lithoclasts occupy approximately 10% of the samples. Crystaloclasts, vitroclasts, and lithoclasts are situated in the fine-grained matrix which consists of volcanic ash, clay minerals, and volcanic glass shards and it occupies approximately 10% of the sample.

According to the ratios of crystaloclasts, vitroclasts, and lithoclasts and partially welded structure, saples from this unit can be determined as **ignimbrite deposits dominated by vitroclastic and crystalloclastic particles**.

6.1.2. Eger unit

Tuff from the Eger unit consists of crystalloclasts (quartz, plagioclase, sanidine, and bitotite), vitroclasts, and lithoclasts. Crystalloclasts occupy approximately 30-40% of the samples. They are presented by 5% quartz, 10-30% plagioclase, 2% sanidine, and 5% biotite. Some quartz grains exhibit rounded habit (*pyroclastic quartz*), while some quartz and plagioclase grains exhibit jigsaw-fit texture indicating fragmentation during transport. Plagioclase crystas also show zoning. Biotite is chloritized where chlorite occupies up to 5% of the sample. According to polarisation microscopy, apatite occurs in the sample from this unit, but it is not confirmed with certainty by the XRD analysis. Clay minerals occupy approximately 10-40% of the samples, depending on the method. XRD identifies them as mostly smecite, with less quantities of clay mineral which could be either from the illite or smectite group. Vitroclasts are presented predominantly by devitrified volcanic glass shards and occupy approximately 10% of the samples. Lithoclasts occupy approximately 40% of the samples. Crystalloclasts, vitroclasts, and lithoclasts are situated in the fine-grained matrix which consists of fine sized volcanic ash, clay minerals, and volcanic glass shards and it occupies approximately 10-15% of the sample.

According to the ratios of crystaloclasts, vitroclasts, and lithoclasts this sample can be identified as **lithoclastic tuff**.

6.1.3. Mangó unit

Tuffs from the Mangó unit consist of crystalloclasts (quartz, plagioclase, sanidine, biotite, and hornblende), vitroclasts, and lithoclasts. Crystalloclasts occupy approximately 35-70% of the samples, from which 10-15% quartz, 10-45% plagioclase, 5-10% sanidine, and 5% biotite and hornblende. Some quartz grains exhibit rounded habit (*pyroclastic* quartz) and sporadically with jigsaw-fit texture indicating fragmentation during transport. Plagioclase grains exhibit jigsaw-fit texture and zoning. Biotite is opacitized and chloritized, where opaque minerals occupy approximately 1% of the sample and chlorite approximately 5% of the sample. Opaque minerals have further altered into limonite. In both samples, XRD

analysis shows a possible occurrence of hydroxylapatite, which was determined by polarisation microscopy along with zircon. Clay minerals occupy approximately 10-40% of the samples, depending on the method. XRD identifies them as predominantly smectite. Vitroclasts are mostly devitrified volcanic glass shards and occupy approximately 20% of the samples according to polarisation microscopy. Lithoclasts occupy approximately 20-30% of the samples. Crystaloclasts, vitroclasts, and lithoclasts are situated in the fine-grained matrix which consists of volcanic ash, clay minerals, and volcanic glass shards and it occupies approximately 15% of the sample.

According to the ratios of crystaloclasts, vitroclasts, and lithoclasts and partially welded structure, samples from this unit can be determined as **ignimbrite deposits dominated by lithoclsastic and crystalloclastic particles.**

6.1.4. Demjén unit

Tuffs from the Demjén unit consist of crystalloclasts (quartz, plagioclase, sanidine, biotite, and hornblende), vitroclasts, and lithoclasts. Crystalloclasts occupy approximately 25-60% of the samples, depending on the method, from which approximately 5% quartz, 10-40% plagioclase, 5-10% sanidine, and 5-15% biotite and 1-5% hornblende. Plagioclase exhibit zoning. Biotites were opacitizied and chloritized, where opaque minerals occupy approximately 1% of the sample and chlorite approximately 5% of the sample. Opaque minerals have further altered into hematite and limonite. In the sample Dem-9_E/6 XRD analysis shows 15% hydroxylapatite, which wasn't determined during the polarisation microscopy analysis, indicating that it probably occurs as fine-grained particles in the matrix. In the rest of the samples, XRD analysis shows a possible occurrence of apatite, whereas it was described during polarisation microscopy analysis as an accessory mineral phase with it occupying less than 1% of the sample. The occurrence of calcite was recorded in one sample as a pseudomorphosis using polarisation microscopy, but it wasn't confirmed by the XRD analysis. Clay minerals occupy approximately 10-50% of the samples, depending on the method. XRD identifies them as predominantly smectite, although there is a small percentage of clay minerals that can be determined either as illite or smectite. Devitrified volcanic glass occupies approximately 15-55% of the samples, although non-devitrified volcanic glass is also present. Lithoclasts occupy approximately 10-40% of the samples. Crystaloclasts, vitroclasts, and lithoclasts are situated in the fine-grained matrix which

consists of volcanic ash, clay minerals, volcanic glass shards, and, possibly, apatite, and it occupies approximately 5-25% of the sample.

According to the ratios of crystaloclasts, vitroclasts, and lithoclasts three out of five samples from this unit can be determined as **vitroclastic tuff**, whereas one sample is **crystalo- to vitroclastic** and one sample is partially welded **ignimbimbrite deposit dominated by crystalloclastic and lithoclastic particles.**

6.1.5. Harsány unit

Sample from this unit consists of approximately 25% phenocrystals, from which quartz is 10%, quartz is 10%, sanidine is 2% and biotite is 3%. Biotite was heavily opacitizied and formed opaque minerals occupy less than 1% and were further altered into hematite and limonite. Approximately 75% of the sample is matrix, which mostly consists of volcanic glass, both devitrified and non-devitrified, and clay minerals, precisely smectite, according to the XRD results. Due to the high content of volcanic glass, the texture of this sample can be defined as hypohyaline.

The sample from this unit is identified as **pumice** clast, according to both Harangi (personal communication, 19th October 2022) and polarisation microscopy conducted in this thesis.

6.1.6. Kuchyna tuff

Kuchyna tuff consists of crystalloclasts (quartz, plagioclase, sanidine, and biotite), vitroclasts, and lithoclasts. Crystalloclasts occupy approximately 20-30% of the samples, depending on the method, from which 5% quartz, 10-20% plagioclase, 2-5% sanidine, and 5% biotite. Some plagioclase grains exhibit zoning. Biotite is both chloritized and opacitized where chlorite occupies up to 5% of the sample, whereas opaque minerals occupy less than 1% of the sample. According to XRD, apatite and hornblende possibly occur in this sample, but it cannot be determined with certainty. Clay minerals occupy approximately 30% of the sample. XRD identifies them as mostly smectite, with less quantities of clay mineral which could be either from the illite or smectite group. Vitroclasts are predominantly devitrified volcanic glass shards and occupy approximately 45% of the samples. Lithoclasts occupy approximately 5% of the sample. Crystalloclasts, vitroclasts, and lithoclasts are situated in

the fine-grained matrix which consists of volcanic ash, clay minerals, and volcanic glass shards and it occupies approximately 10-15% of the sample.

According to the ratios of crystaloclasts, vitroclasts, and lithoclasts this sample can be identified as **vitroclastic tuff.**

6.1.7. Alterations and implications for pyroclastic processes

Opacitization is a deuteric alteration that results in the formation of opaque minerals, usually starting at the rims of the altered mineral. Hydrous minerals are affected, such as biotite which is the case in the samples from this study and is a sign of devolatilization. It occurs when the mentioned minerals release their structurally bound water into the magma as a response to a decrease in water pressure in magma as it ascends to the surface (Cox et al., 1979).

Devolatilization of biotite, presented as opacitisation, and zoning of plagioclase are both signs of crystal formation in an imbalanced state such as rapid cooling and decompression.

Chloritization is a hydrothermal reaction usually occurring at temperatures between 400 and 100 °C. Chlorite, which is a phyllosilicate mineral during its reaction with certain types of hydrothermal fluids. Chloritization of biotite is usually characterized by an increase in MgO, FeO_t, and MnO, with a decrease in SiO_2, K_2O, and TiO_2 (Yamini et al., 2017).

Opaque minerals, determined as possible pyrite and magnetite according to their habitus. In some of the analysed samples these mineral phases show alteration to opaque hematite and further limonite, which are determined by polarisation microscopy, but not by XRD due to their low contents.

Jigsaw-fit textures in quartz and plagioclase is a result of crystalloclast fragmentatnion during the transport in the pyroclastic flow. The fragments stay in place due to high density of the flow and only slightly change the original habit of the initial mineral grains. Plagioclase shows zonation due to the imbalanced state caused by an incomplete continuous reaction between the remaining melt and the crystalizing solid solution, due to the two-stage cooling (McPhie et al., 1993).

Volcanic glass can be found as devitrified or non-devitrified. Volcanic glass is an amorphous product of rapid cooling of magma; but is quite unstable and susceptible to alterations, such as devitrification. Therefore, all volcanic glass older than the Mesozoic is devitrified (Cox et al., 1979). Since analysed samples are Miocene in age, it is not unusual to find both non-devitrified and devitrified volcanic glass. According to Vrkljan et al. (2018), devitrification is a process of replacement of the amorphous matter with anisotropic, fine-grained mineral aggregate.

Welded structure is described in almost all samples by polarisation microscopy. According to Grunder et al. (2005) and references therein, it is expressed by loss of pore space, flattening of pyroclastic particles, and sintering of glassy shards. It is usually controlled by the temperature and water content of magma, where the presence of water in pyroclastic rocks reduces their viscosity and enhances welding. This aligns with Biró et al. (2020) who state that the type of eruption that generated pyroclastic in the Bükkalja Volcanic Field was phreatoplinian *sensu lato* with the increasing influence of water during the eruption, increasing its explosivity.

All of the samples, except KMJ-01, are poorly sorted which indicates the proximity of the source of the pyroclastic material, which aligns with Hencz et al. (2021) who state that the source of the pyroclastic material found in the Bükkalja Volcanic Field is eastward, but in the proximity of the aforementioned volcanic field. The sample KMJ-01 is well sorted, which indicates further transport.

6.2. CORRELATION OF CHEMISTRY AND MINERALOGY

The chemical composition of the analysed samples was obtained via X-ray fluorescence analysis.

All of the samples analysed in this study, except one sample from the Demjén unit have SiO_2 content higher than 63%, determining them as a product of silicic magmatism, which is in accordance with Harangi (2001).

In the Figure 6-1. it is visible that a high percentage of SiO_2 content is usually related to the high percentage of volcanic glass along with quartz. Harsány unit has the highest

percentage of SiO_2 along with the highest percentage of volcanic glass and quartz, indicating that the SiO_2 in that unit mostly comes from volcanic glass and quartz. Demjén unit has the lowest percentage of SiO_2 and also the lowest percentage of quartz and volcanic glass, but it also shows the biggest difference in their percentages. SiO_2 also comes in the structure of other mineral phases, such as felspars, biotite, hornblende, and clay minerals, which are also more abundant in that specific unit in comparison to others. Alongside that, the aforementioned unit has more crystaloclasts and lithoclasts than others, so both percentages of volcanic glass and SiO_2 are quite low in comparison with the other units.

All of the samples analysed in this study, except one sample from Demjén, the unit have SiO_2 content higher than 63%, determining them as a product of silicic magmatism, which aligns with Harangi (2001). Harangi (2001) defines Miocene silicic volcanism in the BVF as either potassic or ultrapotassic, but it cannot be confirmed or denied in the frame of this study because of the missing Na_2O contents due to the method limitations.

Harsány unit has the highest SiO_2 content (73,96%) which corresponds to the fact that the analysed sample is categorized as a pumice clast with volcanic glass being the most abundant element in the aforementioned sample. Eind Kalnik, Eger, and Mangó have similar contents with them ranging from 71,62% in the Eger, 71,63-72,98% in the Mangó unit, and 70,95-72,97% in the Wind-Kalnik unit. Samples from the Demjén unit show a wide range of SiO_2 concentrations, from 61,27% to 73,18%, whereas the Kuchyna tuff sample shows the second lowest concentration of 66,24%.

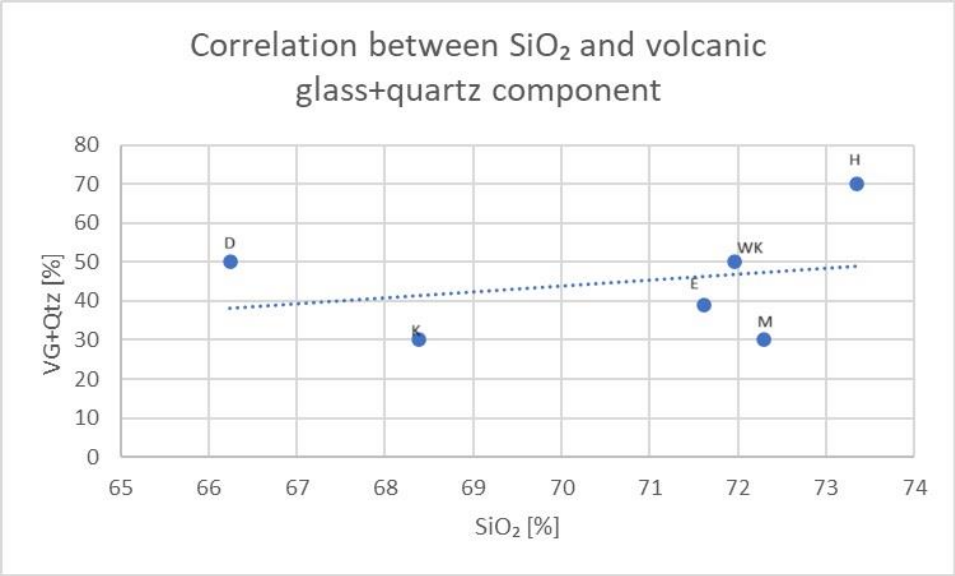

Figure 6-1. Correlation between average SiO_2 and quartz+volcanic glass content. D -Demjén unit; K- Kuchyna tuff; E – Eger unit; WK – Wind-Kalnik unit; H- Harsány unit; M- Mangó unit

According to the result of SiO_2/K_2O ratios, analysed pyroclastic rocks can further be classified according to the magmatic series. Graph with the mentioned classification is given in the Figure 6-2. Harsány unit along with the one sample from the Demjén unit falls into the category shoshonite (alkaline) series due to the extreme enrichment in potassium. Kuchyna tuff belongs to the Calc-Alkaline series whereas the Wind-Kalnik unit, Eger unit, Mangó, and other samples from the Demjén unit correspond to the high-K calc-alkaline series.

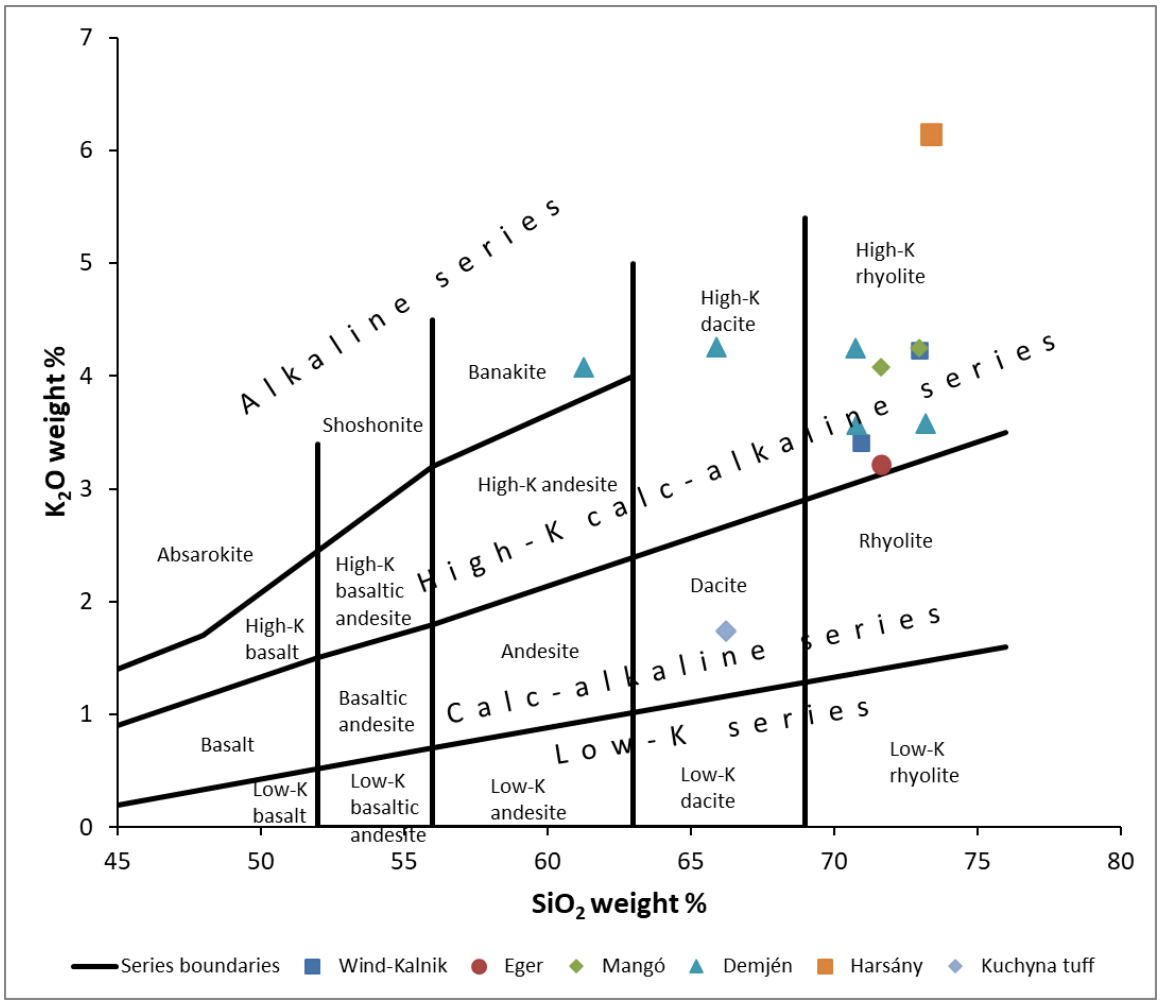

Figure 6-2. Magmatic series according to Ewart (1982) with the classifications for the analysed samples

Potassium appears in the analysed samples mostly as a part of K-feldspar (sanidine), biotite, and hornblende. In Figure 6-3, the comparison of K_2O content obtained by the XRF with percentages of sanidine, biotite, and hornblende is given. Wind-Kalnik unit has the highest percentage of mentioned minerals, but that is not followed by extremely high K_2O content, whereas the Harsány unit has the highest K_2O content (6,14%) and high sanidine content according to the XRD analysis, but not according to the polarisation microscopy, which may be the result of the small surface area of the thin section. Kuchyna tuff sample has the second highest K_2O content (4,53%). Wind-Kalnik (3,41-4,23%), Eger (3,20%), and Mangó u(4,08-4,25%) units have similar K_2O content, whereas it is the lowest in the Demjén unit, where it ranges from 2,36 to 2,38%. All samples except Kuchyna tuff are potassium-rich, hence them being in the High-K Calc-Alkaline and Alkaline series.

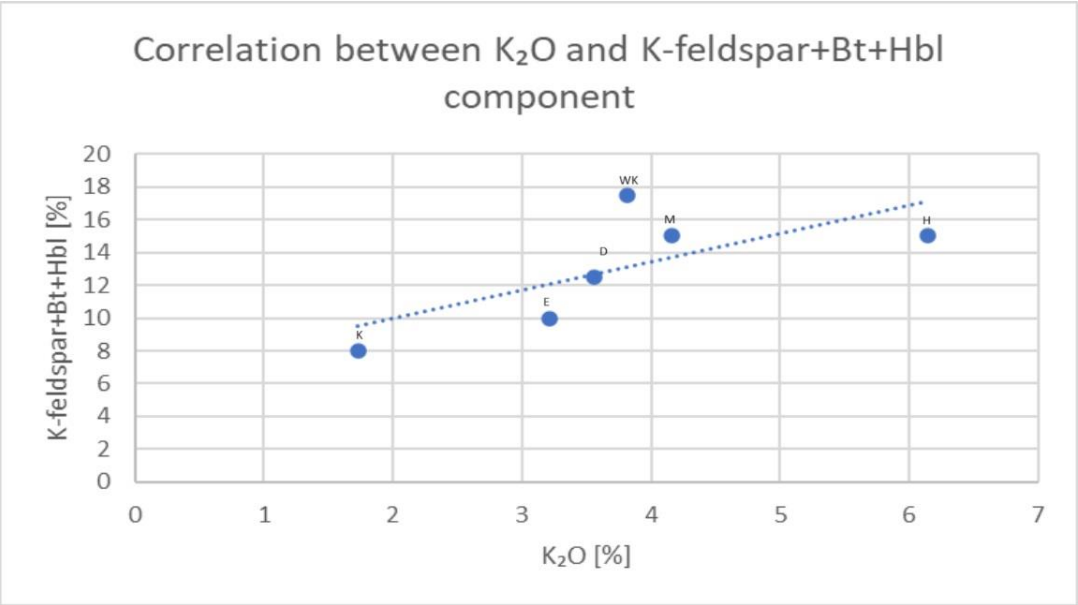

Figure 6-3. Correlation between average K2O and K-feldspar+biotite+hornblende component. D -Demjén unit; K- Kuchyna tuff; E – Eger unit; WK – Wind-Kalnik unit; H- Harsány unit; M- Mangó unit

Iron and aluminum can mostly be found in the crystal structure of biotite. In Figure 6-4 a comparison of Al_2O_3 content and percentage of biotite is given and in Figure 6-5 comparison of FeO content obtained by the XRF with percentages of biotite is presented.

Al_2O_3 content is the highest in the Kuchyna tuff sample at 16,18%, but it isn't followed by a high percentage of biotite in a sample from that unit, indicating that aluminum is mostly found in other minerals, such as feldspars. Most of the samples from Wind-Kalnik, Eger, Mangó, and Demjén units all have Al_2O_3 content from 12-13%.

In the Wind-Kalnik unit, almost all of the aluminum is found in biotite, which is not the case in the rest of the samples. Iron contents are close to the contents of biotite in all units except the Wind-Kalnik unit, however, aluminum is also present in the crystal structure of chlorite, an alteration of biotite, whereas iron can be found in some opaque minerals and hematite and limonite as their alterations. The lowest Al_2O_3 content is in the sample from the Harsány unit, where it is 16,18%.

Total iron oxide is highest in the Kuchyna tuff sample at 4,53% where its percentages are similar to those of biotite, which indicates that almost all iron is incorporated in the biotite crystal structure. Wind-Kalnik (1,87-2,79%), Eger (2,82%), Mangó (2,05-2,17%), Démjen (1,99-4,05%) and Harsány (1,48%) unit have similar total iron oxide contents, except one sample from Demjén unit, where it is 4,05%, although that sample does not show higher biotite content than the rest of the samples from these units.

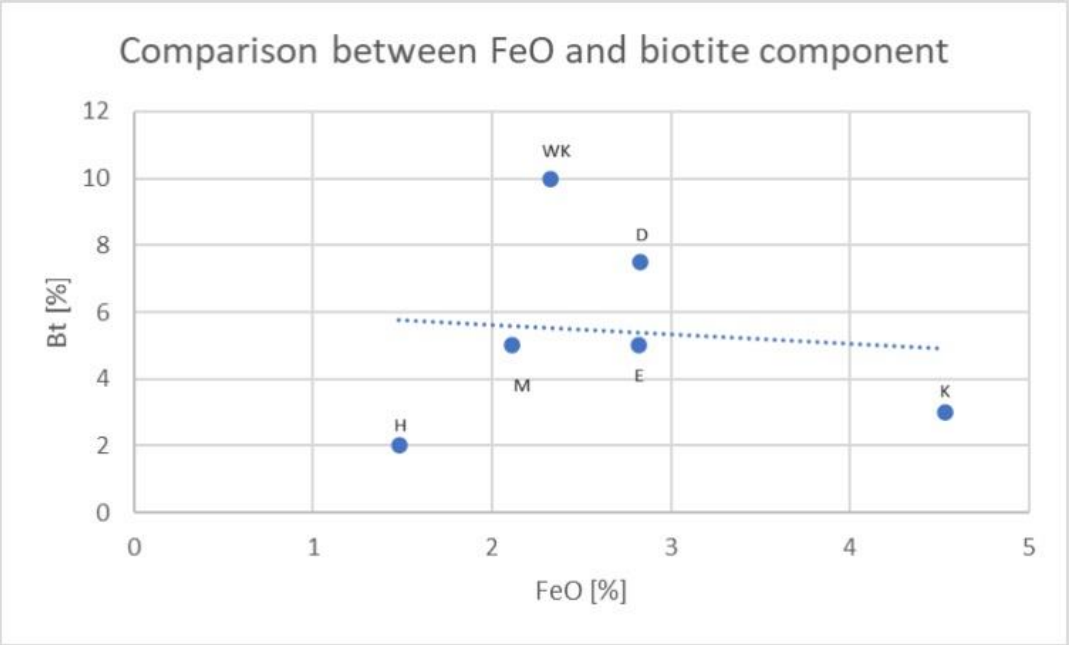

Figure 6-4. Comparison between average FeO and biotite component. D -Demjén unit; K- Kuchyna tuff; E – Eger unit; WK – Wind-Kalnik unit; H- Harsány unit; M- Mangó unit

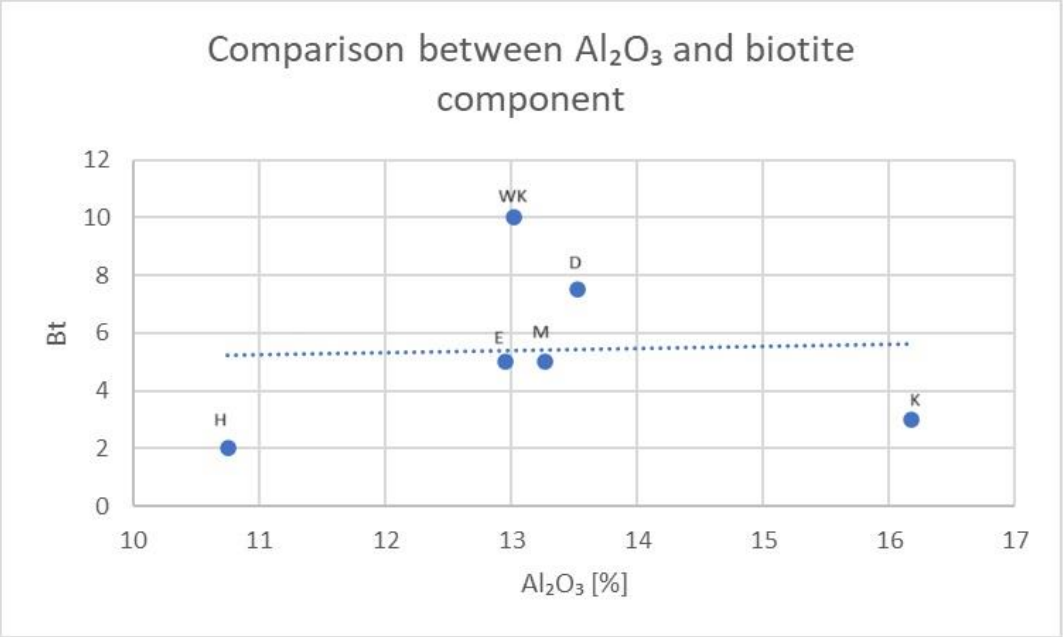

Figure 6-5. Comparison between average Al_2O_3 and biotite component. D -Demjén unit; K-Kuchyna tuff; E – Eger unit; WK – Wind-Kalnik unit; H- Harsány unit; M- Mangó unit

Calcium is found in the crystal structure of plagioclase which has more anorthite in composition. The concentration of CaO ranges from approximately 1-3% in all of the analysed samples except Dem-9_E/6 from the Demjén unit, where it is 8,19%. According to both polarisation microscopy and XRD that sample has quite a high percentage of plagioclase, which is, according to the XRF abundant in anorthite component.

Magnesium is found in the crystal structure of hornblende, which is not present in all analysed samples, and sporadically in biotite. However, hornblende occupies 1-3% of samples according to XRD, which is not enough for that result to be eligible for comparison.

MnO and TiO_2 concentrations are below 1% in all analysed samples, which corresponds to the results of polarisation microscopy and XRD as they aren't a part of the crystal structure of any of the more abundant mineral phases.

P_2O_5 concentrations are below 1% in all samples except one sample from the Demjén unit. Phosphorus is found in the crystal structure of apatite, which occupies less than 1% of all the analysed samples according to the polarisation microscopy. However, according to the XRD, hydroxylapatite content in the sample Dem_E/6 is 15%, which corresponds to the

3,78% of P_2O_5 in that sample, indicating that apatite could be found as fine grains in the matrix of the aforementioned sample.

Microelements found in the analysed samples show normal values, with some of them being only slightly higher or lower than in the bulk composition of continental crust according to Rudnick and Gao (2003), therefore no significant conclusions can be made.

6.3. LITHIUM AND BORON

Lithium contents were determined by atomic absorption spectrometry and boron concentrations were determined by atomic emission spectrometry.

Results of polarisation microscopy and x-ray diffraction indicate that the metasomatic alteration of biotite into chlorite and metasomatic alterations of feldspars into sericite and clay minerals could be the potential carrier of lithium and, possibly, boron, mineralization.

6.3.1. Lithium

In the non-magnetic fractions of the analysed samples lithium concentrations are below the detection limit in 7 samples, whereas in the other samples, they range from 4,2 to 21,7 mg/kg. Lithium concentrations in the magnetic fractions ranged from 15.2 to 41.2 mg/kg. Lithium concentrations in <125 μm fractions, and non-magnetic fractions are below the detection limit in 5 samples, whereas in the other they range from 1,8 to 20 mg/kg.

Biotite is a phyllosilicate mineral with a 2:1 structure from the mica group. Its formula is $K(Fe^{2+},Mg)_2(Al,Fe^{3+},Mg,Ti)([Si,Al,Fe]_2Si_2O_{10})(OH,F)_2$ where iron, magnesium, and titanium are susceptible to substitutions where K^+ (r=1,38 Å) could be replaced with Li^+ due to the same charge, whereas Mg^{2+} (r=0,65-0,72 Å) could be replaced with Li^+ (r=0,76-0,90 Å) due to their similar atomic radius. The correlation between lithium and K_2O content can't be determined in analysed samples.

Chlorite, as a form of alteration of biotite, can also be a carrier of Li mineralization as a form of cookeite, which is a di, trioctahedral clay mineral whose formula is $(LiAl_4)[AlSi_3O_{10}](OH)_8$.

Another possibility is that clay minerals are, carriers of lithium mineralization. Their occurrence is determined by polarisation microscopy and XRD. Both methods show high contents of clay minerals in all of the analysed samples and XRD determined those clay minerals as predominantly smectite. Smectite is characterized by an extremely large reactive surface, therefore lithium could adhere to the surface as the result of absorption, rather than adsorption in the crystal structure.

Swinefordite is a dioctahedral clay mineral from the smectite group which could also be a potential carrier of the lithium mineralization, according to its formula $Li(Al,Li,Mg)_3((Si,Al)_4O_{10})_2(OH,F)_4 \cdot nH2O$.

Lithium concentrations by fractions are given in the Figure 6-6. Undoubtedly, there is a difference between magnetic and non-magnetic fractions, except in the Kuchyna tuff sample, where all the fractions show similar concentrations. Magnetic fractions are composed mostly of biotite and, in some samples, hornblende and show several times higher concentrations than non-magnetic fractions, which indicates that biotite is the carrier of lithium mineralization. Within non-magnetic <125 μm fractions we have found low lithium concentrations, which indicates that lithium-rich smectites don't occur in analysed samples. Although there is a difference in lithium concentrations between analysed fractions, even the values for magnetic fractions aren't much higher than the average bulk composition of the continental crust according to Rudnick and Gao (2003).

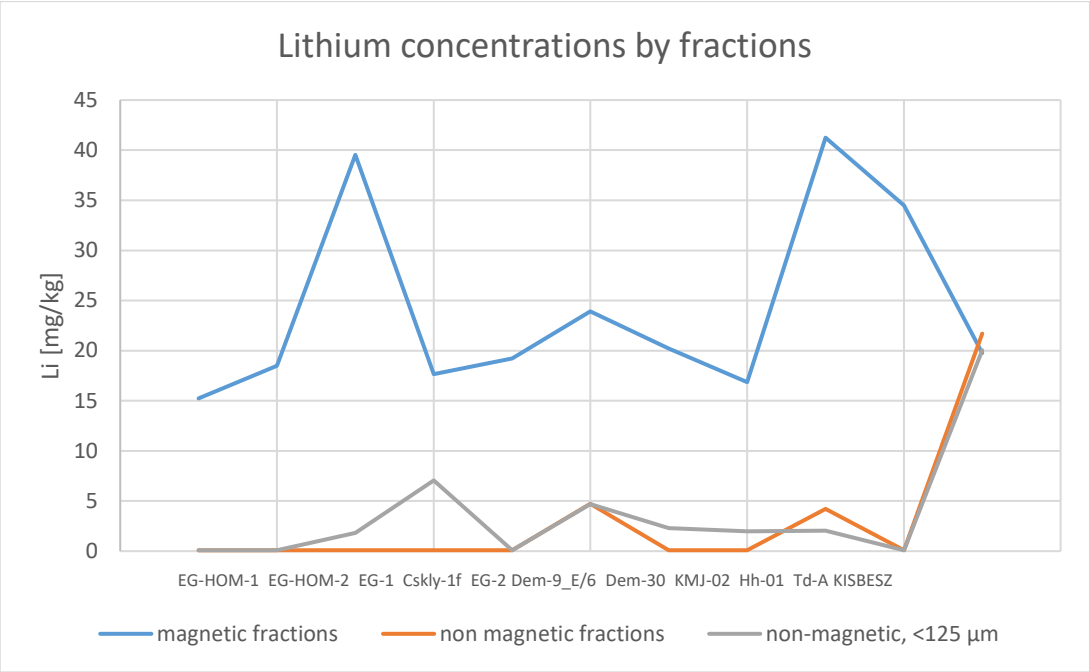

Figure 6-6. Lithium concentrations by fractions

Cheng et al. (2019) have proved that in laboratory conditions, in K-rich biotite after being subjected to the hydrothermal reaction for 8 hours at 80°C, 92,3% of potassium is exchanged with lithium, which indicates a possibility of high-percent K-Li substitution during hydrothermal reactions.

Positions of 001 peaks of biotite in the analysed samples are given in Table 6-1. According to Cheng et al. (2019), K-biotites before substitution show peaks at position d=1,006 mm and position d=1,275 mm after substitution. Peaks in samples analysed in this study more correlate to those in which substitution didn't occur, therefore in analysed samples it is likely that no K-Li exchange took place, and weak increase of lithium is related to chloritization or lithium-bearing fluid inclusions

Table 6-1. Positions of 001 peaks in biotite according to the XRD

sample	unit	position 001 (Å)	position 001 (nm)
EG-HOM-1	Wind-Kalnik	10,0217	1,00217
EG-HOM-1		10,0341	1,00341
EG-1	Eger	10,0234	1,00234
Cskly-1f	Mangó	10,0453	1,00453
EG-2		10,0127	1,00127
Dem-9_E/6	Demjén	10,0012	1,00012
Dem-30		9,9955	0,99955
KMJ-01		10,011	1,0011
KMJ-02		10,0318	1,00318
Hh-01		10,0445	1,00445
Td-A	Harsány	10,0265	1,00265
KISBESZ	Kuchyna tuff	10,024	1,0024

Lithium-rich tuffs have been analysed in several studies so far. Segovia-Moro et al. (2023) researched lithium-rich tuffs from the Neogene Macusani Volcanic Field in Peru. The mentioned volcanic field has a 0,9Mt reserve of Li which occurs in lithium-rich tuff with concentration of 3000-4000 ppm Li. Host minerals for lithium mineralization are in micas, precisely, zinwaldite and lepidolite.

Benson et al. (2017) studied ignimbrites from the Middle Miocene McDermitt Volcanic Field in southeastern Oregon and northern Nevada, USA. Obtained lithium concentration average at 1000 pm for melt inclusions. This study shows that out of all present minerals that crystalize in rhyolitic magmas, lithium is only compatible with biotite, which was also proved by measured Li concentrations, which were highest in biotite out of all the minerals, such as feldspars, quartz, Na-amphibole, and zircon, that occur in analysed samples.

Lin et al. (2020) proved that lithium in the tuffs in the eastern Sichuan basin is fixed onto the illite or illite-smectite clays and leached from the volcanic ashes during alteration processes, which indicates that lithium in tuffs from Sichuan basic possibly originates from a magmatic source.

Li et al. (2021) describe a newly discovered lithium deposit where clay minerals are host minerals for lithium mineralization. Host rocks are extremely altered volcanic rocks where lithium mineralization is related to processes of monmotillonitization and chloritization and Li is probably found between the layers of crystal structure as an adsorbed ion.

Ellies et al. (2021) have researched Li in biotites from rhyolithic Bishop Tuffs from California and Kos Plateau from Greece. Those biotites show lithium concentrations up to 2.300 ppm. As other mineral phases analysed in the aforementioned study don't support the idea of Li-rich melt, authors suggest that lithium occurs in the magmatic volatile phase between the layers of biotite, due to the fact that in rhyolitic magma suites, it crystallizes at low temperatures trapping the coexisting fluid phase.

Peng et al. and references therein (2022) have researched lithium-rich tuffs in the Sichuan basin. They have based their research on the theory that in the clay-type, volcanogenic lithium deposits lithium was leached from the rhyolitic lavas and volcanic ashes via meteoric and hydrothermal fluid during the alteration processes. Lithium-bearing rocks are Early-Middle Triassic felsic volcanogenic tuffs named green-bean rocks due to their yellowish-green colour. Lithium content is 2.86-957 ppm. The aforementioned tuffs are highly altered into clay minerals, which are predominantly illite with the addition of mixed layer illite-smectite and minor occurrences of kaolinite.

According to the Dupont de Dinechin (2023) and references therein, the mantle is low in lithium, with an average concentration of 19 ppm in mantle's peridotites, but in subduction zones, Li-rich slab can metasomatize mantle rocks during dehydration. In felsic lavas lithium concentrations range between 5 to 35 ppm, however, some rhyolites can be enriched in Li, such as topaz rhyolite with concentrations of around 140 ppm and Macusani rhyolite with concentrations higher than 1000 ppm. Rhyolitic volcanic glasses usually have lithium concentrations of about 50 ppm, but values up to 400 ppm were recorded, although according to Prelević et al. (2005), the mantle could be locally enriched in lithium. In comparison with that, both magnetic and non-magnetic, as well as <125μm non-magnetic fractions analysed in this paper can't be considered lithium-rich.

6.3.2. Boron

Boron concentrations in the non-magnetic fraction range from 835 to 4505 mg/kg, while the boron concentrations in the magnetic fractions range from 3044 to 26204 mg/kg in this study.

Boron usually occurs in borate minerals and in tourmaline, which hasn't been recorded in allayed samples, and clay minerals such as smectite. According to Nellessen et al. (2021) in water boron appears as borate or boric acid. Its absorption into the clay minerals is determined by the pH. In alkaline water, it appears as a borate mineral, and it will be absorbed into 2:1 phyllosilicates. Water with a pH of 8-9 is the most suitable for absorption and can yield up to 300 ppm boron in the clay mineral.

Due to their similar ionic radiuses, boron as B^{3+} (r=2,3 Å) could replace Al^{3+} (r=5,4 Å) in the crystal structure of alumosilicates; such as biotite, due to their same ionic charges. Significant correlations between Al_2O_3 and boron content can't be determined in both magnetic and non-magnetic fractions of analysed samples.

According to Bailey et al. (2019) boron can be found in minerals other than borates, such as dumortierite, which is igneous in origin, and prismatin, which originates from anatectic melts. Various boron-bearing minerals can be found in metasediments and metamorphic rocks, but none of the aforementioned minerals have been found in the samples analysed in this study.

Boron concentrations by fractions are given in the Figure 6-7. Magnetic fractions of analysed samples, which consist of biotite with the addition of hornblende, show several times higher concentrations of boron than non-magnetic fractions. Although possible interference with iron could appear in magnetic fractions causing up to 20% higher values, it still proves that there is a big difference in boron concentrations in magnetic and non-magnetic fractions which indicates that biotite and its alterations could be boron-bearing. Both non-magnetic and magnetic fractions show boron concentration much higher than the average bulk composition of the continental crust according to Rudnick and Gao, (2003).

Chlorite, as a form of alteration of biotite, can also be a carrier of boron mineralization as a form of borocookeite, which is a di, trioctahedral clay mineral whose formula is $(LiAl_4\square)[BSi_3O_{10}](OH)_8$. As chlorite is present in most of the analysed samples as an alteration of biotite, it is a possibility that this mineral from the chlorite series is present, explaining the high boron concentrations in the magnetic fraction.

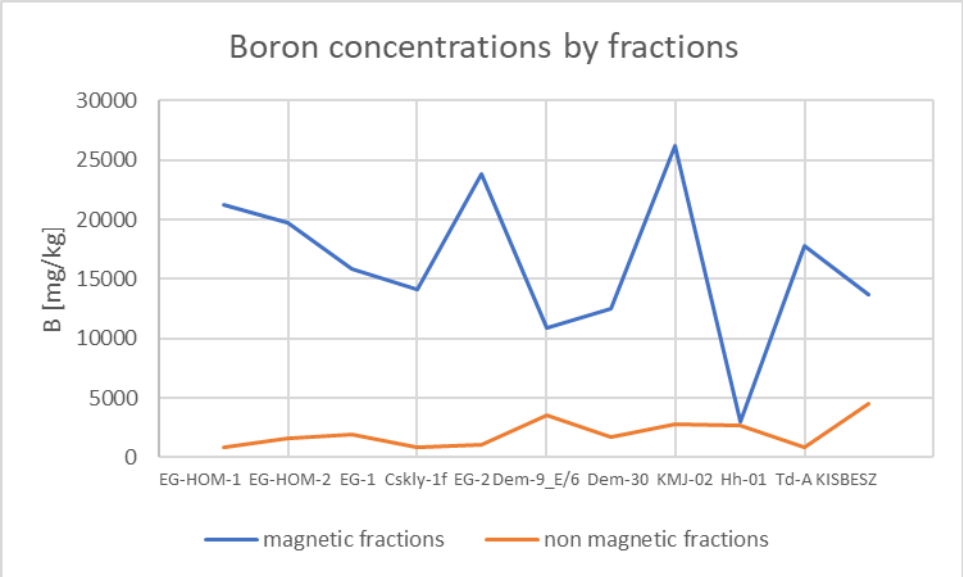

Figure 6-7. Boron concentrations by fractions.

Gméling et al. (2007) analyzed boron and other immobile element concentrations in different volcanic fields. One of the analysed volcanic fields is the Bakony-Balaton Volcanic Field situated in Hungary. The main rock types found in this volcanic field are alkali olivine basalt and basanite dating from 7,5 to 2,8 Ma. Boron concentrations in samples from the aforementioned volcanic field range from 1,6 to 12,4 ppm, which is lower to around average in comparison with bulk continental crust according to Rudnick and Gao (2003).

According to Floyd et al. and references therein (1998), Miocene borate deposits in Western Turkey can be associated with extensive medium to high K- calc-alkali ignimbrites. They analysed ignimbrite samples from Kirka locality which are coeval with the lacustrine-developed borate deposits in their geographical proximity. They claim that boron can be mobile in the subduction environment where calc-alkaline melts are generated.

Boron-rich fluid inclusions are usually common in Li-rich pegmatites (Sirbescu, 2013), however even if fluid inclusions were found in some samples analyzed in this Master's thesis, due to high boron concentrations it couldn't be the only source of boron enrichment, especially due to the fact that they are found in quartz in feldspars, whereas biotites show higher boron contents.

6.3.3. Correlation of lithium and boron

In Figure 6-8, the comparison between lithium and boron concentration in non-magnetic fractions is given. Although the graph shows some correlation between these two elements, because most of the samples from the non-magnetic fraction have lithium concentration below the detection limit, no further conclusions can be made with certainty.

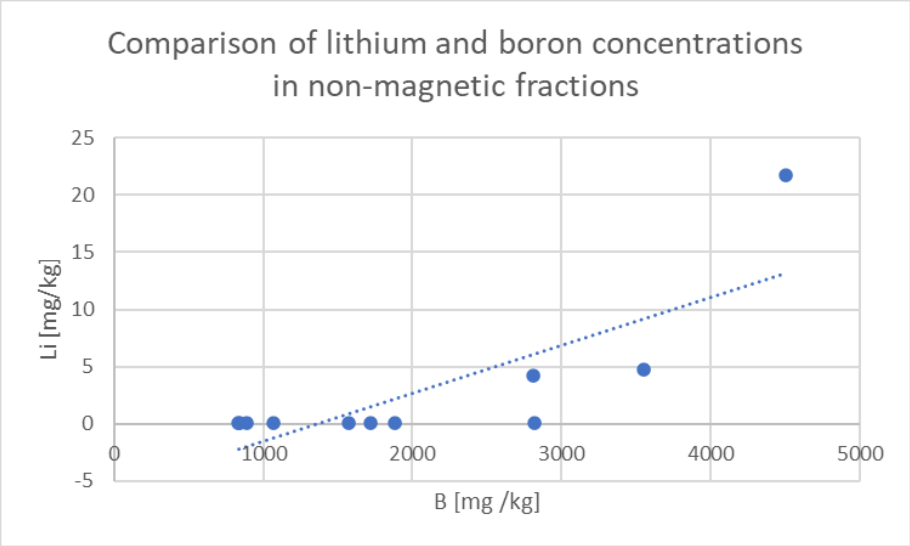

Figure 6-8. Comparison of lithium and boron concentrations in non-magnetic fractions

In Figure 6-9, the comparison between lithium and boron concentration in magnetic fractions is given. It shows a slight negative correlation, where the samples with the biggest lithium concentration don't show higher boron concentrations.

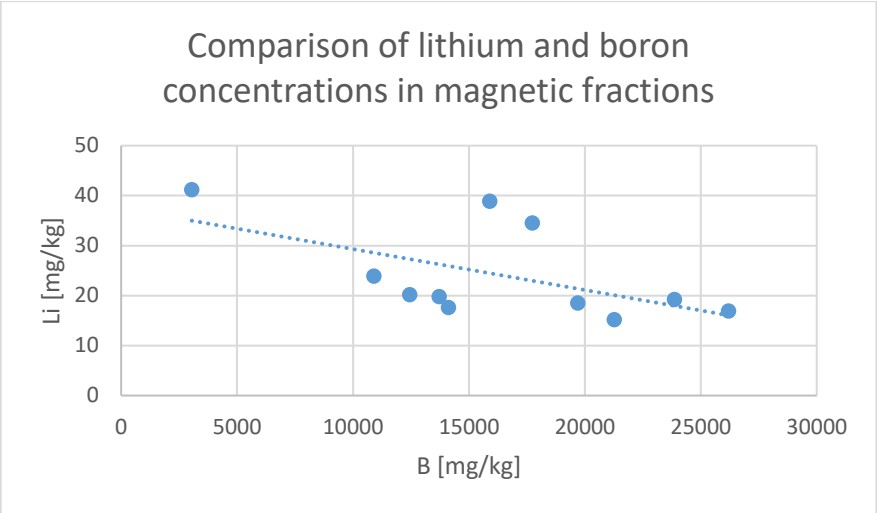

Figure 6-9. Comparison between lithium and boron concentrations in magnetic fractions

6.3.4. Correlation with Western Balkan Li-B metallogenic zone

According to Borojević Šoštarić and Brenko (2022) Western Balkan Li-B metallogenic zone can be traced for 1500 km and is positioned subparallel to the Sava-Vardar and Western Vardar zone toward the Izmir-Ankara-Erzincan zone. Potential lithium-boron deposits can be traced from Motacija Mt. to the end of the Izmir-Ankara-Erzincan zone, except in North Macedonia and Greece, where Li-B mineralization hasn't been discovered so far. Mostly, Li-B mineralization in the Western-Balkan Li-B zone can be found associated with Miocene granitic rocks.

Lithium-boron mineralization is often stratabound and occurs interlayered with tuffitic sediments within lacustrine basins. Although Middle Miocene volcanism is not directly observed in the Western Balkan Li-B metallogenic zone, tuffaceous sediments from analyzed lacustrine basins can be related to Miocene silicic volcanism from Bükkalja Volcanic Field. As shown in Figure 6-10, tuffs found in the Dinarides probably originated from the same eruptions as the tuffs from pyroclastic units analysed in this paper (Borojević Šoštarić and Brenko, 2022 and references therein).

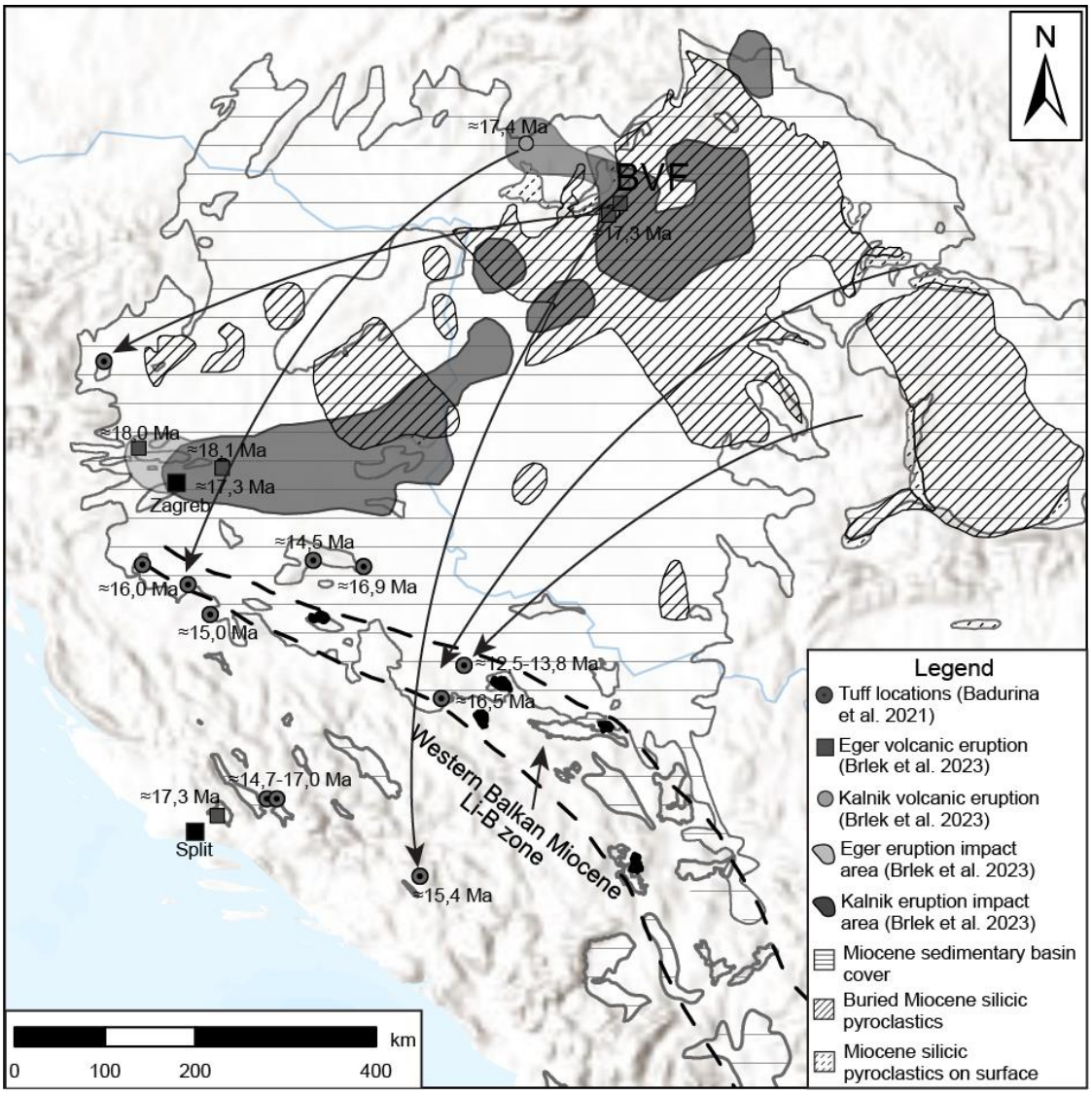

Figure 6-10. Overview map with Miocene volcanism and tuff in Pannonian Basin depicting spatial and temporal distribution according to HENCZ et al. (2021); BADURINA et al. (2021), BOROJEVIĆ ŠOŠTARIĆ & BRENKO (2023) and BRLEK et al. (2023). Abbreviations: BVF – Bükkalja Volcanic Field.

6.3.5. Correlation with tuffs from Dinarides

According to Brlek et al. (2023), Miocene tuffs found in the Dinarides are the product of two separate eruptions. Kalnik, which is dated at 18,1 Ma, and Eger, which is dated at 17,3 Ma. Mentioned eruptions are coeval with the eruption phases in the Bükkalja Volcanic Field. Products of the eruptions were massive rhyolithic ignimbrites which can be found in Kalnik and Požeška gora Mts.

According to Marković et al. (2021), Middle Miocene tuffs can be found in the Zagorje-Mid-Transdanubia zone, precisely in Čučerje and Nježić localities.

According to the aforementioned references, tuffs from the Dinarides are coeval with those from the Bükkalja Volcanic Field and possibly have the same source (Figure 6-10) therefore a comparison with lithium and boron contents from Hergotić (2023) is given.

Hergotić (2023) analysed several tuffs from Dinarides. Two of the analysed samples are from the Zagorje-Mid-Transdubia zone, whereas 4 of the analysed samples are from Outer Dinarides, precisely Sinj and Livno basin, however according to Marković et al (2021) and Brlek et al. (2023) they are all said to have the same source. They are all Middle Miocene in age. The mineral composition is similar to the samples analysed in this paper, consisting mainly of quartz, plagioclase, and biotite with the addition of orthoclase, calcite, titanite, muscovite, and clinopyroxene. Lithium and boron contents were also analysed. Lithium contents in non-magnetic fractions and <32 μm fractions are mostly below the detection limit, whereas lithium contents in magnetic fractions are higher, up to 187,9 ppm. Boron concentrations are also much higher in the magnetic fractions, in some samples even over 10.000 ppm. Boron concentrations in non-magnetic fractions range is much lower than in magnetic fractions, ranging from 1.500 ppm to 6.537 ppm, whereas the fraction <32μm concentrations range from 2.013 ppm to 9.653 ppm. Biotite is suspected to be both Li- and B-bearing minerals, which is also the case regarding the samples analysed in this paper.

7. CONCLUSION

For this master's thesis, 11 pyroclastic rocks from the Bükkalja Volcanic field were analysed along with one Kuchyna tuff sample.

Quartz, plagioclase, K-feldspar, biotite, and clay minerals, precisely, smectite, were determined as the most abundant mineral phases in all samples, whereas hornblende, apatite, and mixed-layer illite-smectite occur only in some of the analysed samples. Chlorite and opaque minerals, which represent alteration products of biotite, and to a smaller extent, hornblende, were determined using polarisation microscopy. Analysed samples were separated into magnetic fractions alongside biotite and hornblende. Volcanic glass, along with the pumice fragments, both devitrified and non-devitrified are abundant in every sample according to the polarisation microscopy, whereas andesitic to rhyolitic lithoclasts occur in most of the samples.

According to the SiO_2 to K_2O ratios most of the samples belong to the high K calc-alkaline magmatic series.

Lithium concentrations are undoubtedly higher in magnetic compared to non-magnetic and <125μm non-magnetic fractions, indicating that lithium could be found in biotite or its alteration product, such as chlorite. Although tuffs around the world have been researched as the source of lithium mineralization, concentrations in tuffs analysed in this study aren't of great significance. Allfractions exhibit low concentrations of lithium with the used methods.

Concentrations of boron are much higher in magnetic fractions compared to non-magnetic fractions, although both fractions are boron-rich indicating that boron could be found both on biotite and its alteration products, as well as adsorbed onto the clay minerals which separated into the non-magnetic fraction. There hasn't been any significant research regarding boron enrichment in biotite which leaves the mechanisms of the mentioned enrichment quite unclear and a potential topic for future research.

Lithium and boron are both elements of great interest due to their use in various branches of industry owing to the high demand for both elements alternative sources of potentially useful mineralization are of critical necessity.

8. REFERENCES

Badurina, L., Šegvić, B., Manfić, O., Slovenec, D. 2021. *Miocene tuffs from the Dinarides and Eastern Alps as proxies of the Pannonian Basin lithosphere dynamics and tropospheric circulation patterns in Central Europe.* Journal of the Geological Society, 178, p 202–262.

Bailey, D. G., Lupulescu, M. V., Darling, R. S., Singer, J. W., Chamberlain, S. C. 2019. *A review of boron-bearing minerals (excluding tourmaline) in the Adirondack region of New York* State. Minerals. 9(10), p. 644.

Benson,T., Mahood, G.A., Grove, M., 2017. *Geology and $^{40}Ar/^{39}Ar$ geochronology of the middle Miocene McDermitt volcanic field, Oregon and Nevada: Silicic volcanism associated with propagating flood basalt dikes at initiation of the Yellowstone hotspot*. GSA Bulletin. 129 (9-10), p 1027–1051.

Biró T., Hencz M., Németh K., Karátson D., Márton E., Szakács A., Bradák B., Szalai Z., Pécskay Z., Kovács I.J. 2020*: A Miocene Phreatoplinian eruption in the North-Eastern Pannonian Basin, Hungary: the Jató Member*. Journal of Volcanology and Geothermal Research. 401, p. 1–21

Borojević Šoštarić, S., Brenko, T. 2022. *The Miocene Western Balkan lithium- boron metallogenic zone*. Miner Deposita 58, p. 639-658.

Brlek, M., Tarpster, S.R., Schindlbeck-Belo, J., Gaynor, S.P., Hauf, K.F., Georgiev, S.V., Trinaistić, N., Šuica, S., Brčić, V., Wang, K.L., Lee, H.Y., Beier, C., Abersteiner, A.B., Mišur, I., Peytcheya, I., Kukoč, D., Németh, B., Trajanova, M., Balen, D., Guillong, D., Lukács, R. 2023. *Tracing widespread Early Miocene ignimbrite eruptions and petrogenesis at the onset of the Carpathian-Pannonian Region silicic volcanism*,Gondwana Research, 116, p. 40-60.

Cheng, Y., Huang, Z., Yao, D., Wu, C. 2019. *Extraction of Potassium from Biotite by Lithium Ion Exchange and Its Electrochemical Properties*. IOP Conference Series: Materials Science and Engineering. 678.

Cox, K.G., Bell, J.D., Pankhurst, R.J. 1979. *The Interpretation of Igneous Rocks*. Springer Dordrecht.

Czuppon, G., Harangi, S., Ntaflos, T., Lukács, R., Szabó, Cs., Koller, F. 2001. *Mixed andesite-rhyolite ignimbrite from the Miocene Bükkalja Ignimbrite Volcanic Field, Northern Hungary: evidence for magma mixing*. Mitt. Osterr. Mineral. Ges. 146, p. 61– 63.

Dupont de Dinechin, M., Balcone-Boissard, H., Martel, C., Rusiecka, M. 2023. *Lithium in felsic magmas: a volcanological perspective*. Front. Earth Sci. 11, p 1-13.

Ellis, B. S., Neukampf, J., Bachmann, O., Harris, C., Forni, F., Magna, T., Laurent, O., Ulmer, P. 2022. *Biotite as a recorder of an exsolved Li-rich volatile phase in upper-crustal silicic magma reservoirs*. Geology, 50(4), p. 481–485.

Ewart, A., 1982. *The mineralogy and petrology of Tertiary-Recent orogenic volcanic rocks: with special reference to the andesitic-basaltic compositional range*; p. 25-95 in, Thorp, R.S., ed., Andesites: Orogenic Andesites

Fisher, R.V. 1966. *Rocks composed of volcanic fragments*. Earth Sci Rev 1, p. 287-298.

Floyd, P.A., Helvaci, C., Mittwede, S.K.1998. *Geochemical discrimination of volcanic rocks associated with borate deposits: an exploration tool?* Journal of Geochemical Exploration, 60(3), p. 185-205.

Fordinál K., Baráth I., Šimon L., Kohút M., Nagy A. Kučerová J. 2010: *New data on the Devínska Nová Ves Formation (Vienna Basin, Slovakia)*. 16th Conference on Upper Tertiary Brno. Geol. Výzk. Mor. Slez., Brno, p. 32–34.

Gméling, K., Németh, K., Martin, U., Eby, N., Varga, Z. 2007. *Boron concentrations of volcanic fields in different geotectonic settings.* Journal of Volcanology and Geothermal Research, 159(1–3), p. 70-84.

Grunder, A. L., Laporte, D., Druitt, T. H. 2005. *Experimental and textural investigation of welding: Effects of compaction, sintering, and vapor-phase crystallization in the rhyolitic Rattlesnake Tuff.* Journal of Volcanology and Geothermal Research, 142(1–2), p. 89-104.

Harangi, S. 2001. *Neogene to Quaternary volcanism of the Carpathian–Pannonian region — a review.* Acta Geologica Hungarica 44, p. 223– 258.
Harangi, S., Lukács, R., Czuppon, Gy., Szabó, Cs. *2002. Magma mixing in a compositionally layered magma chamber: a silicate melt inclusion study*. Workshop on Volcanic Systems, Seiano, Italy, Proceedings, p. 101– 106.

Harangi S, Mason PRD, Lukács R. 2005. *Correlation and petrogenesis of silicic pyroclastic rocks in the Northern Pannonian Basin, Eastern-Central Europe: in situ trace element data of glass shards and mineral chemical constraints*. J Volcanol Geoth Res. 143(4), p. 237–257.

Harangi S, Lenkey L. 2007. *Genesis of the Neogene to Quaternary volcanism in the Carpathian-Pannonian region: role of subduction, extension, and mantle plume*. Geol. Soc. Am. Spec. Pap. 418, p. 67–92

Harangi S., Lukács R. 2019. *The Neogene to Quaternary volcanism and its geodynamic relations in the Carpathian–Pannonian Region*. Földtani Közlöny 149, p. 197–232.

Hencz, M., Biró, T., Cseri, Z., Karátson, D., Márton, E., Nemeth, K., Szakács, A., Pécskay, Z., Kovacs, I. 2021. *A Lower Miocene pyroclastic-fall deposit from the Bükk Foreland Volcanic Area, Northern Hungary: Clues for an eastward-located source.* Geologica Carpathica. 72, p. 26-47.

Hergotić, L. 2023. *Mineraloška i geokemijska svojstva odabranih magmatita i tufova iz Dinarida – s osvrtom na litij i bor.*Master's thesis. Zagreb: Faculty of Mining, Geology and Petroleum Engineering, University of Zagreb.

Konečny, V., Lexa, J., Hojstricová, V. 1995. *The Central Slovakia Neogene volcanic field: a review.* Acta Vulcanol. 7, p. 63– 78.

Li, C., Li, Z., Wu, T., Luo, Y., Zhao, J., Li, X., Yang, W., Chen, X. 2021. *Metallogenic Characteristics and Formation Mechanism of Naomugeng Clay-Type Lithium Deposit in Central Inner Mongolia, China*. Minerals, 11, p. 238.

Lin, Y. J., Zheng, M. P., Zhang, Y. S., Xing, E. Y., Redfern, S. A. T., Xu, J. M., Zhong, J. A., Niu, X. S. 2020. *Mineralogical and geochemical characteristics of Triassic lithium-rich K-bentonite deposits in Xiejiacao section, South China.* Minerals, 10(1), p 69-85.

Lukács R, Harangi S, Ntaflos T, Mason PRD. 2005. *Silicate melt inclusions in the phenocrysts of the Szomolya Ignimbrite, Bükkalja Volcanic Field (Northern Hungary): implications for magma chamber processes*. Chem Geol 223(1–3), p. 46–67.

Lukács R., Harangi Sz., Bachmann O., Guillong M., Danišík M., Buret Y., von Quadt A., Dunkl I., Fodor L., Sliwinski J., Soós I., Szepesi J. 2015: *Zircon geochronology and geochemistry to constrain the youngest eruption events and magma evolution of the Mid-Miocene ignimbrite flare-up in the Pannonian Basin, eastern-central Europe*. Contributions to Mineralogy and Petrology. 170, p. 1–26.

Lukács R., Harangi Sz., Guillong M., Bachmann O., Fodor L., Buret Y., Dunkl I., Sliwinski J., von Quadt A., Peytcheva I. Zimmerer M. 2018: *Early to Mid-Miocene syn-extensional massive silicic volcanism in the Pannonian Basin (East-Central Europe): Eruption chronology, correlation potential and geodynamic implications*. Earth Science Reviews 179, p. 1–19.

Lukács, R., 2022. Electronic mail to Sibila Borojević Šoštarić, 19th October 2022.

Marković, F., Kupier, K., Coric, S., Hajek Tadesse, V., Hernitz Kucenjak, M., Bakrač, K., Pezelj, Đ., Kovačić, M. 2021. *Middle Miocene marine flooding: New 40Ar/39Ar age constraints with integrated biostratigraphy on tuffs from the North Croatian Basin*. Geologia Croatica, 74 (3), p 237-252.

Márton, E., Fodor, L., 1995. *Combination of palaeomagnetic and stress data—a case study from North Hungary.* Tectonophysics. 242(1–2), p. 99–114.

Márton E, Pécskay Z., 1998. *Complex evaluation of paleomagnetic and K/Ar isotope data of the Miocene ignimbritic volcanics in the Bükk Foreland, Hungary*. Acta Geol Hung 41, p. 467–476

McPhie J, Doyle M, Allen R 1993. *Volcanic textures—a guide to the interpretation of textures in volcanic rocks.* Centre for Ore Deposit and Exploration Studies, University of Tasmania.

Nellessen, M. A., Crossey, L., Gasda, P., Peterson, E., Lanza, N., Reyes-Newell, A., Delapp, D., Yeager, C., Labouriau, A., Wiens, R. C., Clegg, S., Legett, S., Das, D. 2021. *Boron adsorption onto clay minerals: Insight into Martian groundwater geochemistry.* Presented at the 52nd Lunar and Planetary Science Conference. University of New Mexico; Los Alamos National Laboratory; McGill University.

Németh, N., Petho, G. 2009. *Geological mapping by geobotanical and geophysical means: A case study from the Bükk Mountains (NE Hungary).* Central European Journal of Geosciences, 1, p. 84-94.

Noszky J. 1931. *The Oligocene–Miocene stratigraphy of the northeastern part of the Hungarian Mid-Mountains: II. The Miocene.* Annual report of the Geological Institute of Hungary 27, p. 160–236.

Peng, Y., Zheng, M., Zhang, Y., Xing, E., Gui, B., Zuo, F. 2022. *Geochronology and geochemistry of lithium-rich tuffs in the Sichuan basin, Western Yangtze: Implication for the magmatic origin and final closure of eastern Paleo-Tethys.* Geoscience Frontiers, 14(1)

Pettijohn, F.J. 1975. *Sedimentary Rocks*. Harper.

Prelević, D., Foley, S. F., Romer, R. L., Cvetković, V., Downes, H. 2005. *Tertiary ultrapotassic volcanism in Serbia: Constraints on petrogenesis and mantle source characteristics*. Journal of Petrology, 46(7), p. 1443–1487.

Rudnick, R.L., Gao, S., 2003. *The Composition of the Continental Crust* Treatise on Geochemistry, Vol. 3, The Crust, Elsevier-Pergamon, Oxford, 1-64.

Rybár, S., Kuiper, K., Fordinál, K., & Teodoridis, V., Šarinová, K., Sant,K., Kováčová, M., Vojtko, R., Reiser, M., Nováková, P., Vlček, T. 2019. *New 40 Ar/ 39 Ar, fission track and sedimentological data on a middle Miocene tuff occurring in the Vienna Basin: Implications for the north-western Central Paratethys region*. Geologica Carpathica. 70, p. 386-404.

Schréter Z., 1939. *Geological properties of the southeastern side of the Bükk Mountains*. Annual report of the Geological Institute of Hungary 1933-35, p. 511–532.

Segovia-More, M., Torró i Abat, L., Villanova-de-Benavent, C., Briones, J., Vallance, J., Monnier, L., Laurent, O., Salvi, S., Baby, P., Proenza, J., Nieto, F. 2023. *High-resolution mineralogy of Lithium-rich Tuff from the Macusani Volcanic Field, Puno, Peru*. . 17th SGA Biennial Meeting on Mineral Resources in a Changing World. Zurich,Switzerland. p.303–306

Sirbescu, M.-L. C.; Krukowski, E. G.; Schmidt, C.; Thomas, R.; Samson, I. M.; Bodnar, R. J. 2013. *Analysis of boron in fluid inclusions by microthermometry, laser ablation ICP-MS, and Raman spectroscopy: Application to the Cryo-Genie Pegmatite, San Diego County, California, USA* Chemical Geology. 342, p. 138–150.

Szakács A., Márton E., Póka T., Zelenka T., Pécskay Z., Seghedi I. 1998: *Miocene acidic explosive volcanism in the Bükk Foreland, Hungary: Identifying eruptive sequences and searching for source locations*. Acta Geologica Hungarica 41, p. 413–435.

Šimon L., Fordinál K., Kollarová V., Kováčiková M. 2009: *The Kuchyna tuff — Finding of neovolcanics in Záhorie lowland*. Congress paper, Bratislava, 1–262.

Vrkljan, M., Borojević Šoštarić, S., Tomašić, N. 2018. *Optička mineralogija*. Zagreb: University of Zagreb.

Yamini, M., Tutti, F., Yamini, M., Ahmadian, J., Wan, B., 2017. *Examination of chloritization of biotite as a tool for reconstructing the physicochemical parameters of mineralization and associated alteration in the Zafarghand porphyry copper system, Ardestan, Central Iran: mineral-chemistry and stable isotope analyses.* Mineralogy and Petrology. 111(5).

Web sources

Döbelin, N. 2020. Phase quantification using calibrated peak lists. URL: https://www.profex-xrd.org/tutorials/phase-quantification-using-calibrated-peak-lists/ (05.02.2024)

European Comission. 2023. *Critical Raw Materials Act.* URL: https://single-market-economy.ec.europa.eu/sectors/raw-materials/areas-specific-interest/critical-raw-materials/critical-raw-materials-act_en (29.01.2024.)

Geographical position of the Bükk Mountains. URL: https://earth.google.com/web/ (14.09.2023.)

Royal Society of Chemistry. 2024a. Lithium. URL: https://www.rsc.org/periodic-table/element/3/lithium (29.01.2024.)

Royal Society of Chemistry. 2024b. Boron. URL: https://www.rsc.org/periodic-table/element/5/boron (29.01.2024.)